Investigating the Performance of Parabolic Trough Solar Collector with Thermal Energy Storage System for Injera Baking Applications

By

Bonsa Reta Mosisa

A Thesis Submitted to Department of Thermal and Aerospace Engineering

School of Mechanical, Chemical and Materials Engineering

Office of Graduate Studies

Adama Science and Technology University

November, 2020

Adama, Ethiopia

Investigating the Performance of Parabolic Trough Solar Collector with Thermal Energy Storage System for Injera Baking Applications

By

Bonsa Reta Mosisa

Advisor: Dr. Addisu Bekele

A Thesis Submitted to Department of Thermal and Aerospace Engineering

School of Mechanical, Chemical and Materials Engineering

Office of Graduate Studies

Adama Science and Technology University

November, 2020

Adama, Ethiopia

DECLARATION

I hereby declare that this M.Sc. thesis entitled *"INVESTIGATING THE PERFORMANCE OF PARABOLIC TROUGH SOLAR COLLECTOR WITH THERMAL ENERGY STORAGE SYSTEM FOR INJERA BAKING APPLICATIONS"* in partial fulfilment of the requirements for the award of the degree of Master of Science in Thermal Engineering is an authentic record of my own work under the supervision of Dr. Addisu Bekele, Assistant Professor of Thermal Engineering, Adama Science and Technology University.

The matter embedded in this thesis has not been submitted for the award of a degree or diploma in any other university. All relevant resource information used in this paper has been duly acknowledged.

Bonsa Reta Mosisa	______________	____________
Candidate	Signature	Date

This is to certify that the above statement made by the candidate is correct to the best of my knowledge and belief. This thesis has been submitted for examination with my approval.

Dr. Addisu Bekele	________________	________________
Advisor	Signature	Date

APPROVAL OF BOARD OF EXAMINERS

We, undersigned, members of the board of examiners of the final open defense by **Bonsa Reta Mosisa** have read and evaluated his thesis entitled "***Investigating the Performance of Parabolic Trough Solar Collector with Thermal Energy Storage System for Injera Baking Applications***" and examined the candidate. This is, therefore, to certify that the thesis has been accepted in partial fulfilment of the requirements of the degree of Masters of Science in Thermal Engineering.

______________________	______________________	______________
Name of student	Signature	Date
______________________	______________________	______________
Advisor	Signature	Date
______________________	______________________	______________
External Examiner	Signature	Date
______________________	______________________	______________
Internal Examiner	Signature	Date
______________________	______________________	______________
Chair Person	Signature	Date
______________________	______________________	______________
Head of Department	Signature	Date
______________________	______________________	______________
School Dean	Signature	Date
______________________	______________________	______________
Post Graduate Dean	Signature	Date

ACKNOWLEDGEMENT

First of all, I would like to thank almighty God for his constant love and support. Without his help and guidance being here is impossible.

I would like express gratitude towards my advisor Dr. Addisu Bekele, for his much needed support, uncountable advices, his patience and precious inputs throughout the this thesis work.

Last but not the least, I would like to thank my family and friends for support during tough times and motivating me throughout my life and for their constructive suggestions and the inspiration.

ABSTRACT

Every human being needs energy in their lives for different propose. One of energy intensive activity is cooking. This cooking energy demand is mostly fulfilled by biomass, natural gas and electricity. Solar energy is also one of the promising solutions for meeting the energy demand.

In this paper the performance of parabolic trough solar collector integrated with phase change material is investigated for Injera baking application. The system is designed to fulfill the Injera demand for an average family size (45 Injera). Energy absorbed by the parabolic trough collector is studied for four different tracking techniques under the climatic conditions of Adama. The cylindrically encapsulated capsules with $NaNo_3$ are used for the storage system. The performance of a solar parabolic trough collector and charging process of the designed thermal energy storage are studied using one dimensional explicit Finite difference method .The transient analysis of the ceramic baking pan done using Matlab pdepe solver to compare the heating up time for a heating fluid type of shell Thermia B and Sythrem 800 oil.

The result from numerical simulation shows that four parabolic trough solar collectors connected in parallel required fulfill the demand and 168.1 Kg mass of PCM encapsulated in 277 cylindrical capsules are required. Polar East–West and horizontal East–West tracking systems were best appropriate for a parabolic trough collector throughout the entire year.

Key words: *Injera, Phase change material, Parabolic trough,* $NaNo_3$*, Solar energy, Thermal Energy storage*

TABLE OF CONTENTS

LIST OF FIGURES

LIST OF TABLES

LIST OF ACRONYMS AND ABBREVIATIONS

NOMENCLATURE

C	Specific heat capacity (J/kg.K)
g	Gravity (m/s^2)
h	Convective heat transfer coefficient (W/m^{2}K)
L	Characteristic length (m)
Nu	Nusselt number
Pr	Prandtl number
T	Temperature (K or ^{o}C)
V	Volume (m^3)
S_o	Sunshine hour
G_{on}	Extraterrestrial solar Radiation(w/m^2)
H	Global daily radiation (W/m^2)
I	Global hourly radiation (W/m^2)
m	Mass of storage material (Kg)

GREEK SYMBOLS

θ	Angle of incidence
ϕ	Latitude
Δ	Change
β	Slope
γ	Surface azimuth angle

δ	Declination
ε	Porosity
ω	Hour angle

SUBSCRIPTS

A	receiver tube
ab	energy absorbed
cv	convection
ext	external
f	working fluid
g	glass envelope
int	internal
ext	external
max	maximum
min	minimum
r	radiation
st	storage

ABBREVIATIONS

DR	Daily range temperature of the day
HTF	Heat Transfer Fluid
LHTES	Latent Heat Thermal Energy Storage
PCM	Phase Change Material
PTSC	Parabolic Trough solar collector

SNL	Sandia National Laboratories
ST	local solar time
TES	Thermal Energy Storage
HCE	Heat collecting element
PDE	Partial Differential Equation

CHAPTER 1

INTRODUCTION

1.1 Background of the Study

Energy is vital to any economic development and societal well-being. It is very important in every aspects of human being life and connected to all human activities. Statistics from the International Energy Agency (IEA) World Energy Outlook 2019 show that the total energy demand in the world rises by 1.3% each year up to 2040. There are different sources of energy which are under category of renewable and non-renewable. Beside high effort to utilize various types of energy, now day's Global attention has focused on mitigation of environmental issues by increasing energy efficiency and reducing carbon emissions. Over 30% of total energy consumed in developing countries is used for household energy consumption. Cooking is one of daily practices in which energy is highly needed and it accounts for about 90% of domestic energy consumption in these countries. A majority of rural households use biomass fuels to meet their heating and cooking needs with firewood constituting about 95% of fuel consumed for cooking in villages. Each year about 16 million hectare of forests are consumed as cooking fuel and the harmful emissions from the burning of this biomass fuel are responsible for three million deaths per year globally (Sedighi & Salarian, 2017). Most of the people living in the developing countries cook food-using biomass as their primary energy sources. In Ethiopia, cooking accounts for over 50% of all primary energy consumption in the country. Unless new sustainable and more cleaner source of energy is used, the number of people relying on biomass for cooking will increase to 2.7 billion by 2030 because of population growth (Adem & Ambie, 2017).

Injera is spongy flat bread like processed of different cereals such as Teff, millet, sorghum, maize, wheat and rice or combinations of those. It is staple food item predominantly consumed in Ethiopia and some parts of East Africa. In most households of Ethiopia, the energy demand for baking Injera largely met with bio-fuels such as fuel wood, agricultural residue and dung cakes. Most of the people living in Ethiopia bake Injera using biomass on open-fire stoves that is unhealthy and inefficient. Whereas, electricity is used in some of the urban households (Abulkadir & Demiss, 2013)

Currently, biomass is the dominant source of energy used for Injera baking followed by electricity. According to data from World Energy Outlook 2019 only 45% of population have access to electricity in 2018. Below half of the population still don't have electricity access. Therefore, alternative energy sources such as Solar, thermal gasification and biogas should considered highly.

Solar energy is a suitable solution to limit deforestation caused by the exploitation of firewood to provide domestic energy needs and to minimize the abusive use of energy derived from the fossil sources. Solar energy is considered a suitable alternative for cooking purpose. It is an abundant renewable resource, freely available everywhere in adequate amount, making it one of the most promising, clean, non-polluting sources. There different method of harnessing this abundantly occurring renewable resources to use it for different purpose applications. Using solar thermal collectors is one way of changing solar energy into another usable form of energy. The use of solar energy for the purpose of cooking food presents a viable alternative to the use of fuel wood, kerosene, and other fuels traditionally used in Ethiopia.

Ethiopia is rich with solar radiation resources. The study based on Modeling solar radiation and GIS analysis results show that there is a very high potential of solar power generation in wide-ranging areas of Ethiopia all over the year and this is due to the geographical location which is close to the equator with large high altitude lands (Tekle, 2014).

1.1.1 Working principle of solar thermal system integrated with PCM for Injera baking application

In this study the performance of parabolic trough solar collector with Thermal energy storage system for Injera baking purpose is investigated. The system contains parabolic trough solar collector, Injera baking assembly and phase change material based thermal energy storage device as a main component. The PTSC is the source of energy where solar energy converts into thermal energy that used to bake Injera and the storage unit, which is called as packed bed, is a cylindrical storage tank filled with cylindrically encapsulated capsules containing a PCM. The system considered for this study contains two modes of operation these are Charging and Discharging mode.

During charging process, the heat transfer fluid coming from PTSC flow over the packed bed from the top to the bottom, and the PCM in the cylindrical capsules melts. At the end of this process thermal energy needed for baking stored for later usage. During discharging process, the heat transfer fluid flows over the packed bed from the bottom to the top, and the PCM in the cylindrical capsules solidifies. The HTF oil that exit from storage tank during discharging process meet the required temperature under the baking pan

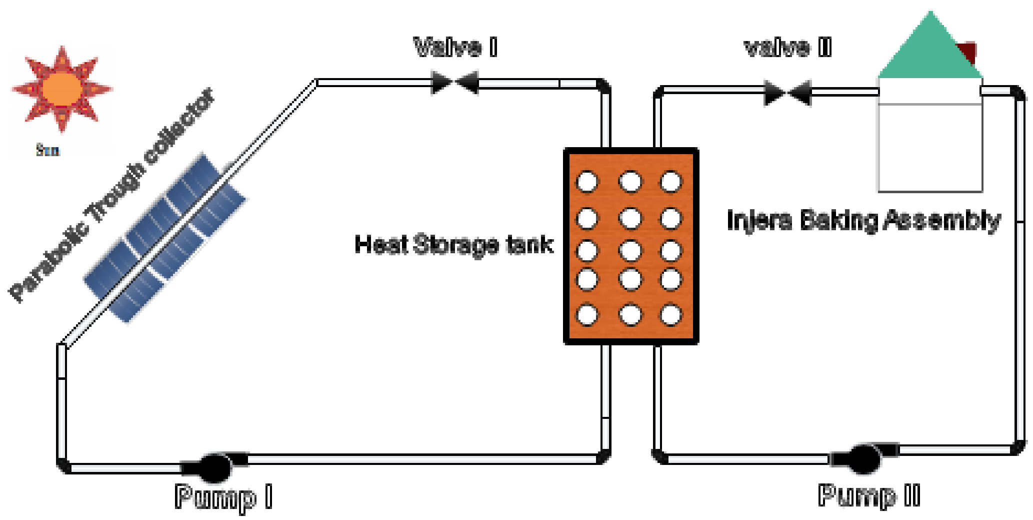

Figure 1-1 Schematic diagram of solar thermal system integrated with PCM for Injera baking application.

1.2 Statement of the Problem

Most of the people living in Ethiopia bake Injera using biomass on open-fire stoves. The inefficient open-fire stove consumes large amounts of firewood and produces high indoor air pollution and CO_2 emission. This highly affects the health of women whom actively involved in Injera baking process (Adem & Ambie, 2017). In rural part of the country still there is no enough electricity infrastructures, according to data from World Energy Outlook 2019 only 45% of population have access to electricity (IEA, 2019). So there should be a means of utilizing alternative renewable energy for a cooking. Solar energy is abundantly available but the efforts on developing solar cookers have been limited with direct solar cookers and solar cookers with sensible storage type. Direct solar cookers have not been widely accepted because they are not suitable for indoor and night use. Due to intermittent nature of solar energy there is mismatch between the load and the available energy, therefore thermal storage system that fulfill the required energy has to be designed. The problem related with both traditional and solar Injera baking system can be solved by conducting the performance analysis of parabolic trough solar collector integrated with latent heat storage system.

1.3 Objectives of the study

1.3.1 General objective

The main objective of this thesis is to investigate the performance of parabolic trough solar collector with thermal energy storage system for Injera baking application.

1.3.2 Specific objectives

- ✓ To determine and compare solar energy absorbed by parabolic trough solar collector for different sun tracking modes.
- ✓ To investigate the optical and thermal performance of a parabolic trough solar collector under the climate conditions of Adama.
- ✓ To size and design the Layout of parabolic trough solar collector Solar Field that satisfy the Injera baking demand for average family size.
- ✓ To size PCM thermal energy storage system required for Injera baking demand for average family size.
- ✓ To analyze the transient thermal behavior of the PCM system during charging process .

1.4 Scope and Limitations

1.4.1 Scope of the Study

The study aims at transient numerical performance analysis of parabolic trough solar collector integrated with PCM thermal energy storage for Injera baking application. This work includes simulation of parabolic trough solar collector particularly at Adama weather condition and investigation of thermal storage system that satisfies the heat demand of Injera baking.

1.4.2 Limitation of the Study

The numerical simulation analysis conducted only on the main component of the system parabolic trough solar collector and PCM thermal energy storage. The baking cycle and temperature distribuation study on the baking pan not considered here.The financial and economic, hydrodynamic analysis of the system were not included.

1.5 Significance of the Study

The study contributes a solar thermal system as an Injera baking technology. This numerical investigation of the system paves a way for development of the similar system that will be a best candidate for cooking system. With regard to the environmental protection and human health this study will come up with cleaner baking system.

CHAPTER 2

LITERATURE REVIEW

2.1 Basics of Solar Energy

Solar energy is the electromagnetic energy emitted by the sun. It is a natural source of energy that is not exhausted by its usage. The emission of this energy is a result of a progression of radiation and convection processes occurs with successive emission, absorption and re-radiation. There are several fusion reactions that supply the energy radiated by the sun. The sun is the largest member of the solar system which is compass of powerfully warm gassy substance having a diameter of $1.39x10^9$m, is at an average distance of $1.5x10^{11}$m from the Earth. It is a sphere of intensely hot gaseous matter. The Sun rotates on its axis approximately once every 4 weeks. The sun has effective blackbody surface temperature of 5777K. Sun is responsible not only to produce directly most of the renewable energy sources, but also responsible for providing indirect sustenance for non-renewable sources such as fossil fuels. (Tiwari, 2016)

2.1.1 Solar Energy Utilization

The use of solar energy has three major objectives: to produce electricity, make fuels, and directly collect and use heat.to accomplish this three objectives there three conversion mechanism, those are:

a. Solar thermal conversion
b. Solar photovoltaic and
c. Solar thermo-photovoltaic conversion

The solar thermal conversion implies the capturing of the solar heat and using it in many processes. Solar photovoltaic and thermo-photovoltaic are the means for conversion of solar energy directly to electricity. The solar thermal energy is captured by the various types of solar collectors. The solar photovoltaic effect is achieved by the semiconductor devices which can directly produce electricity when the photons are incident on it. Thermo-photovoltaic devices directly convert heat to electricity.

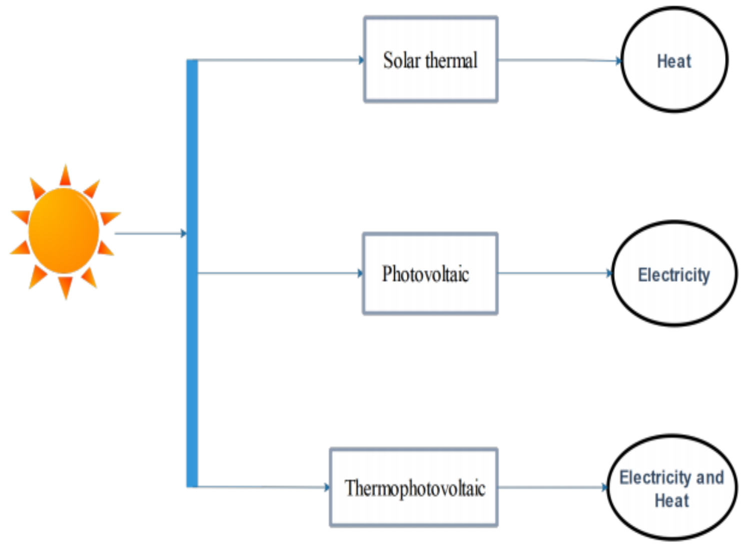

Figure 2-1 Solar energy conversion (Kreith & Goswami, 2007)

2.1.2 Solar Radiation Components

To predict the performance of a solar process in the future, we use past measurements of solar radiation at the location in question or from a nearby similar location. Solar radiation data are used in several forms and for a variety of purposes. The most detailed information available is beam and diffuse solar radiation on a horizontal surface, by hours, which is useful in simulations of solar processes. Detailed information about solar radiation availability at any location is essential for the design and economic evaluation of a solar energy system. Long-term measured data of solar radiation are available for a large number of locations in the world. Where long term-measured data are not available, various models based on available climatic data used to estimate the solar energy availability (Kreith & Goswami, 2007).

Extraterrestrial radiation: is the radiation that received in the absence of the atmosphere. There are two sources of variation in extraterrestrial radiation. The variation in the radiation emitted by the sun and Variation of the earth-sun distance (range of ±3.3 %). However, for engineering purposes, in view of the uncertainties and variability of atmospheric transmission, the energy emitted by the sun considered as fixed. Extraterrestrial solar radiation predicted with certainty but radiation levels on the earth are subject to considerable uncertainty resulting from local climatic interactions. The most useful solar radiation data are based on long-term (30 years or more) measured average values at a location, which unfortunately are not available for most locations in the world. For such locations, an estimating method (theoretical model) based on some measured climatic parameter may be used.

Beam Radiation: The solar radiation received from the sun without having been scattered by the atmosphere.

Diffuse Radiation: The solar radiation received from the sun after its direction changed by scattering by the atmosphere.

Total Solar Radiation: The sum of the beam and the diffuse solar radiation on a surface. Solar radiation is a total radiation on a horizontal surface, often referred to as global radiation on the surface

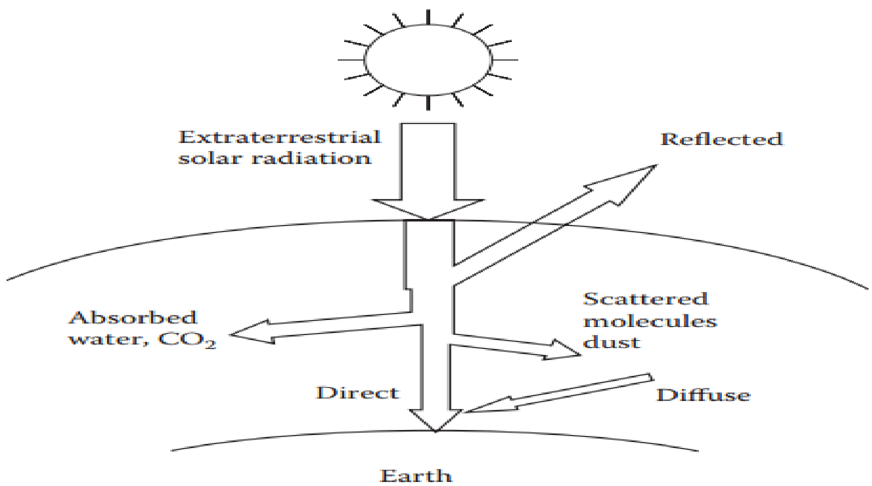

Figure 2-2 Attenuation of solar radiation as it passes through the atmosphere (Kreith & Goswami, 2007)

2.2 Solar Collectors

Solar collectors are devises that collect solar radiation, convert it in to thermal energy to run some applications. The major components of any solar collector include the reflector, absorber and heat transportation medium. There are two types of collectors: concentrating (stationary) and non-concentrating. While concentrating collectors use different areas of intercepting and focusing, non-concentrating collectors use same or nearly same areas of intercept and focus.

The different areas of intercept and focus in concentrating collectors give high radiation fluxes at their focus; making them suitable for high-temperature applications (Tian & Zhao, 2013).

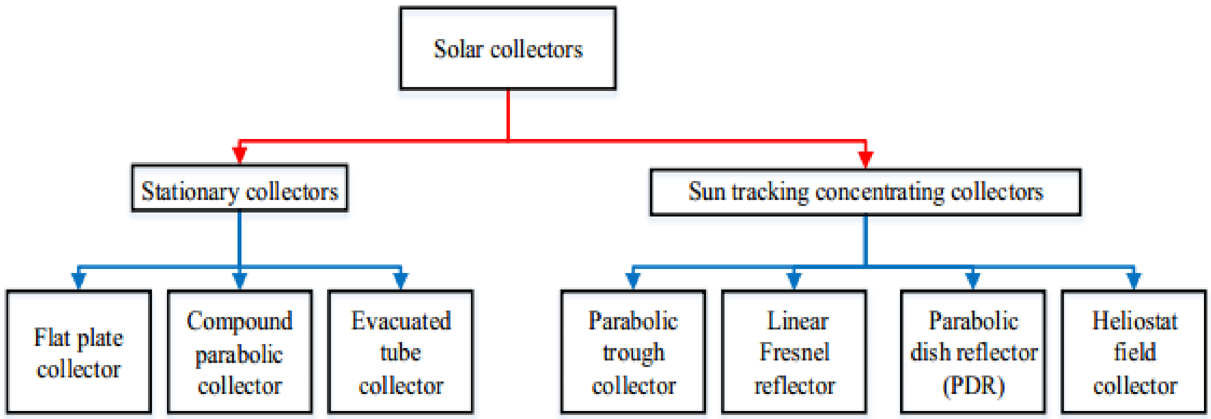

Figure 2-3 Classification of solar collectors *(Kalogirou, 2014)*

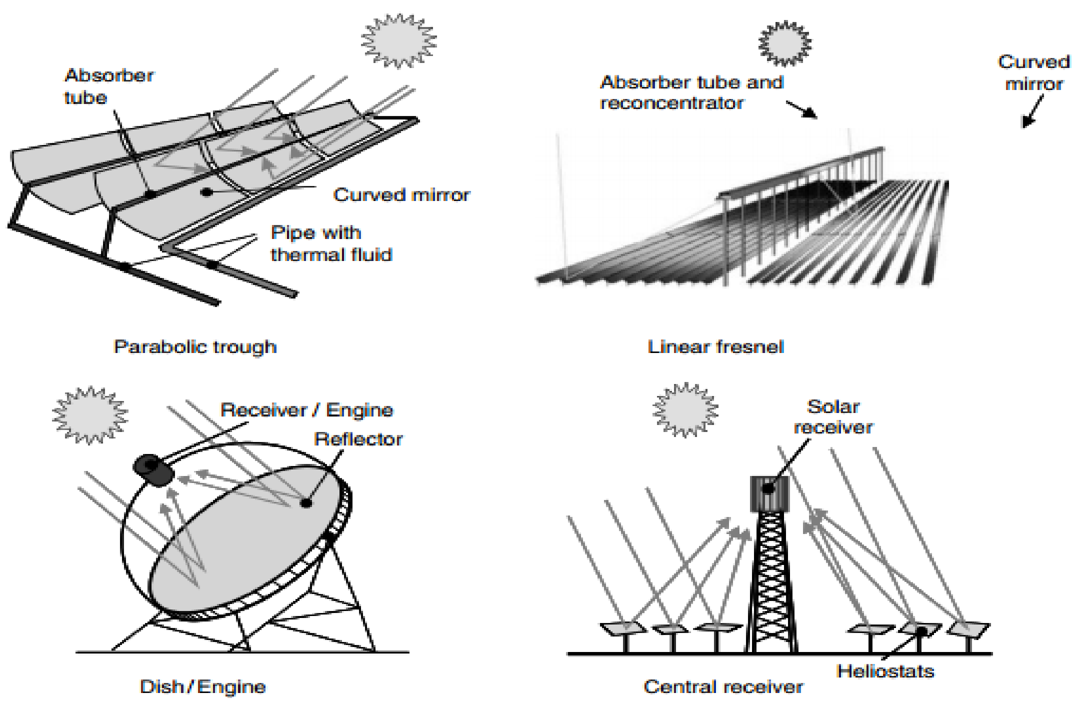

Figure 2-4 Schematic diagrams of the four concentrating collectors systems (Kreith & Goswami, 2007)

Stationary collectors used for low temperature application while sun tracking concentrating collectors used for medium and high temperature application range. When we compare different solar energy collectors by their Indicative working temperature range the parabolic trough collector reaches up to 400 ^{o}C (Kalogirou, 2014).

Table 2-1 Types of solar collector with their respective temperature range of application

low temperature	Medium temperature	High temperature
Flat plate 30-80 °C	Linear Fresnel 60-250 °C	Parabolic dish collector 100 -1500°C
Evacuated tube 50-200 °C	Cylindrical parabolic 60-300°C	Heliostat field collector 150-200°C
Compound parabolic 60-240 °C	Parabolic trough 60-400 °C	

2.3 Parabolic Trough Solar Collector

PTSC is a dominant technology available today in both commercial and industrial scale among the medium-temperature solar collectors. They are made up of a parabolic trough-shaped mirror that reflects direct solar radiation, concentrating it onto a receiver tube located in the focal line of the parabola. The concentrated radiation heats the fluid that circulates through the receiver tube, thus transforming the solar radiation into thermal energy in the form of the sensible heat of the fluid.

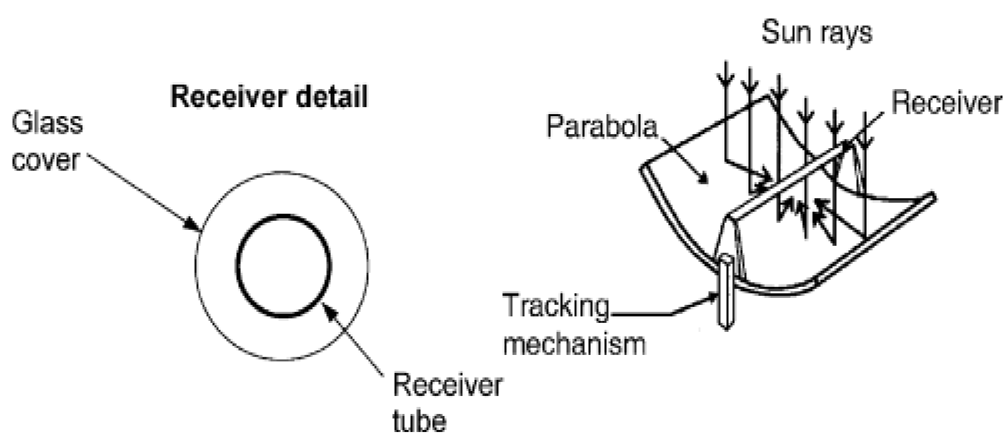

Figure 2-5 Schematic of a parabolic trough solar collector (Kalogirou, 2014)

2.4 Review on Performance Analysis of Parabolic Trough Solar Collector

Many studies have been developed and carried out regarding modeling of parabolic trough solar collector (PTSC) technology.

Compared to the multi-dimensional models the 1-D model is superior, because it involves less solution time and complexity. The review study on different models indicate that 1-D energy balance gives reasonable results for short HCEs (< 100 m) The 1-D model becomes insufficient with increasing HCE length, and thus the discretization through the axial direction is needed to reduce the deviation(Yılmaz & Mwesigye, 2018).

(Kalogirou, 2012), Presented a detailed thermal model of parabolic trough solar collector (PTSC) implemented in Engineering Solver Equation software. The proposed model takes into account the three mechanisms of heat transfer: conduction, convection, and radiation. A verification of the proposed model is carried out with experimental data done by Sandia National Laboratories. The results of the model and the experimental data indicate a good agreement with each other.

(Ouagued et al., 2013),Studied the performance of a tracking solar parabolic trough collector using heat transfer model by dividing he receiver into several segments and applying heat balance in each segment over a section of the solar receiver under Algerian climate. Different tilted, tracking collectors and oils are considered so as to determine the most efficient PTSC system. It was indicated that Syltherm 800 is suitable as working fluid over the year compared to the other synthetic working fluids.

(Mokheimer et al., 2014), Investigated the hourly, daily and monthly performance of the PTSC using simulation code developed using EES software under Dhahran, Saudi Arabia weather conditions. Euro Trough solar collector (ET-100) and for LUZ solar collector LS-3 PTSC were considered for this study. They concluded that the maximum optical efficiency that can be reached in Dhahran is 73.5%, whereas the minimum optical efficiency is 61%. These results were validated using available experimental data and against the results obtained by THERMOFLEX code.

(Marif et al., 2014),Investigated the optical and thermal performance of a solar parabolic trough collector under the climate conditions of Algerian Sahara one dimensional implicit finite difference method with energy balance approach. The absorber model based on an energy balance in each section of the glass envelope, absorber pipe and the fluid developed. Two fluids (liquid water and TherminolVP-1™ synthetic oil)and different tracking systems were considered for the study. They found out that the high optical efficiency is obtained with full tracking equal to 73.92% and the one axis polar East–West and horizontal East–West tracking systems were most desirable for a parabolic trough collector throughout the whole year.

(C Tzivanidis et al., 2015), designed small parabolic trough collector model using commercial Software called Solid works and simulated for different operating conditions. Flow Simulation environment of Solid works used for the simulation purpose simulation results was validated with simple 1-D numerical model developed with FORTRAN. The results of the simulation indicate that solar radiation direction is very important for the efficiency of the collector, especially for its optical efficiency.

(D. Kumar & Kumar, 2015),developed one dimensional steady state heat transfer in order to estimate the through-out year performance characteristics in terms of water temperature rise, heat energy generation, optical and thermal efficiency for the climactic conditions of Bhiwani city in India. These all parameters were evaluated for horizontal and vertical plane using analytical simulation by Mat lab R2012a. They concluded that higher heat energy generation is found to be 2.38 kW h/day in May on horizontal plane, 2.46 kW h/day in April on inclined plane, the maximum optical efficiency is attained as 72.26% and 72.4% on horizontal and an inclined plane respectively. The peak instantaneous thermal efficiency is accomplished as 66.78% in July on horizontal plane, 65.77%in September on inclined plane of collector. The result was validated with existing experimental results of Sandia National Laboratories (SNL).

(Marefati et al., 2018) investigate optical and thermal analysis of PTSC for four cities of Iran with different weather conditions and the solar energy potential of the collector compered. Different parameters such as concentration ratio, incident angle correction factor, collector mass flow rate are considered and their effect on output of the system studied. Steady heat transfer model developed and Mat lab software used for this numerical analysis. They come up with conclusion of that Shiraz city is the best region to use solar concentrator systems, with an average annual thermal efficiency of 13.91% and annual useful energy of 2213 kWh/m^2.

(Lamrani et al., 2018) investigated thermal performance of a PTSC under transient climatic conditions. One dimensional transient model that based on energy balance equation of collector components developed and solved by implicit finite difference method using Mat lab software. Results obtained show that the length of the receiver tube has a great effect on HTF outlet temperature and using synthetic oil as working fluid is suitable compared to water.

2.5 Solar Cookers

A solar cooker is a device, which utilizes solar energy to cook food by converting it to thermal Energy. Solar cooking is one of the simplest, the most feasible and attractive method of thermal applications of solar energy. It used for both domestic and institutional cooking. The advantage of solar cooking is that it offers ecological and socio economic benefits. (Lameck Nkhonjera, 2017)

2.5.1 Types of Solar Cookers

There are countless styles of solar cookers in the world based on various art of cooking and types of food cooked. Starting back from the time when first solar cooker introduced numerous, types of solar cookers have been designed and developed and are still being improved by scientists and researchers. Therefore, the classification of solar cookers is a not an easy task. The available solar cookers broadly categorized under two groups, solar cookers without storage and solar cookers with storage.

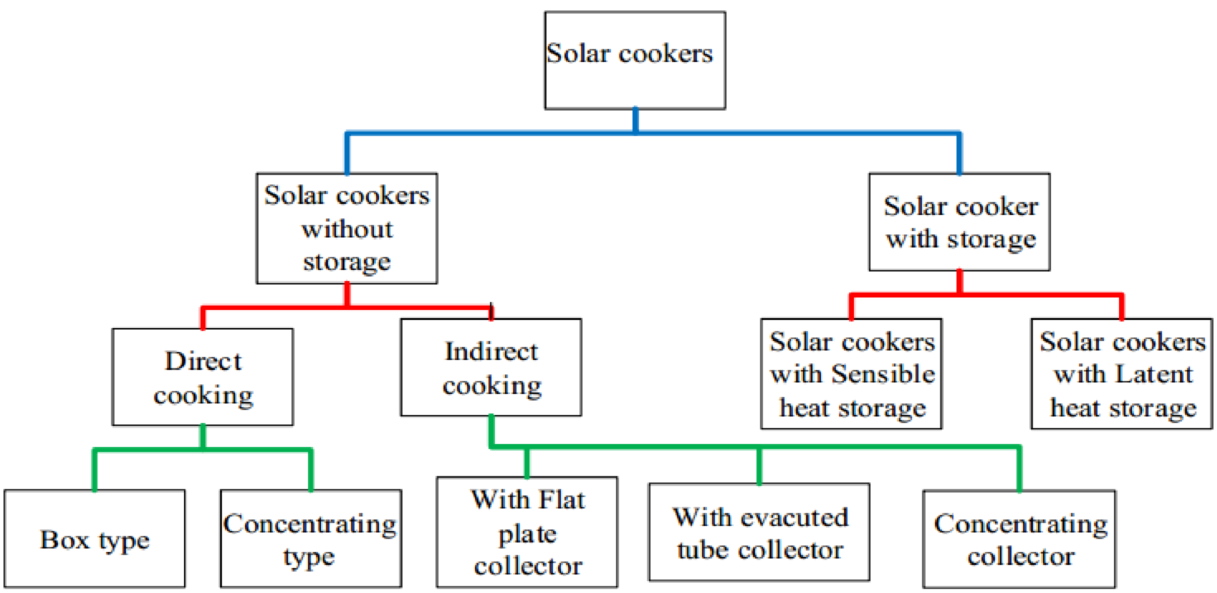

Figure 2-6 Types of solar cookers (Muthusivagami et al., 2010)

1. Solar cookers without storage

Solar cookers without storage don not incorporate any types of thermal Energy. Depending upon the heat transfer mechanism from solar collector to the cooking pot storage, they classified into direct and indirect solar cookers.

i. Direct solar cookers

The cooking process use the solar radiation directly without heat transfer fluid. The most common types of direct solar cookers are box and concentrating type cookers with these type of cookers, a temperature up to 100ºC and 300ºC can achieved respectively (Muthusivagami et al., 2010).

Drawbacks of direct solar cookers are:

- ✓ Takes longer cooking time.
- ✓ Indoor cooking is impossible therefore, users direct exposure to the sun.
- ✓ Direct exposure of the food in the sun.

ii. Indirect Solar cookers

In indirect type solar cookers, the cooking pot and the collector physically separated from each other. Heat transferred to the pot using heat-transferring medium. Solar cooker with flat plate collector, evacuated tube collector and concentrating type collector are commercially available cookers under this category. Advantages of this cooker are possibility of fast cooking, large pot volumes and the possibility of indoor cooking and heat flow control in the pots (Muthusivagami et al., 2010) .

2. Solar cookers with heat storage

Due to the intermittent supply of solar energy from the sun, there is a mismatch between the supply and consumption of energy in solar cooking. The solar cookers must contain a heat storage material to store thermal energy in order to solve the problem of cooking outdoors and impossibility of cooking food due to frequent clouds in the day or during off-sunshine hours. According to the work of (Nkhonjera et al., 2017)based on the mode of heat transport from the solar absorber to the cooking load solar cookers with heat storage are classified into three categories those are 2-satage cookers,3-stage cookers and 4-stage cookers.

i. 2-satage solar cookers

In the first stage heat transported from the solar absorber to the heat storage medium and in the second stage from the storage medium to the cooking load. Solar radiation converted to heat for charging the storage material by solar absorber directly without heat transfer fluid. There are two different Thermal energy storage (TESu) designs in 2-stage cookers:

- TES unit without an integrated cooking vessel (TESncv).
- TES unit with integrated cooking vessel (TESicv).

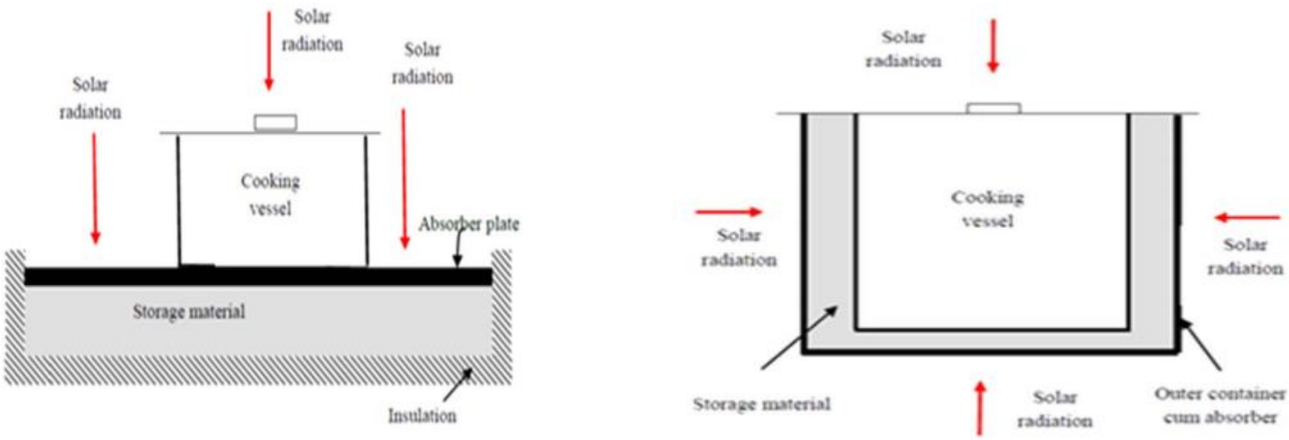

Figure 2-7 Schematics of TESu designs 2-stage solar cooker (Nkhonjera et al., 2017

ii. 3-stage solar cooker

The first stage involved the heat transport from the solar absorber to heat transfer fluid (HTF) then from HTF to the storage medium in the second stage and then from storage medium to cooking load in the final stage

iii. The 4-stage cookers

Transferred heat from the absorber to HTF in first stage then from HTF to storage medium in second stage while the third and fourth stages involved heat flow from storage medium to HTF and then to cooking load.

2.6 Injera Baking Technologies

Injera is soft spongy flat bread with a typical test and texture. It is predominantly eaten as staple food item in Ethiopia and some parts of East Africa. The main ingredient for baking Injera is Teff, also prepared using other cereals such as sorghum, millet and barley. The average thickness, diameter and weight of Injera are 3–5 mm, 58 cm and 330g respectively (Jones et al., 2017).

Preparation of Injera is time consuming cooking. The first step is mixing Teff flour with water then it left for ferment. The fermentation is a long process it usually takes two to four days depending on the weather condition of the locations. It takes less time in warmer locations. Approximately four to six hours before baking, a layer of bitter fermentation product is removed and hot water is added to reactivate fermentation, then the batter is poured on top of the hot baking pan surface (Tsegay, 2011).

Baking Pan

Baking pan (locally named mated) is a round circular disk with a smooth top surface suitable for Injera baking application. The traditional mated is made of clay materials and the required top surface temperature for baking is 180^{o}c to 200 ^{o}c. On average Conventional baking pans are 58 - 60cm in diameter. The energy efficiency of the mated made of clay is very poor, around 52 to 55 %. New ceramic manufactured and it Showed Injera baked at a reduced temperature of 147 to 150^{o}c with less quality. (Tsige, 2015).

The requirements for good material of Injera baking pan material (Tsige, 2015)

- ✓ Higher thermal shock resistance. The baking pan is subjected to high temperature and suddenly drops when dough (lit) pours to it.
- ✓ The ability to withstand moderate mechanical loads applied to clean the surface of the bake pan from baking residuals
- ✓ Should have a non-stick top surface for the quality of the Injera baked; i.e. the baking disc should be effective during baking cycles.
- ✓ Should withstand stress due to temperature gradient across the thickness.
- ✓ Should be free of health problems.

2.6.1 Type of Injera Baking Technologies

I. Three-stone open-fire stove

This the old and traditional method of Injera baking. Most of the people living in Ethiopia bake Injera-using biomass on open-fire stoves. There are three stones with equal size placed in a triangle to support or carry the baking pan with a diameter of 60 cm and thickness of 20 cm on average. Then, firewood inserted into the openings between the stands for burning. While burning is taking place below the pan, Injera baked on it. Disadvantage of three stone open fire stoves are they consumes large amounts of firewood and produces high indoor air pollution and CO2emission (K.D. Adem and D.A. Ambie, 2017)

II. Improved Biomass Injera baking stoves

Development effort for efficient biomass Injera baking start in 1980s by governmental institutions since then some non-government and government organization came up with various Improved stoves such as Ambo mud-stove, Burayou mud-stove, Tigrian stove, Sodo Injera baking stove, Mirt stove, Gonziye and Awramba stove. The common performance evaluation criteria's used to compare different types of stove were thickness and seasoning skill of the mated, fuel consumption and easiness to use (K.D. Adem and D.A. Ambie, 2017).

III. Biogas Injera baking stoves

Biogas is a relatively clean gaseous fuel produced mainly from cattle dung and other biomass waste in an anaerobic digester. Combustion of methane using proper fuel-to-air ratio will create a non-polluting and comfortable kitchen for Injera baking. biogas stove used for Injera baking have a problem of consuming a large amount of gas from the plant, loses a large amount of heat out and pressures are not equally distributed on the holes. To get optimum cooking heat distribution of Injera baking burner optimum design size, number of holes on burner, proper mixing of air and fuel flow rate was analyzed (Bezuayehu et al, 2017).

IV. Electric Injera baking stoves

Frist electric Injera baking stove (electric Injera mated) introduced to Ethiopia before 40 years. However, almost no design improvements have taken place on the first stove and not standardized yet. It is estimated that 530.000 Injera electric baking stoves currently in use in Ethiopia. 3.5-6 kW per cooker power consumed by existing electric mated which consume approximately 60–70% of the Ethiopian hydro-based grid power.

The shortcoming of electric Injera baking stove summarized as follow (Jones et al., 2017)

- ✓ The high resistance, inadequately sized electric wiring, and incorrectly adjusted heating element;
- ✓ Use of poor construction materials;

- ✓ Poor insulation: dissipation of energy during the baking session is said to roughly range from 40 to 50 percent;
- ✓ Lack of temperature control device such as a thermostat encouraging loss of heat
- ✓ Overall, sub-optimal/poor and inefficient design and workmanship.

2.7 Thermal Energy Storage

Since the nature of solar energy is diluted and intermittent, thermal energy storage (TES) required stores energy for a particular time and provides this energy for later usage. The energy storage is used to correct the mismatch between the time of energy supply and energy demand. Solar energy can be stored in different forms as electrical, chemical, mechanical and thermal energy. The heat that is not required by the process during sun hour can be stored to use later when there is no solar irradiation. This stored heat used for water heating, space heating, desalination, cooking, thermal power system etc. Based on the nature of the change that occur on the storage material different techniques are used for thermal energy storage. These energy storage mechanisms are (Stutz et al., 2017):

a. Sensible heat storage
b. Latent heat storage
c. Thermochemical thermal heat-storage systems

Sensible Heat Storage

Thermal energy is stored by raising the temperature of a storage medium by using its heat capacity. The thermal energy stored by sensible heat can be expressed as(A. Kumar & Shukla, 2018):

$$Q = mC_p\Delta T \qquad (2.1)$$

Where: m is the mass (kg),

C_p is the specific heat capacity (kJ/ kg.K) and

ΔT is the raise in temperature during charging process.

The amount of thermal energy stored in the form of sensible heat depends on mass, value of the specific heat of the material used to store the thermal energy and the temperature change. Some of the most common sensible heat storage materials are water, mineral oil, molten salts, liquid metals and alloys, rock, concrete, sand and bricks (Alva et al., 2018).

Latent Heat Storage

Latent heat storage is the heat released or absorbed by a thermodynamic system during a constant-temperature phase change process. Latent heat of a material is the heat that carries a phase change of the material, with no change in the chemical composition. It Involves the heat absorbed or released when a material changes from one physical state to another and the sensible heat.

The total energy stored in latent heat thermal energy storage system can be determined using the following equation (A. Kumar & Shukla, 2018):

$$Q = m[C_{ps}(T_m - T_L) + \Delta H_m + C_{pl}(T_H - T_m) \qquad (2.2)$$

where m is mass of heat storage medium T_m is the melting point , Cps and Cpl are the specific heat of the PCM in solid and liquid state respectively, and ΔHm is the phase change enthalpy.

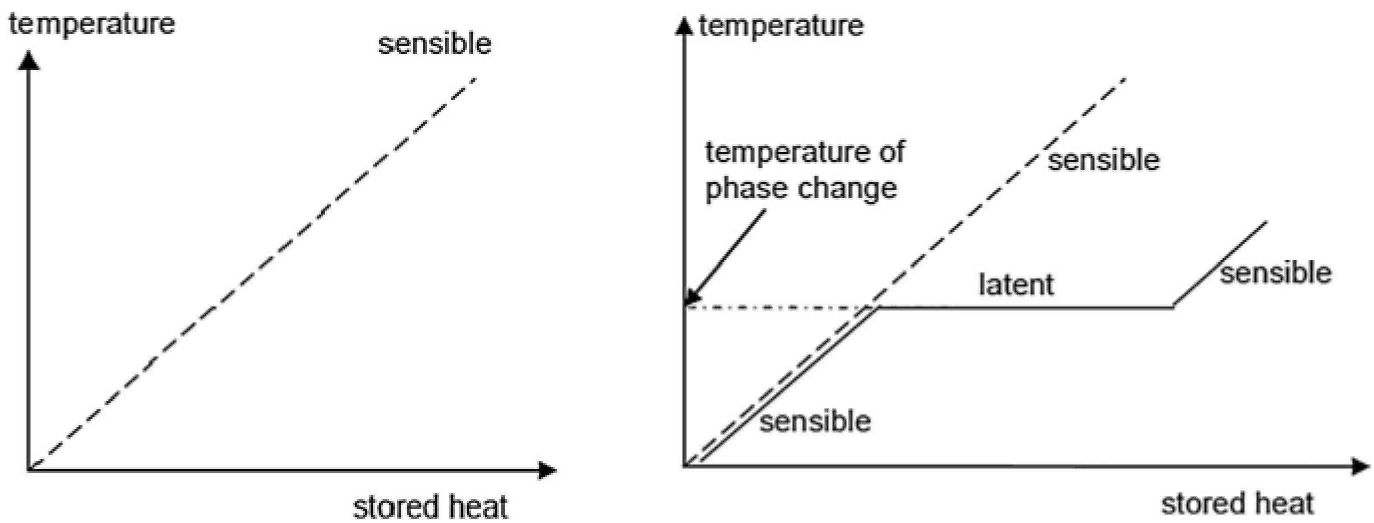

a) b)

Figure 2-8 Stored sensible heat (a) and stored latent heat (b) along with Temperature(Crespo et al., 2018).

Thermochemical thermal heat-storage

Thermo-chemical storage uses reversible chemical reactions of reactants to store and release the required heat energy. The charging process is forward endothermic reaction in wich a chemical reactant dissociates into products. During this course the storage medium absorbs heat and store it until released by undergoing backward exothermic reaction.

2.7.1 Comparison between Sensible, Latent and Thermochemical Thermal Energy Storage

Sensible heat storage systems are simpler in design than latent heat systems. However, they suffer from the disadvantage of being bigger in size. Latent thermal energy storage requires less volume than sensible thermal energy storage . In latent heat storage TES systems, the outlet temperature of the HTF is steady during discharge .While, sensible heat systems cannot store or deliver energy at a constant temperature. As the thermal discharge continues, the outlet temperature of the HTF gradually starts decreasing with the time. Compared to latent heat, specific heat of sensible heat storage materials is 50-100 times smaller and therefore the thermal energy storage density is smaller (Alva et al., 2018).

Energy density stored in thermochemical heat storage is higher compare to both sensible and latent heat storage materials. However thermochemical storage technology is still at laboratory stage, whereas sensible and latent heat technologies are matured and are at industrial stage (Alva et al., 2017). Latent heat storage has many advantages over sensible and thermochemical thermal storage. Latent heat storage can achieve heat storage and release even when there is almost no temperature variation, and its storage capacity per unit volume is 5–14 times higher than sensible heat storage (Wei et al., 2018).

2.7.2 Phase change materials (PCM)

Latent heat storage materials also called as phase change materials (PCM). There is a phase change process during charging and discharging process. Depending on the type of phase change of the material PCM can be classified into three groups :solid-liquid, solid-solid and liquid-vapor.

Comparing with solid-liquid PCM the solid-solid PCM have no leaking problem so no need of encapsulation and they are cheaper and easy to handle. However they are not used for commercial applications due to the lower heat of phase change. In case of liquid-vapor PCM,because of the volume increased in the vapor phase, the tank would have either to support very high pressure or have a very large volume. Therefore, they are not used as latent heat storage materials (Crespo et al., 2018).

2.7.2.1 Classification of Phase Change Materials

Based on the composition the solid-liquid phase change materials are classified into three groups: organic, inorganic and eutectic materials.

a. Organic PCM

Organic PCMs produced primarily from natural fats, oils or petrochemical products, including paraffin and non-paraffin organics.

- ✓ Paraffin organics

Paraffin are mineral oil products, and consist of mixture of mostly straight chain alkanes which have the general formula (C_nH_{2n+2}). The paraffin's are a family of saturated hydrocarbons with similar properties. The crystallization of the (CH_3)-chain can store or release latent heat.

- ✓ Non paraffin organics

These organic materials are subdivided into fatty acids and other non-paraffin organic. Fatty acids are classified and produced by animals and plants and they are among the rare renewable feedstock which has the same properties. Few of their properties such as density, specific heat, latent heat and thermal conductivity of fatty acids as PCM has been discovered and analyzed(Magendran et al., 2019).

b. Inorganic PCM

Inorganic materials can be further subdivided into salt hydrate and metallic

- ✓ Salt hydrate

The most commonly used inorganic compounds are the hydrated salts. Suitable to be used in a wide range of applications, salt hydrates are the most important group of PCMs and have been studied comprehensively in latent heat thermal energy storage systems. Salt hydrates are mostly consisting of salt and water, which mixtures form a crystalline matrix when they solidify. salt hydrates could also be used for solar applications (Crespo et al., 2018).

- ✓ Metallic

Metallic materials; which include low melting metals and metal eutectics are not widely used due to their heavy weights. Thermal energy storages that employ metallic however might have an advantage on their physical sizes as metallic materials have high heat of fusion per unit volume, apart from their higher thermal conductivities compared to other types of PCMs.

c. Eutectic materials

The eutectic is a composition of two or more components, such as organic–organic, organic–inorganic and inorganic–inorganic

Table 2-2 Advantages and Disadvantages of different PCM (Mofijur et al., 2019)

Type of Materials	Advantage	Disadvantage
Organics PCMs	• Available in a large temperature range • No super cooling • Compatible with other materials • No separation • Chemically PCMs are stable • These are safe to use • Non-reactive in nature • Can be recycled	• Low thermal conductivity • large volume changes • Flammable • Expensive except technical grade paran wax
Inorganic PCMs	• High volumetric latent heat • Less expensive • Easily available • Thermal conductivity is higher • The thermal fusion of these PCMs are very high • Lower volumetric variation • These PCMs are non- flammable	• Changed volume is remarkably high • Super cooling • Corrosiveness
Eutectics	• The melting point of these PCMs are sharp • High volumetric storage density	Less thermophysical properties data is available

2.7.3 Selection principles and required thermo-physical properties of PCM

The performance of the selected materials in various aspects will directly affect the heat storage ability and thermal storage efficiency. Therefore phase change material must meet certain criteria and possess certain material characteristics.

The following six major requirement types given in detail on the basis of thermodynamics, kinetics, chemistry and economics of the PCM (Wei et al., 2018).

1. Thermal performance requirements.

The melting temperature of material must much with application temperature to get the maximum efficiency. For the same phase change temperature, high latent and specific heat makes the thermal storage density as great as possible. Relatively large thermal conductivity required to have improved system efficiency of the storage design. To avoid phase separation phenomena caused by density differences between the solid and liquid states the PCM should have consistent chemical composition in both phases.

2. Physical performance requirements.

- ✓ Good phase equilibrium
- ✓ Low vapor pressure
- ✓ High density
- ✓ Small volume change in the phase change process

3. Dynamic performance requirements

As low as possible during solidification, and no super-saturation during melting. Fast crystallization required to raise the dynamic response ability of the whole thermal storage system.

4. Chemical performance requirements

- ✓ Good chemical stability
- ✓ Minimal corrosiveness and anti-oxidation
- ✓ Material should be non-toxic, non-flammable, non-explosive and safe to use.

5. Economic performance requirements

The PCM that are low cost and possess good industrial utility.

6. Technical performance requirements: The selected material should be technically efficient, compact, reliable and applicable.

2.8 Review on Related Works

(Goytom, 2016) studied transient heat transfer analysis of solar powered Injera baking system using Matlab Software. Simulate the heat balance model of baking pan by discretizing it with explicit finite difference method. The heating up of the baking pan evaluated by varying its thickness and the temperature of the hot oil. The result showed that 5 mm thick pan with heated oil temperature of 255^{o}C gives better heat up and baking time.

(Hassen et al., 2011),designed and manufactured a laboratory prototype for an oil based Injera baking glass stove system and analyze its performance experimentally. Tempered Glass pan used as baking pan for this prototype. The heat transferring fluid Shell Thermia oil B heated by 2 kW electrical heater that used to provide equivalent with parabolic trough solar collector. The temperature variations in the heating and storage tank, baking pan inlet, baking pan outlet and on the surface of the baking pan investigated using K-type thermocouples and the baking test performed after the baking pan reached 191 ^{o}C.

(Tesfay et al, 2013) investigated the charging behavior of solar salt and its potential for Injera baking. In this study electric based and solar based laboratory models that works principle of natural circulation boiling- condensation developed, in both cases a HTF was steam. Small-scale parabolic dish with fixed receiver used in the solar-based laboratory model. The thermal storage designed with 10 salt cavities of same size, 0.032 m diameter and 0.15 m height and loaded with two kilos of solar salt was experimented and simulated in COMSOL. This work come up with that PCM completely melted after it charged by an average power of 650W for 4.5 hours and a useful heat can be stored for more than one day. Despite other literatures, they found out that 135-160oc is enough to bake Injera.

(Hailu et al., 2017), designed direct solar fryer Injera baking system that use parabolic dish collector and aluminum made baking plate. The size of baking pan was 550 mm in diameter and 12.5 mm in thickness. The designed system have two operational modes these were continuous heating and baking and alternating heating and baking modes. A prototype developed for both types of operational modes then it performance investigated experimentally. The result show that heating up time for the direct solar fryer model with continuous heating and baking mode is 30 minutes to reach baking temperature of 120-130 o c and its average baking time is 7 minutes per Injera. Solar fryer thermal efficiency including the solar collector efficiency, found to be 37 %.

(Hassen et al., 2011) designed and manufactured a laboratory model for solar powered Injera baking oven system. This system proposed to use parabolic trough solar collector as the source of energy. However, for the laboratory model, electrical heater used instead to heat the heat transfer fluid. Frist he designed different of components of the laboratory model such as Baking Pan Assembly, Heat Transfer Fluid Gallery, Oil Heating and Storage System, Electrical Heater and Piping System. Then after he manufactured each part to conduct an experiment. In the laboratory model developed, the baking pan (mated) and the heat storage system placed separately. The Thermal oil (Thermia oil B) used to transfer heat from the heat storage unit to baking pan assembly by convection and conduction heat transfers mechanisms. The fluid circulation is forced circulation he used a pump to transfer fluid from heat storage tank to baking pan assembly (oil gallery). He used flat and circular baking pan witch dimension of 8mm thickness and 580mm diameter. He found out that it is possible to bake Injera using heat transfer Fluid heated by solar or other energy source by forced circulation loop.

(Tesfay et al., 2014) Experimental set up that consist a parabolic dish solar collector coupled with latent heat storage constructed. A solar salt (40% KNO3 and 60% NaNO3) selected as heat storage material and the storage charged with self-circulating steam loop. A cooking pan is integrated with an aluminum block with three-steam channels and ten salt cavities. They conduct the Experiment and the result compared with simulation results of COMSOL Multiphysics. The aluminum block efficiently separates the salt from the high-pressure steam, but the numbers of steam channels are few and this limit the heat transfer process.

(Tesfay et al., 2015), the system storage has a capacity of about 250ºC and retains the heat for about two days. The storage is coupled polar mounted concentrator with fixed receiver and steam heat transfer fluid. The steam circulates naturally between the evaporator and condenser in a closed loop. The study has demonstrated indirect charging, simultaneous charging-discharging and discharging of the stored heat. The frying pan is a custom-made aluminum plate casted by embedding a 10mm coiled stainless steel steam pipe as heating element. The pan is 500mm in diameter and 30mm thick, and the fins are 20mm in diameter and 140mm long. The fins immersed into a 20kg PCM, which coupled to a 1.8m diameter parabolic dish collector. The solar fryer demonstrates Injera baking for average family size on top of a heat storage charged by a solar energy. This baked Injera able to cover three to four days food consumption of the family.

2.9 Conclusion from the literature review

Moreover, a review of the literature infers that considerable efforts invested in research and development of solar cookers with and without storage. Limited research works reported on solar Injera baking machine integrated with Thermal energy storage, particularly, parabolic trough type solar cookers with a PCM storage system for Injera baking. Regarding parabolic trough solar collector there is no detailed study available on the year-round performance using PTSC under the Adama weather conditions where the plentiful solar energy is available.

CHAPTER 3

SOLAR ENERGY POTENTIAL ANALYSIS

3.1 Solar Radiation Model

Solar radiation model used to calculate input data that will be utilized for performance analysis of PTC. For determine and assessing the amount of solar energy for any application the primary task is estimating the solar radiation available in selected area. The main goal of this analysis is to determine and compare solar energy absorbed by parabolic trough solar collector for different sun tracking modes The solar energy potential of the selected area depends on the local weather conditions at the site. The better understanding of Sun–Earth angles is essential for estimating solar intensity throughout year for any surface at any place with a desired inclination and orientation. Therefore some important terms are defined and explained below:

Latitude (ϕ): is the angle made between the radial line joining the observer (location) with the center of the Earth, and its projection on the equatorial plane ($-90^o \le \phi \le 90^o$). Latitude of Adama is 8.51447^o North.

Declination (δ): The angular position of the sun at solar noon (i.e., when the sun is on the local Meridian) with respect to the plane of the equator, north declination designated as positive. ($-23.45^o \le \delta \le 23.45^o$). The declination, δ, in degrees for any day of the year calculated as(Duffie & Beckman, 2013):

$$\delta = 23.45 \sin\left[\frac{360}{362}(284+n)\right] \tag{3.1}$$

Where: n is day of the year.

Hour angle (ω): The angular displacement of the sun east or west of the local meridian due to rotation of the earth on its axis at 15^0per hour; morning designated as negative, afternoon positive (Kalogirou, 2014).

$$\omega = (ST - 12) * 15^o \tag{3.2}$$

Where: ST is the local solar time. The values of the hour angle in the northern hemisphere are listed in Table 3.1

Table 3-1 The value of hour angle with time of the day for the northern hemisphere (Tiwari et al., 2016).

Time of the day (h)	6	7	8	9	10	11	12
Hour angle (°)	-90	-75	-60	-45	-30	-15	0
Time of the day (h)	12	13	14	15	16	17	18
Hour angle (°)	0	15	30	45	60	75	90

Slope (β): The angle between the plane of the surface in question and the horizontal; (0◦≤β≤180◦.(β>90◦) means that the surface has a downward - facing component.)

Surface azimuth angle (γ): The deviation of the projection on a horizontal plane of the normal to the surface from the local meridian, with zero due south, east negative, and west positive; ($-180^0 \leq \gamma \leq 180^0$)

Angle of incidence (θ): the angle between the beam radiation on a surface and the normal to that surface. For a horizontal plane the incidence angle and the zenith angle are the same.

The general expression for the angle of incidence given as (Duffie & Beckman, 2013).

$$\begin{aligned}\mathrm{Cos}\,\theta = {} & (\cos\phi\cos\beta + \sin\phi\sin\beta\cos\gamma)\cos\delta\cos\omega + \sin\delta(\sin\phi\cos\beta - \cos\phi\sin\beta\cos\gamma) \\ & + \cos\delta\sin\beta\sin\gamma\sin\omega\end{aligned} \tag{3.3}$$

Zenith angle (θ_Z): The angle between Sun's rays; the line perpendicular to a horizontal plane is known as the "zenith angle. It is the angle of incidence of beam radiation on a horizontal surface.

Solar Altitude Angle (α_s):The angle between the horizontal and the line to the sun, that is, the complement of the zenith angle($\theta_Z + \alpha_s = 90^o$).

The mathematical expression for the solar altitude angle is (Kalogirou, 2014):

$$\sin\alpha_s = \sin\phi\sin\delta + \cos\phi\cos\delta\cos\omega \tag{3.4}$$

Solar azimuth angle (γ_s): The angular displacement from south of the projection of beam radiation on the horizontal plane. Displacements east of south are negative and west of south are positive.

Sunshine hour (S_o): The total duration in hours of the Sun's movement from sunrise to sunset. It is defined in terms of the hour angle as (Kalogirou, 2014):

$$S_o = \frac{2 * \omega_s}{15} \tag{3.5}$$

Where ω_s sunset hour angle, obtained from Equation 3.8 when $\alpha_s = 90^o$ and it is given by

$$\omega_s = \cos^{-1}(-\tan(\phi)\tan(\delta)) \tag{3.6}$$

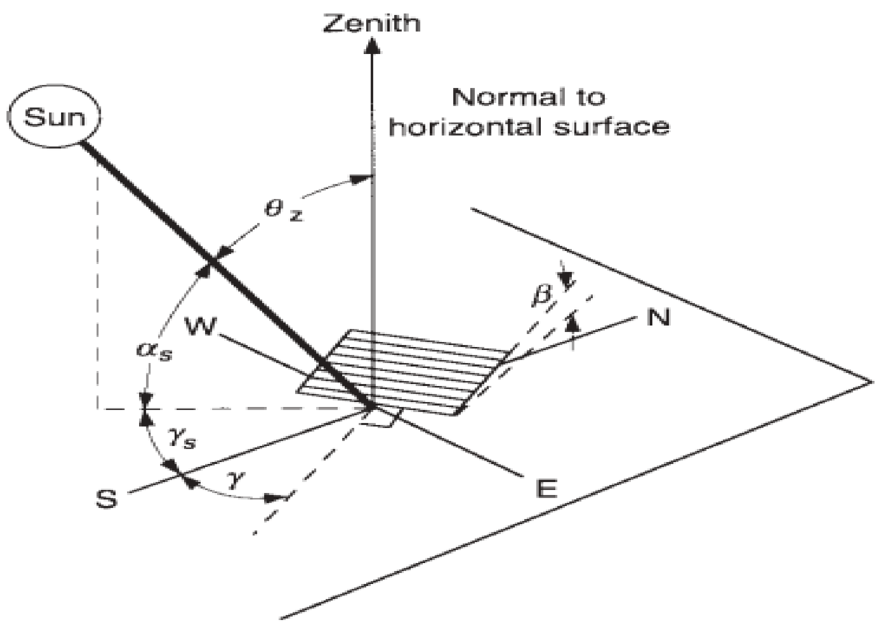

Figure 3-1 Zenith angle, slope, surface azimuth angle, and solar azimuth angle for a tilted surface (Duffie & Beckman, 2013)

Since adequate solar radiation, information is seldom available in developing countries such as Ethiopia so Several empirical methods and models have been proposed to estimate daily radiation from commonly observed meteorological parameters such as sunshine hours, temperature, and cloud cover.

3.2 Extraterrestrial Solar Radiation

The extraterrestrial radiation measured on the plane normal to the radiation on the n th day of the year for a whole year can be calculated by. (Kalogirou, 2014).

$$G_{on} = G_{sc}(1+0.033\cos\frac{360n}{365}) \tag{3.7}$$

Where G_{on} =extraterrestrial radiation measured on the plane normal to the radiation on the n th day of the year (W/m^2).

G_{SC} =the solar constant, 1367 W/m^2 and n is the day of the year

Solar constant: The amount of solar energy per unit time, at the mean distance of the earth from the sun, received on a unit area of a surface normal to the sun (perpendicular to the direction of propagation of the radiation) outside the atmosphere .

The extraterrestrial solar radiation incident on a horizontal surface placed parallel to the ground outside of the atmosphere given by (Kalogirou, 2014):

$$G_{oH} = G_{on}\cos\theta_z \tag{3.8}$$

$$G_{oH} = G_{on} = G_{sc}(1+0.033\cos\frac{360n}{365})\sin\phi\sin\delta+\cos\phi\cos\delta\cos\omega \tag{3.9}$$

3.2.1 Monthly Average Daily Extraterrestrial Radiation on horizontal surface

The daily total extraterrestrial radiation on a horizontal surface over the period from sunrise to sunset during a day given by (Duffie & Beckman, 2013):

$$H_o = \frac{24*3600*G_{SC}}{\pi}\left[1+0.033\cos\left(\frac{360n}{365}\right)\right]\left(\frac{2\pi\omega_s}{360}\sin\phi\sin\delta+\cos\phi\cos\delta\cos\omega\right) \tag{3.10}$$

Where: ω_s is the sunset hour angle, in degrees and H_o is daily total extraterrestrial radiation on horizontal surface (J/m^2).

The monthly average daily extraterrestrial radiation on horizontal surface ($\bar{H}_o$) calculated from above equation using n and δ obtained for mean day of the month. The Average Days for Months and Values of n by Months suggested by Klein given in Table 3.2 below.

Recommended average days of months for the average radiation of the month given in Table 3.2 below (Duffie & Beckman, 2013).

Table 3-2 Declination and number of day for representative day of the month

Month	Representative day of the month	n for the mean day of the month	Declination
January	17	17	-20.917
February	16	47	-12.9546
March	16	75	-2.41773
April	15	105	9.414893
May	15	135	18.79192
June	15	166	23.31441
July	17	198	21.18369
August	16	228	13.45496
September	15	258	2.216887
October	15	288	-9.5994
November	14	318	-18.912
December	10	344	-23.0496

3.3 Terrestrial radiation

To study the long term performance of the given solar system Daily and hourly solar radiation should be known and studied from the metrological data.

3.3.1 Monthly Average daily Global radiation on horizontal surface

If sunshine duration data are available, the classical form of Angstrom–Prescott model used successfully to estimate monthly average daily Global radiation on horizontal surface from the Extraterrestrial Radiation. The original Angstrom type regression equation modified by Page and others given by (Duffie & Beckman, 2013)

$$\frac{\bar{H}}{\bar{H}_o} = a + b\frac{S}{S_o} \tag{3.11}$$

Where $\bar{H}$ is the monthly average daily global radiation, $\bar{H}_o$ is the monthly average daily extraterrestrial radiation, S is the monthly average daily hours of bright sunshine(h), S_o is the monthly average day length (h), and a and b are empirical coefficients.

The regression coefficients a and b can be determined as follows (Tiwari et al., 2016)

$$a = -0.110 + 0.235\cos\phi + 0.323(S/S_o) \tag{3.12}$$

$$b = 1.449 - 0.553\cos\phi - 0.694(S/S_o) \tag{3.13}$$

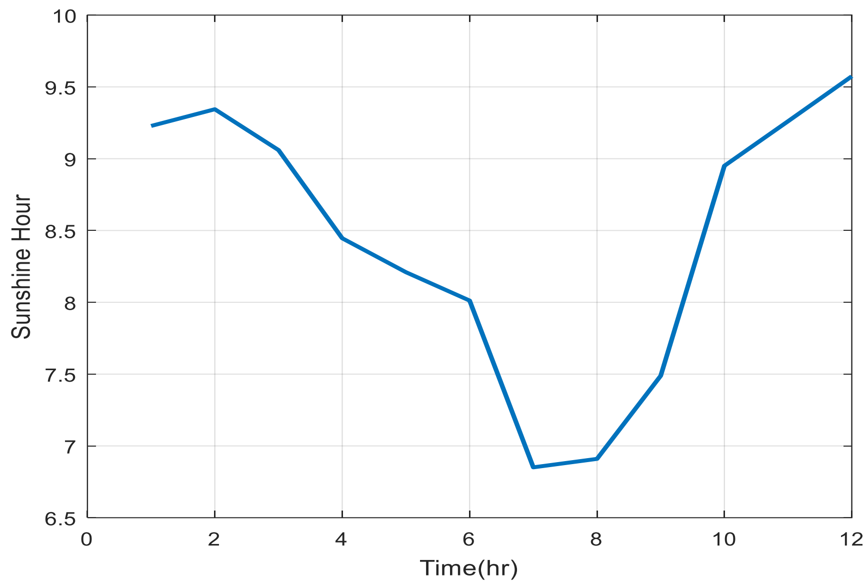

Figure 3-2 Monthly Average Daily Sunshine Duration for Adama City

3.3.2 Monthly average daily diffuse and beam radiation on horizontal surface

Extraterrestrial solar radiation that passes through the atmosphere of the earth is reduced due to reflection, absorption , and scattering. The part of the energy that is directly received at the surface of the earth without being essentially scattered is called direct of beam radiation.

$$\frac{\bar{H}_d}{\bar{H}} = 0.931 - 0.814\frac{S}{S_o} \tag{3.14}$$

Monthly Average daily beam radiation on horizontal surface calculated as follow:

$$\bar{H}_b = \bar{H} - \bar{H}_d \tag{3.15}$$

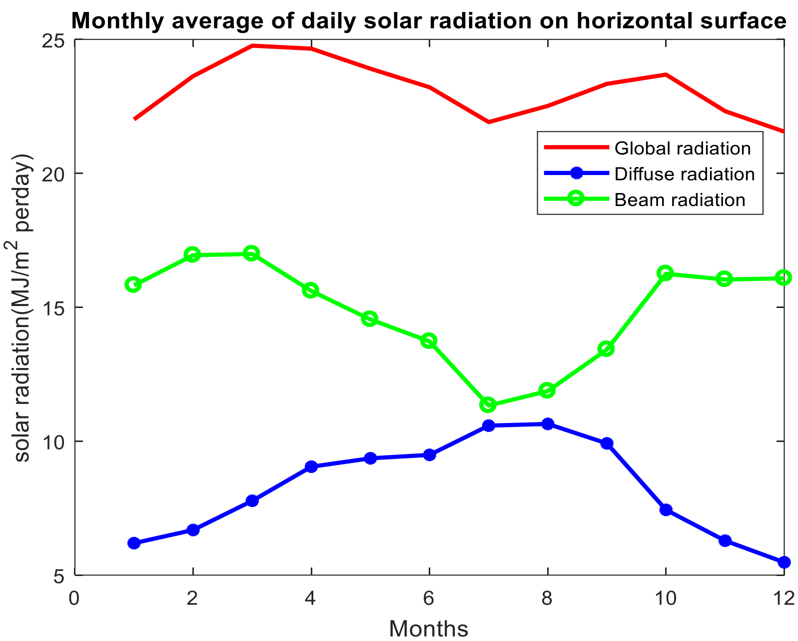

Figure 3-3 Monthly average daily global, beam and diffused radiation on a horizontal surface

3.3.3 Estimation of Hourly solar irradiance on horizontal surface

To predict the performance of a solar system, hourly values of radiation are required. It is possible to estimate hourly values from calculated daily solar radiation data.

3.3.3.1 Monthly average hourly global solar irradiance on horizontal surface

Monthly average hourly total solar irradiance on horizontal surface can be estimated from monthly average daily global radiation on horizontal surface ($\bar{H}$), hour angle (ω) and sunset hour angle (ω_s) .

Monthly average hourly global solar irradiance on horizontal surface in W/m^2 given as (Tiwari et al., 2016):

$$\bar{I} = \frac{r_t \bar{H}}{3600} \tag{3.16}$$

Where $\bar{H}$ is monthly average daily global radiation on horizontal surface in J/m^2 and r_t is the ratio of hourly total to daily total radiation as a function of day length and the hour in question from Collares-Pereira and Rabl correlations (Tiwari et al., 2016).

$$r_t = \frac{\pi}{24}\left(a_1 + b_1 \cos\omega\right)\frac{\cos\omega - \cos\omega_s}{\sin\omega_s - \frac{2\pi\omega_s}{360}\cos\omega_s} \tag{3.17}$$

The coefficients a_1 and b_1 are given by

$$a_1 = 0.409 + 0.5016\sin(\omega_s - 60) \tag{3.18}$$

$$b_1 = 0.6609 - 0.4767\sin(\omega_s - 60) \tag{3.19}$$

3.3.3.2 Estimation of Monthly average hourly diffuse and beam solar irradiance on horizontal surface

From Liu and Jordan correlations, the ratio of hourly diffuse to daily diffuse radiation, as a function of time and day length given by (Kalogirou, 2014):

$$r_d = \left(\frac{\pi}{24}\right)\frac{\cos\omega - \cos\omega_s}{\sin\omega_s - \frac{2\pi\omega_s}{360}\cos\omega_s} \tag{3.20}$$

Where ratio of hourly diffuse radiation to daily diffuse radiation is given by

$$r_d = \frac{I_D}{H_D} \tag{3.21}$$

Monthly average hourly beam solar irradiance on horizontal surface

$$\bar{I}_B = \bar{I} - \bar{I}_D \tag{3.22}$$

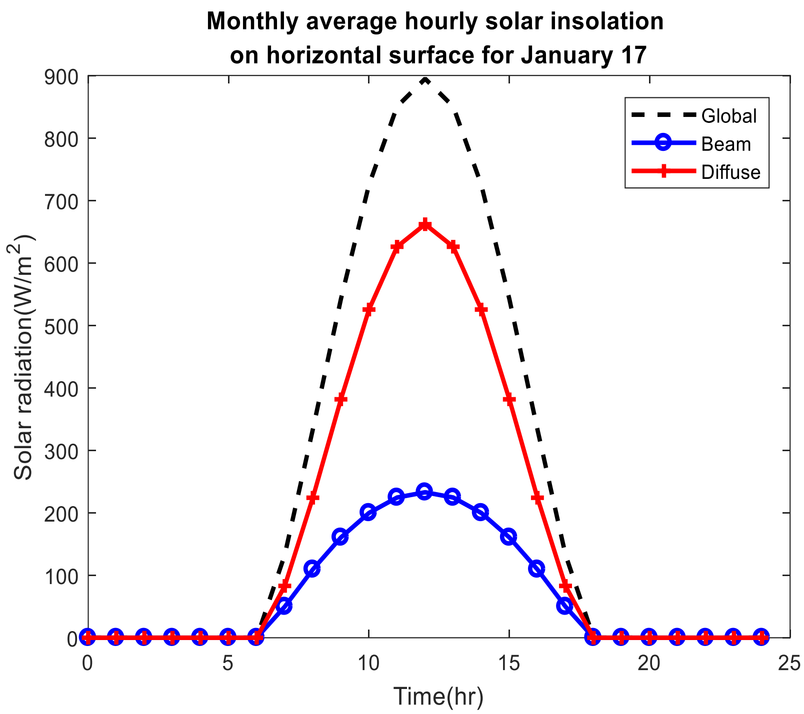

Figure 3-4 Monthly mean hourly Global, Diffuse and Beam radiation on horizontal surface for January 17

3.3.4 Monthly Average of hourly beam incident solar radiation on inclined surface

The long-term performance and system behavior can be monitored by estimating hourly direct normal beam insolation from available meteorological inputs on particular day (nearer to middle of the month) in each month as suggested by Klein. Since PTCs are imaging collectors with a specific image of the sun in the receiver only the beam radiation can be exploited from it (Christos Tzivanidis & Bellos, 2016). Beam radiation on a tilted surface, expressed as (Kalogirou, 2014)

$$\overline{I_{Bt}} = \overline{I_B}\,\frac{\cos\theta}{\cos\theta_Z} \tag{3.23}$$

Where: θ and θ_Z are the incidence angle and zenith angle. $\overline{I_B}$ represents the hourly beam radiation on a horizontal surface

Angle of incidence

The incidence angle is the angle between the sun's rays and the normal on the collector surface. Since they are using only direct beam sunlight, PTSCs need tracking mechanisms to preserve them focused toward the sun. Four tracking strategies analyzed in the current investigation: full tracking, polar, E-W and N-S tracking. The cosine of incidence angle estimated depending the tracking mode. (Kalogirou, 2014)

a) Full tracking

Obviously, the full-tracking mode ensures that the incidence angle is practically equal to zero, depending on the accuracy of the used mechanism. Hence:

$$\cos\theta = 1 \tag{3.24}$$

b) Polar N–S axis with E–W tracking

For a surface rotated about a north–south axis that is parallel to the earth's axis, with regular adjustment, the angle of incidence given by

$$\cos\theta = \cos\delta \tag{3.25}$$

c) Horizontal E–W axis with N–S tracking

For a surface rotated about a horizontal east–west direction with regular adjustment, the angle of incidence takes the form:

$$\cos\theta = \sqrt{1-\cos^2(\delta)\sin^2(\omega)} \tag{3.26}$$

d) Horizontal N–S axis with E–W tracking

For a surface rotated about a horizontal north –south direction with regular adjustment, the angle of incidence written as

$$\cos\theta = \sqrt{\left(\cos\delta\sin\phi\cos\omega - \cos\delta\cos\omega\right)^2} \tag{3.27}$$

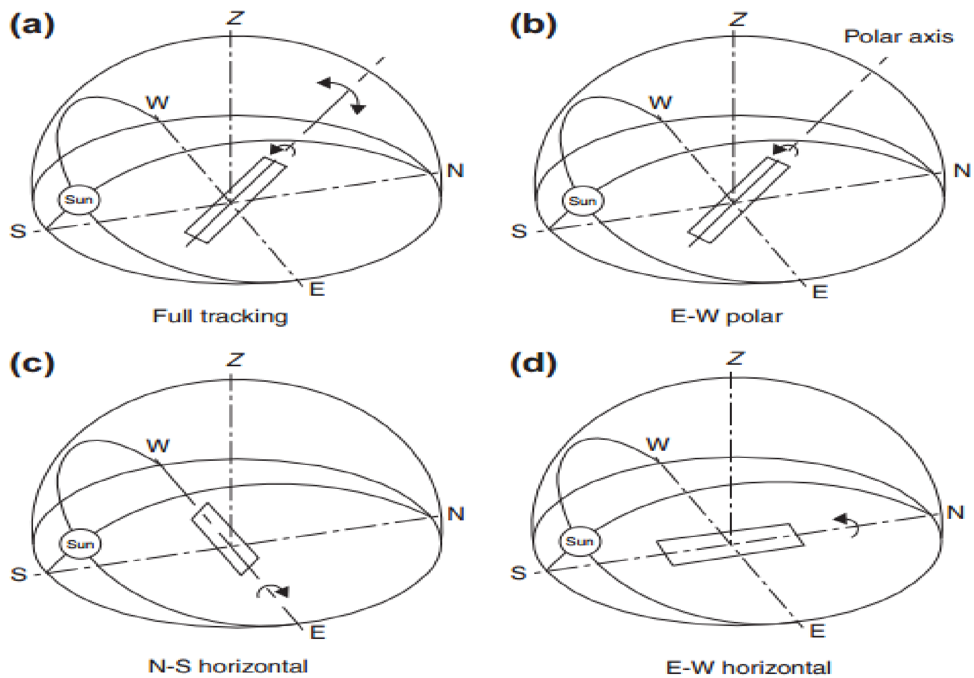

Figure 3-5 Collector geometry for various modes of tracking (Kalogirou, 2014).

3.3.5 Estimation of Hourly Variation of Atmospheric Temperature

In the design and simulation of parabolic trough solar collector atmospheric temperature is one of necessary input. The hourly variation of outdoor temperature estimated by mathematical model that use minimum and the maximum temperatures of the day. The daily ambient temperature can be calculated by using (Bellos et al., 2017):

$$T_{am} = T_{am,\min} + \frac{DR}{2}\cos(2\pi * \frac{(t_h - t_{h,\max})}{24}) \tag{3.28}$$

Where $T_{am,\min}$ is mean daily temperature of the day

DR is daily range temperature of the day

t_h is time of the day

$t_{h,\max}$ is times for the occurrence of daily maximum temperatures

It assumed that the ambient temperature is usually maximized at 14:00 and thus the parameter $t_{h,\max}$ is selected to be equal to 14 h (Bellos et al., 2017).

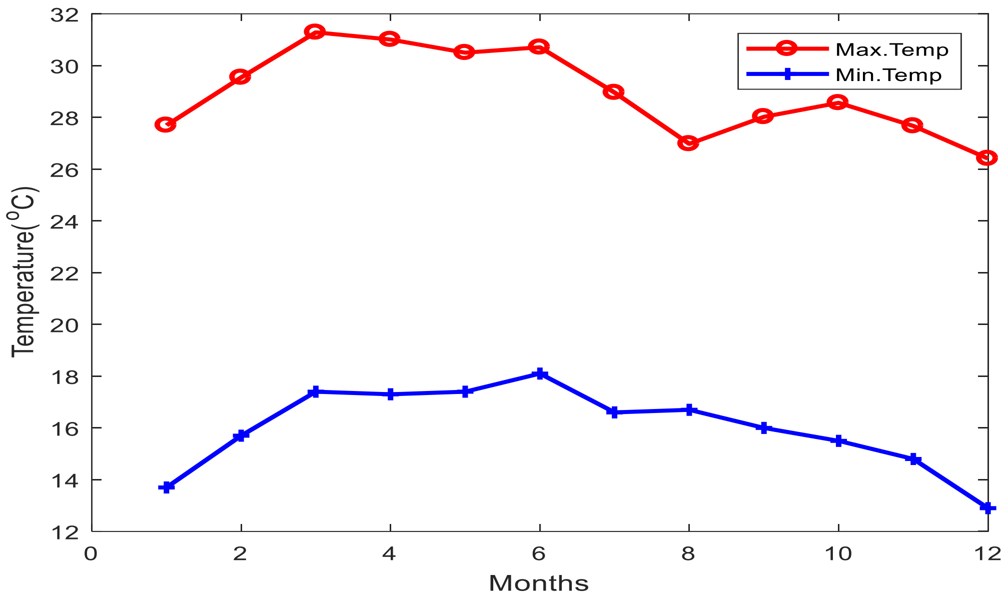

Figure 3-6 Monthly average maximum and minimum variation of Temperature

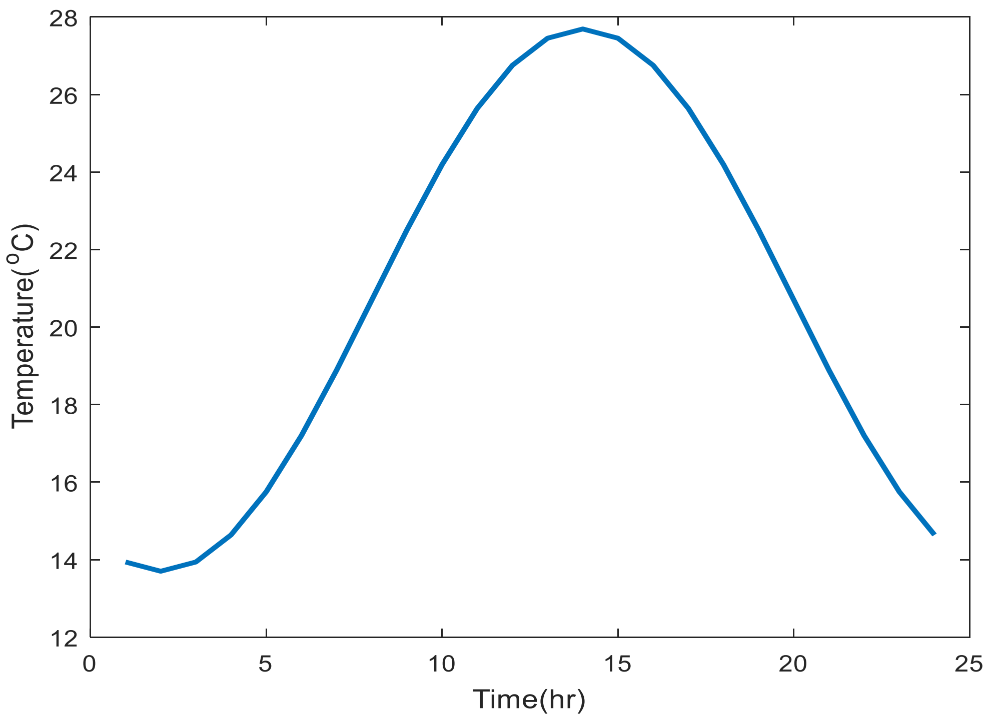

Figure 3-7 Hourly Ambient Temperature pattern on January 17

CHAPTER 4

COOKING DEMAND AND PERFORMANCE ANALYSIS OF THE SYSTEM

4.1 Injera Baking Process

Injera is soft spongy flat bread with a typical test and texture. It is predominantly eaten as staple food item in Ethiopia and some parts of East Africa. The main ingredient for baking Injera is Teff, also prepared using other cereals such as sorghum, millet and barley.

Preparation of Injera is time-consuming process. There is little difference in production process with type of cereals used as ingredient. The production process for Teff is considered since it is the most common ingredient. Detailed process shown below in the Figure 4.1. The fermentation takes two to four days depending on the weather condition of the locations.

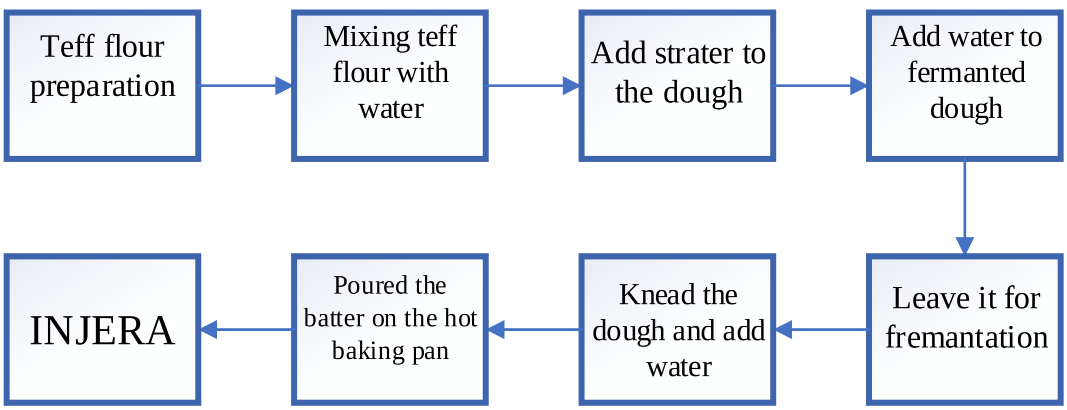

Figure 4-1 Injera preparation processes

4.1.1 Heat Demand of Injera Baking

Thermal design and sizing of solar baking device is based on the Injera baking energy requirement. The total energy required for baking process is the energy utilized for baking plus energy used for heating up the pan.

Baking Energy

The Energy utilized for baking given can be defined as the energy necessary to raise the batter to a particular temperature, and evaporate the amount of water that is observed to be lost during the baking process. It is assumed that the energy utilized in cooking the Injera is the energy required in raising the batter from room temperature to the boiling point of water which is called sensible heat, plus the energy required to evaporate the water which is called latent heat.

From the experimental and numerical investigation done previously on the baking pan and Injera, the thermo-physical properties of Injera and baking pan are listed under Table 4.1 and considered for this study.

Table 4-1 Thermo-physical properties of Injera and baking pan(Ambaw, 2015)

Properties	Value
Specific heat capacity of Teff flour	1.625
Teff mass fraction in the dough	0.2732
Initial mass of batter	0.4315 kg
Mass of Injera	0.3455kg
Moisture content of the dough(water mass fraction)	0.7268
Density of ceramic pan	2400 kg/m^3
Diameter of ceramic pan	0.58m
Thickness of ceramic pan	0.008m
Thermal conductivity of ceramic pan	0.8 W/m.K
Mass of ceramic pan	12.5kg
Specific heat of ceramic pan	960 J/kg.K

The actual utilized heat energy calculated based on the following assumptions (Getenet, 2011)

- The average mass of Injera and moisture loss for every single Injera is constant.
- The heat capacity of the batter is nearly equal to the heat capacity of water.
- The difference in weight between the baked Injera and the initial batter is equal to the weight of moisture loss during baking.

Mathematically, this baking energy given by (Hailu et al., 2017):

$$Q_{baking} = m_{batter} * c_p * (T_{bt} - T_r) + h_{fg} * m_w \tag{4.1}$$

Where $m_w =$ mass of the evaporated water

T_{bt} = Boiling temperature of water in Adama (T_{bt} =94.352ºC).

T_r = the room temperature in the kitchen (20ºC).

h_{fg} = the latent heat of vaporization of water (2260 kJ/kg).

c_p =specific heat capacity of water (4.187 kJ/kg.K).

Mass of the evaporated water

Based on above assumptions the mass of evaporated water given by

$$m_w = m_{batter} - m_{injera} \tag{4.2}$$

By assuming safety factor of 1.2 for losses (Tsegay, 2011)and Using equation 4.1 the baking energy required for one Injera is 394.43KJ.

The total baking energy for a session of Injera baking for an average family size for three days calculated as:

$$Q_{baking} = 394.43 * n_b \tag{4.3}$$

Where: n_b = number of Injera, Number of Injera for average family size (5 persons) for three days is 45. The total energy utilized for average family size is 17749.35KJ

The time taken for cooking of one Injera is assumed to be about 2 to 3 minutes taking 3 minutes;

the power required for one Injera baking can be calculated as:

$$p_{baking} = \frac{Q_{baking}}{\Delta t} \tag{4.4}$$

The power required for one baking session calculated by multiplying the Eq.4.4 by number of Injera baked. The power required for baking one Injera is 2.2KW and the total baking power for one baking session will be 99KW.

Heating up Energy

The heat-up Energy is the amount of energy required to increase the surface temperature of the pan from its initial temperature(20-25ºC) to the temperature required for the baking of Injera (180-220ºC).

Mathematically, this Heating energy given by (Hailu et al., 2017):

$$Q_{heatup} = m_{pan} c_{p,pan} (T_h - T_i) \tag{4.5}$$

Where m_{pan} = mass of pan.

$c_{p,pan}$ =Specific heat of pan.

T_h = required baking temperature and

T_i = initial temperature of the pan

Using equation 4.5 energy required for heat up is 2400KJ.

The heating up power can be calculated as:

$$P_{heating} = \frac{Q_{heating}}{t_{heating}} \tag{4.6}$$

Where $t_{heating}$ is heat up time for the baking pan surface to reach required temperature. The heating up power is 5.5KW.

The total thermal energy required for baking process is the sum of heat energy utilized for baking and heat up the baking plate

$$Q_{total} = Q_{baking} + Q_{heatup} \tag{4.7}$$

$$Q_{total} = 2400 + 17445.15 \text{ KJ}$$

$$= 20149.35 \text{ KJ}$$

Considering others losses and assuming a safety factor of 1.5. The total energy required will be:

$$Q_{total,required} = Q_{total} * 1.5 \tag{4.8}$$

From equation 4.8 the total energy required to bake Injera for one term baking of average family size that used for three days is 30224.025KJ. And the total power is 104KW.

4.2 Performance model and transient analysis of parabolic trough solar collector

4.2.1 Introduction

The performance of PTSC analyzed using collector performance model that comprises three different models. These are solar, optical and thermal model. Solar radiation model is used for estimating the solar radiation that reaches the collector. The goal of optical model analysis is to determine the optical efficiency of the PTSC. A thermal model uses an energy balance between the fluid flowing through the receiver, usually a heat transfer fluid (HTF), and the atmosphere. Its goal is to determine the energy that is absorbed by the heat transfer fluid (HTF) and describe all the heat losses from the receiver to the atmosphere due to heat transfer mechanisms. In order to determine the useful energy obtained from a parabolic trough collector at a particular location, it is necessary to model the trough performance through a computer simulation on an hourly basis to understand what the annual performance will be.

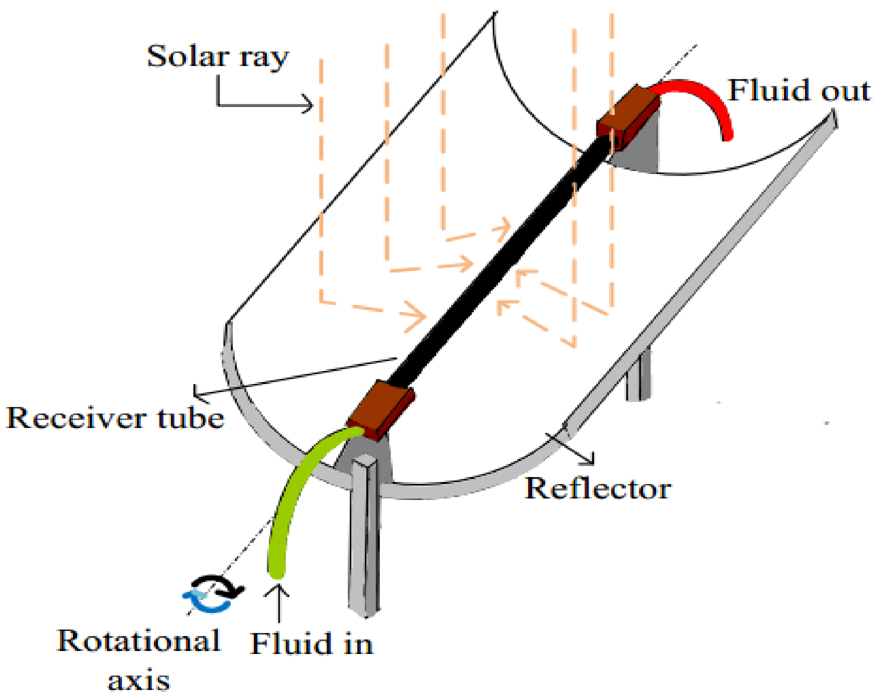

Figure 4-2 Schematic of parabolic trough concentrating solar system(Khairul, 2016)

The dimensions of PTC are taken from a real collector (PT1-IST Company).

Table 4-2 The specification of parabolic trough collector(Christos Tzivanidis & Bellos, 2016)

Engineering parameters		Optical properties	
Parameters	Value	Parameters	Value
Length of the collector	6.1m	Concentration ratio	14.4
Width of the collector	2.3m	Cover emittance	0.88
Receiver inner diameter	47mm	Absorber emittance	0.10
Receiver outer diameter	51mm	Trough reflectance	0.90
Focal distance	0.8m	Receiver absorbance	0.95
cover outer diameter	74mm	Cover transmittance	0.85
cover inner diameter	70mm		

4.2.2 Collector geometry

Geometrical description of a parabolic trough commonly used to characterize the form and size of a parabolic trough. The geometry of the collector obtained using geometrical relations defining the parabolic shape that makes up the collectors system. (Goswami, 2015)

The profile of the collector is defined using x and y coordinate

$$x^2 = 4yf \tag{4.9}$$

Where: f represents the focal length

Focal length (f): Determines the location of the heat collection element. It is distance between the parabolic center and the absorber tube. The focal length is given by. (Goswami, 2015) :

$$f = \frac{w_a}{4\tan(\varphi_r / 2)} \tag{4.10}$$

Where w_a is the collector's aperture width and φ_r is the rim angle.

Rim angle (φ_r): the angle between the optical axis and the line between the focal point and the mirror rim and determines the shape of the cross -section of a parabolic trough.

The rim angle given by (Mwesigye et al., 2018):

$$\varphi_r = \tan^{-1}[\frac{8(f / w_a)}{16(f / w_a)^2 - 1} - 1] \tag{4.11}$$

Where: r_r is the rim radius.

At any point of the collector, the local mirror radius obtained by(Marefati et al., 2018):

$$r = \frac{2f}{1+\cos\varphi} \tag{4.12}$$

Which gives the rim radius r_r when the angle $\varphi = \varphi_r$ as

$$r_r = \frac{2f}{1+\cos\varphi_r} \tag{4.13}$$

When the collector is of perfect shape and alignment, the diameter of a cylindrical HCE needed to intercept all the solar image is determined to be

$$D = \frac{w_a \sin 0.267}{\sin\varphi_r} \tag{4.14}$$

Aperture area (A_a): the product of the aperture width and the collector length. At a given DNI and a given Sun position, it determines the radiation capture.

$$A_a = w_a * L \tag{4.15}$$

Concentration ratio(C): Concentration ratio is the ratio of the collector aperture area A_a, to the receiver area A_r, which are the factors increasing the radiation flux on the energy-absorbing surface(Abdulhamed et al, 2018).

$$C = \frac{A_a}{A_r} \tag{4.16}$$

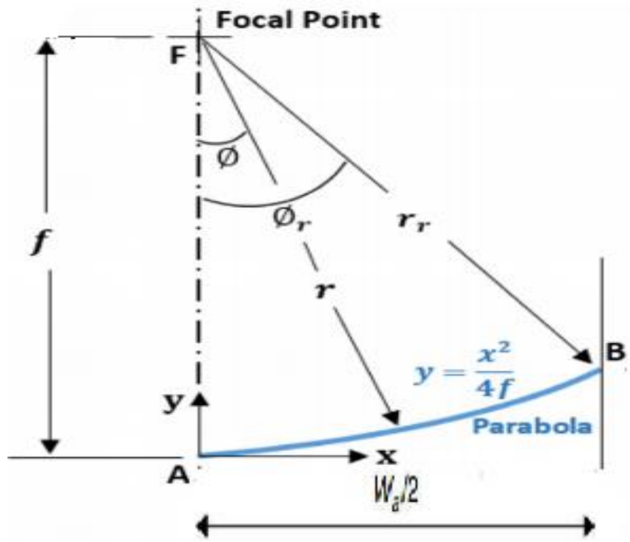

Figure 4-3 Section of a linear parabolic concentrator (Abdulhamed et al, 2018)

4.2.3 Optical Modeling

The aim of optical analysis of the sun rays is to specify thermal output of the examined collector. In ideal conditions, the concentrators reflect all of incident solar energy. However, in reality there is no perfect reflection of solar radiation due to presence of optical losses. The Optical performance of PTCs depends on factors such as tracking error, geometric error and technical failure.

4.2.3.1 Optical efficiency

Optical efficiency of PTSC defined as the ratio of energy reaching the absorber tube to that received by the collector. It indicates how much energy absorbed by its receiver out of the total solar energy incident on the aperture of its mirror. (A.Allouhi et al., 2018)

$$\eta_o = \gamma \, \tau \, \alpha \, r_m k(\theta) \tag{4.17}$$

Where γ is intercept factor, $\tau \alpha$ is transmittance-absorbance product, r_m is reflectance of the mirror and $k(\theta)$ is the incident angle modifier

Incident angle modifier

The incident angle modifier defined as the ratio of thermal efficiency at a given angle of incidence to the peak efficiency at normal incidence. This can be calculated from the equation as stated below. For the IST collector, the incidence angle modifier $k(\theta)$ of the collector given as follow (Kalogirou, 2014)

$$k(\theta) = \cos(\theta) + 0.0003178(\theta) - 0.00003985(\theta)^2 \tag{4.18}$$

Where θ is the incidence angle of beam insolation on collector aperture measured from normal to the aperture.

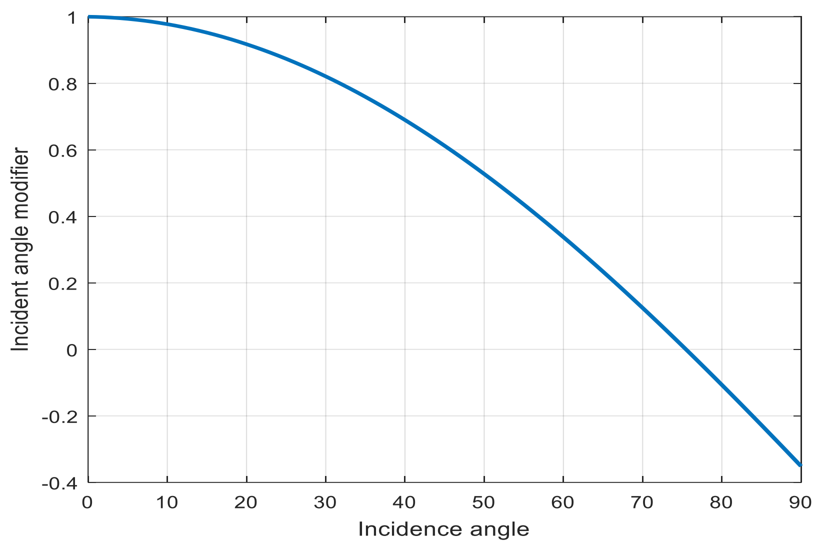

Figure 4-4 Incident angle modifier for incidence angle 0-90^{o}

4.2.4 Thermal model

PTCs are made by bending a sheet of reflective surface into a parabolic shape. Thermal model developed based on the heat transfer process occur in heat collection element (HCE) or Receiver.

4.2.4.1 Components of Heat Collection Element

Glass cover: placed around the Receiver tube to reduce the convective heat loss from the HCE It is an anti-reflective evacuated glass tube which protects the absorber from degradation and reduces the heat losses. The vacuum enclosure is used primarily to reduce heat losses at high operating temperatures and to protect the solar-selective absorber surface from oxidation. It is made typically from Pyrex, which maintains good strength and transmittance under high temperatures (Ouagued et al., 2013).

Receiver tube: is typically stainless steel tube metal black tube placed along the focal line of the receiver. Thermal fluid circulates through this tube and gained heat from absorbed solar radiation. It covered with a selective coating that has a high solar absorptance of 95% for solar radiation, and low thermal emittance (10%, 673 K) for thermal radiation loss(Ouagued et al., 2013).

Heat transfer fluid: Thermal oils are commonly used as the working fluid in these collectors for temperatures above 200°C,because at these high operating temperatures normal water would produce high pressures inside the receiver tubes and piping. Steam is the most common heat transport medium in industry for temperatures below 250 °C where there is a great deal of experience with it.

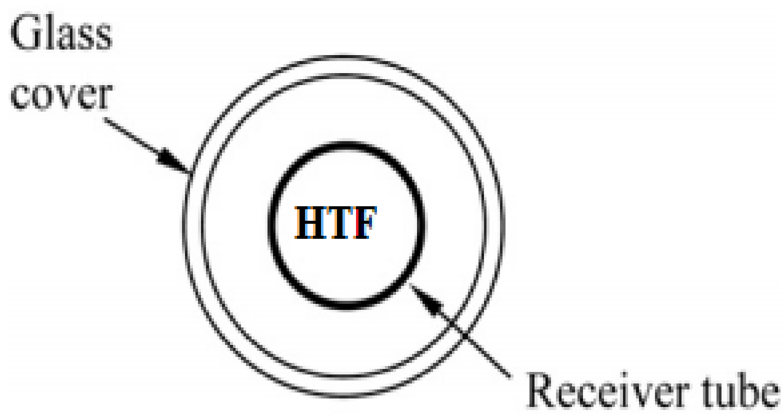

Figure 4-5 Schematic of HCE in detail adopted from (Kalogirou, 2012)

The goal of the thermal model is to determine the energy that is absorbed by the heat transfer fluid (HTF) and describe all the heat losses from the receiver to the atmosphere due to heat transfer mechanisms: conduction, convection, and radiation. In a thermal conversion system a working fluid is used to extract energy from the receiver.

4.2.4.2 Thermal resistance Model of Heat Collecting Element

Thermal resistance model is obtained from an energy balance of the receiver, with assumption that all temperatures, heat fluxes, and thermodynamic properties are uniform around the circumference of the receiver. The heat transfer mechanism occur in HCE explained below

The solar radiation reflected by the reflector mirror is absorbed by the glass cover and the receiver tube. The majority of the energy absorbed by the absorber coating is transferred through the absorber by conduction and then to the heat transfer fluid (HTF) by convection. The rest of the energy transferred back to the receiver tube by radiation and convection. The energy transferred back by convection and radiation is conducted through the glass cover alongside with the energy absorbed by the receiver tube. Then, this energy is lost to the ambient by convection and radiation.(Kalogirou, 2012)

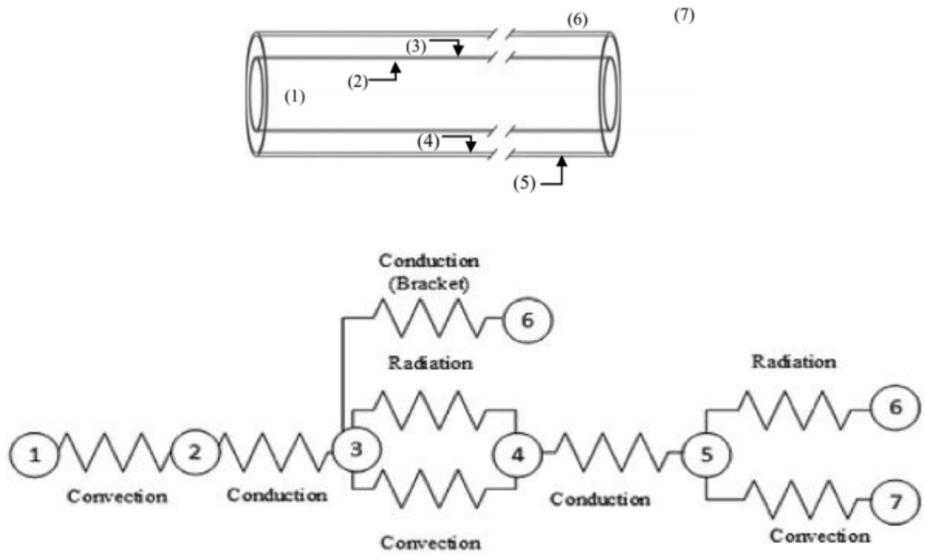

1 HTF, 2 Receiver tube inner surface, 3 Receiver tube outer surface, 4 Glass tube inner surface, 5 Glass tube outer surface, 6 Surrounding air, 7 Sky

Figure 4-6 Schematic of a fragment of HCE (Hafez et al., 2018) and Thermal resistance (Kasaiean et al., 2018)

4.2.4.3 Analysis of Heat Transfer Interactions in HCE

A. Heat transfer between Glass cover and the atomsphere.

Heat transfer from the glass cover to the surrounding ambient air by convection and there is radiation heat transfer process between Glass cover and sky due to temeperature difference.

1. Convection heat transfer

The convection heat transfer is estimated from Newton's law of cooling as shown below (Padilla et al., 2011):

$$q_{go-a} = h_{cv,ext} \pi D_{go} (T_{go} - T_a) \tag{4.19}$$

Where $h_{cv,ext}$ is the convective heat transfer coefficient between the external surface of the glass cover and the ambient air. Determined by below equation (Christos Tzivanidis & Bellos, 2016):

$$h_{cv,ext} = \frac{8.6 v_{air}^{0.6}}{L^{0.4}} \tag{4.20}$$

Where: v_{air} is wind speed in m/s and L is length of collector in m.

2. Radiation heat transfer

Assume that the glass envelope is treated as a small gray convex in a large blackbody cavity which is the sky. The radiation heat transfer between the glass envelope and the sky is given by (Lamrani et al., 2018)

$$q_{go-sky,rad} = \pi D_{go} h_{r,ex} (T_{go} - T_{sky}) \tag{4.21}$$

The heat transfer coefficient by radiation between the glass envelope and the sky is given as follows:

$$h_{r,ext} = \sigma \varepsilon_{go} (T_{go})^2 + (T_{sky})^2 (T_{sky} + T_{go}) \tag{4.22}$$

Where σ is the Stefan–Boltzman constant ($5.67x10^{-8} W / m^2 k^4$) and ε_{go} is the emittance of the external surface of the glass envelope.

The effective sky temperature assumed to be 8°C below the ambient temperature. (Yılmaz & Mwesigye, 2018)

$$T_{sky} = T_{amb} - 8^o C \tag{4.23}$$

B. Heat transfer beween the receiver tube and the glass cover

Heat transfer between receiver tube and glass cover occurs by convection and radition mechanism.

1. Convection heat transfer

Convection heat transfer depends on the annulus pressure. For very small Pressure (< 0.013 Pa), convective heat transfer coefficient considered as zero. At higher pressures heat transfer is by free convection. For pressure greater than 0.013 Pa from Raithby and Holland’s formula the convection heat transfer estimated as follows (Lamrani et al., 2018):

$$q_{ro-gi,cv} = h_{cv,\text{int}} \left(T_g - T_r \right) \tag{4.24}$$

where $h_{cv,\text{int}}$ is estimated through natural convection relations between two horizontal, concentric cylinders and given by(Kalogirou, 2012):

$$h_{cv,\text{int}} = \frac{2\pi k_{eff}}{\ln\left(\frac{D_{gi}}{D_{ro}}\right)} \tag{4.25}$$

The effective thermal conductivity k_{eff} is given by (Kalogirou, 2012):

$$k_{eff} = 0.36 k_{air} \left(\frac{pr_{air}}{0.861 + pr_{air}}\right)^{0.25} \left(R_{ac}\right)^{0.25} \tag{4.26}$$

Where

$$R_{ac} = \frac{\left(\ln\left(\frac{D_{gi}}{D_{ro}}\right)\right)^4}{L_{eff}{}^3 \left(D_{gi}{}^{-0.6} + D_{ro}{}^{-0.6}\right)^5} \left(Gr_{air} . \Pr_{air}\right) \tag{4.27}$$

The critical length is given by $L_{eff} = \frac{D_{gi} - D_{ro}}{2}$

2. Radiation Heat Transfer

The radiation heat transfer between the receiver tube and glass cover is estimated by (Padilla et al., 2011):

$$q_{ro-gi,rad} = \pi D_{ro} h_{r,\text{int}} (T_r - T_g) \tag{4.28}$$

Where the heat transfer coefficient by radiation between the absorber tube and the glass envelope is expressed as follows (Kalogirou, 2012):

$$h_{r,\text{int}} = \frac{\sigma\left(\left(T_r\right)^2 + \left(T_g\right)^2\right)\left(T_r + T_g\right)}{\frac{1}{\varepsilon_r} + \frac{1-\varepsilon_g}{\varepsilon_g}\left(\frac{D_{ro}}{D_{gi}}\right)} \tag{4.29}$$

C. Conduction heat transfer through the receiver tube wall and glass cover .

Conduction heat transfer through the receiver tube wall is determined by the Fourier's law of conduction through a hollow cylinder with assumption that there is no thermal resistance and thermal conductivity of the glass is constant(Kalogirou, 2012).

$$q_{ri-ro} = \frac{2\pi k_r (T_{ri} - T_{ro})}{\ln\left(\frac{D_{ro}}{D_{ri}}\right)} \tag{4.30}$$

Where k_r is receiver tube thermal conductivity of receiver tube at the average temperature $\frac{T_{ri} + T_{ro}}{2}$ (W/m-^{o}C)

The conduction heat transfer through the glass cover uses the same equation as the conduction through the receiver tube wall

D. Heat transfer between the HTF and the receiver tube

From Newton's law of cooling the convection heat transfer from the inside surface of the receiver tube to the HTF is given by (Kalogirou, 2012):

$$q_{f-r,cv} = h_{cv,f} \pi D_{ri} (T_r - T_f) \tag{4.31}$$

The convection heat transfer coefficient at the inside pipe diameter(Incropera et al., 2011):

$$h_{cv,f} = Nu_f \frac{k_f}{D_{ri}} \tag{4.32}$$

Where Nu_f is Nusselt number based on inside diameter of pipe and D_{ri} is inside diameter of pipe The Nusselt number calculated using the Gnielinski correlation (Lamrani et al., 2018).

When the Reynolds number is lower than 2300, laminar flow exists in the receiver tube and the Nusselt number is constant. For pipe flow, the constant value, assuming constant heatflux.

For $\mathrm{Re}_f < 2300$ $\qquad Nu_f = 4.36$ (4.33)

For $\mathrm{Re}_f > 2300$

$$Nu_f = \frac{\left(\frac{f}{8}\right)\left(\mathrm{Re}_f - 100\right)Pr_f}{1 + 12.7\left(\frac{f}{8}\right)^{0.5}\left(\left(Pr_f\right)^{\frac{2}{3}} - 1\right)} \tag{4.34}$$

With f is the friction factor defined as follows(Lamrani et al., 2018):

$$f = \left(1.82\log_{10}(\mathrm{Re}_f) - 1.64\right)^{-2} \tag{4.35}$$

E. Collector heat removal factor

Heat removal factor is defined as the useful energy gained to the energy gained if the entire absorber is at the inlet temperature of the heat transfer fluid. It is a measure of the thermal resistance encountered by the absorbed solar radiation in reaching the collector fluid and it is expressed as (Marefati et al., 2018)

$$F_R = \frac{\dot{m}c_p}{A_r U_L}\left[1 - \exp\left(\frac{-A_r U_L F'}{\dot{m}c_p}\right)\right] \tag{4.36}$$

Where A_r is the receiver area (m^2) and F' is the collector efficiency factor is given by

$$F' = \frac{1/U_L}{1/U_L + \frac{D_{ro}}{h_{fi}D_{ri}} + \frac{D_{ro}}{2k_f}\left[\ln\left(\frac{D_{ro}}{D_{ri}}\right)\right]} \tag{4.37}$$

Where k_f is thermal conductivity of the working fluid (W/m K), D_{ro} is receiver tube inner diameter D_{ri} is receiver tube outer diameter, h_{fi} is convective heat transfer coefficient inside the receiver tube [W/m^{2}K] and U_L is the thermal loss coefficient and given by(D. Kumar & Kumar, 2015):

$$U_L = \left[\frac{A_r}{\left(h_{cv,ext} + h_{r,ext}\right)A_c} + \frac{1}{h_{r,\mathrm{int}}}\right]^{-1} \tag{4.38}$$

F. Thermal efficiency

The thermal efficiency of a solar PTC is defined as the ratio of useful heat gain by the HTF and the heat flux received by the concentrator. It is essential to point that only the beam radiation can be exploited from the PTC because these collectors are imaging collectors with a specific image of the sun in the receiver (Chahine et al., 2018). The instantaneous thermal efficiency given by

$$\eta = \frac{\dot{Q}_u}{I_d A_a} \tag{4.39}$$

A_a is the unshaded collector aperture area given as $A_a = \pi\left(W_a - D_{po}\right)L$ and The useful energy rate to the working fluid in receiver tube can be calculated by the use of the Hottel–Whillier equation given as:

$$\dot{Q}_u = \dot{m}c_p(T_{fo} - T_{fin}) = F_R A_a\left[\eta_o I_d - U_L\,\frac{\left(T_{fin} - T_a\right)}{C}\right] \tag{4.40}$$

The Outlet temperature can be calculated as(D. Kumar & Kumar, 2015):

$$T_{fo} = T_a + \frac{C\eta_o I_d}{U_L} + \left(T_{fi} - T_a - \frac{C\eta_o I_d}{U_L}\right).\exp\left(\frac{-F'U_L A_r}{\dot{m}c_p}\right) = T_{fi} + \frac{\eta A_a I_d}{\dot{m}c_p} \tag{4.41}$$

Mass flow rate analysis Using average daily beam solar radiation of 700W/m^2 estimated from the solar radition model analysis. The variation mass flow rate of the collector with outlet temperature and thermal efficiency analyzed.

As shown in Figure. 4.7, as mass flow rate increases; outlet water temperature decreases. A mass flow rate of 0.0125kg/sec which corresponds to an outlet temperature of 300^{o}C is selected as working fluid mass follow rate for this study.

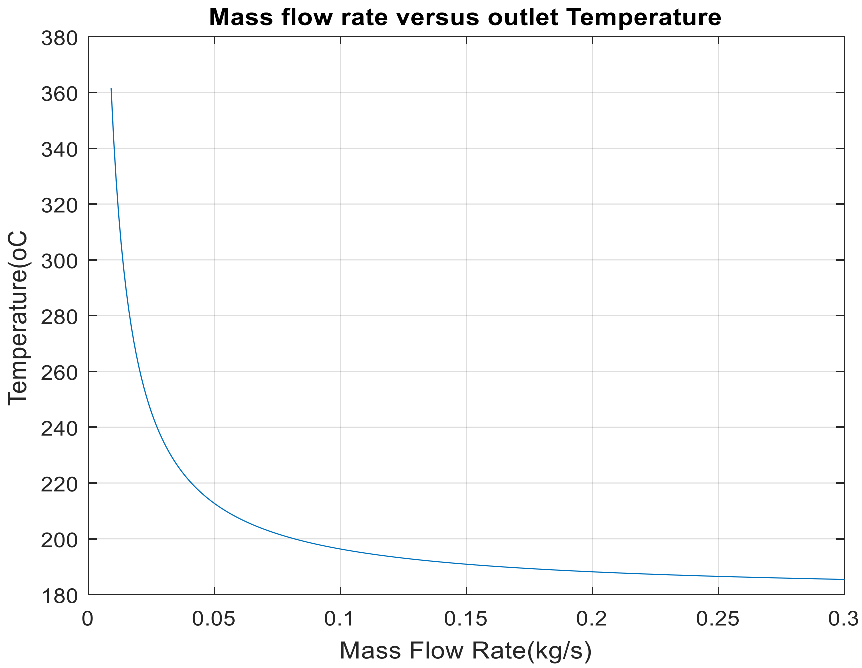

Figure 4-7 Variation of heat transfer fluid outlet temperature as a function of mass flow rate

4.2.5 Transient Analysis of Parabolic Trough solar collector

To study the performance collector under fluctuating climatic conditions transient anlysis should be done. A one-dimensional mathematical model is introduced to study the transient thermal behavior of the PTC. The inputs of the model are the instantaneous ambient temperature, incident beam radiation, mass flow rate, and physical properties of the glass cover, receiver tube and HTF. The model is based on the energy balance between the HTF, receiver tube, glass cover and surrounding then the partial differential equations are obtained by applying the energy balance for each section. Therefore, the receiver tube is divided into N segment and heat propagation occurs according the axial direction. These equations vary during the illumination time (t) for a length (X) of the absorber.The discretization of method finite difference used for solving the nonlinear equations of those heat balance at the receiver tubes. A computer program developed in Matlab to solve these equations.

The following simplifying hypotheses used in the model. (Lamrani et al., 2018)

- The heat transfer by conduction in the receiver tube is neglected
- The receiver tube and the glass cover are assumed to be grey bodies.
- The solar flux on the absorber tube is uniform.

- The heat transfer fluid is incompressible.
- The form factor between the receiver tube and the glass cover is considered equal to 1
- Conduction losses at the ends of receiver tube are neglected
- The flow is unidirectional.
- The glass is considered opaque to infrared radiation
- The parabolic shape is symmetrical

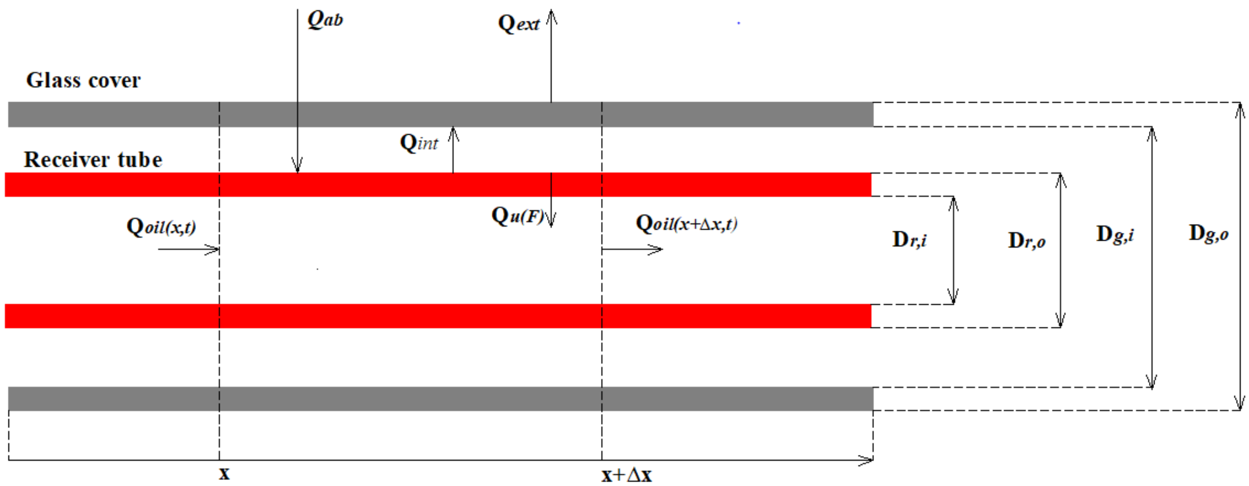

Figure 4-8 Schematic diagram of heat transfer analysis in HCE

A. Energy Balance of Glass cover

The energy balance for the glass envelope is given by (Ghodbane & Boumeddane, 2018):

$$m_g C_g \frac{\partial T_g(x,t)}{\partial t} = Q_{\text{int}} - Q_{ext} \tag{4.42}$$

Where Q_{int} is internal heat transfer between the absorber and the glass cover. The heat transfer is occur by convection and radiation and it is given by:

$$Q_{\text{int}} = Q_{\text{int},cv} + Q_{\text{int},r} \tag{4.43}$$

Q_{ext} is external heat transfer between the glass cover and the ambient atmosphere and the sky.

$$Q_{ext} = Q_{ext,cv} + Q_{ext,r} \tag{4.44}$$

By incorporating all internal and external heat transfer Equation 4.42 can be written as:

$$\rho_g C_g A_g \frac{\partial T_g(x,t)}{\partial t} = \pi D_{r,o} h_{cv,\text{int}}(T_r - T_g) + \pi D_{r,o} h_{r,\text{int}}(T_r - T_g) - (\pi D_{g,o} h_{cv,ext}(T_g - T_{amb}) + \pi D_{g,o} h_{r,ext}(T_g - T_{sky})) \tag{4.45}$$

Where ρ_g, C_g and T_g are the Glass cover density, specific heat and temperature, respectively and A_g is the difference between the inner surface and the outer surface of glass tube (m²).

B. Energy Balance of Receiver tube

The energy balance in the absorber tube is given as follows(Ghodbane & Boumeddane, 2018):

$$m_A C_A \frac{\partial T_A(x,t)}{\partial t} = Q_{ab} - Q_{\text{int}} - Q_u(F) \tag{4.46}$$

Where Q_{ab} is refers to the solar energy absorbed by the heat collecting element, Q_{int} is heat loses by convection and radiation and $Q_u(F)$ is useful heat transfers to the working fluid by convection.

Equation 4.46 can be written as:

$$\rho_A C_A A_A \frac{\partial T_A(x,t)}{\partial t} = I_d \gamma \tau_g \alpha_r r_m W k(\theta) - \pi D_{r,o} h_{cv,\text{int}}(T_r - T_g) - \pi D_{r,o} h_{r,\text{int}}(T_r - T_g) - \pi D_{A,i} h_{cv,F}(T_r - T_F) \tag{4.47}$$

Where: ρ_A, C_A and T_A are the Absorber density, specific heat and temperature, respectively. A_A is the difference between the inner surface and the outer surface of absorber tube (m²).

C. Energy Balance of Heat transfer fluid

Similarly, the energy balance for the heat transfer fluid circulating in the absorber tube is stated by(Ghodbane & Boumeddane, 2018):

$$m_f C_f \frac{\partial T_f(x,t)}{\partial t} + \dot{m} C_f (T_f(x + \Delta x, t) - T_f(x,t)) = Q_u(F) \tag{4.48}$$

where $\dot{m}$ is a flow rate working fluid flows inside the absorber, $Q_u(F)$ is useful heat transfers to the working fluid by convection.

Equation 4.48 can be written as:

$$\rho_f C_f A_f \frac{\partial T_f(x,t)}{\partial t} = \pi D_{r,i} h_{cv,f}(T_r - T_f) - \dot{m} C_f \frac{\partial T_f(x,t)}{\partial x} \tag{4.49}$$

Solution Procedure

The above three differential Equations (4.45,4.47 and 4.49) discretized by an Explicit Finite difference method. The length of HCE $0 \le x \le L$ is divided into Δx equal parts of mesh size. A forward time and centered space finite difference scheme are used to obtain the following Equations

$$\frac{\partial T_g(x,t)}{\partial t} = \frac{T_{g,n}{}^{i+1} - T_{g,n}{}^{i}}{\Delta t} \tag{4.50}$$

$$\frac{\partial T_r(x,t)}{\partial t} = \frac{T_{r,n}{}^{i+1} - T_{r,n}{}^{i}}{\Delta t} \tag{4.51}$$

$$\frac{\partial T_f(x,t)}{\partial t} = \frac{T_{f,n}{}^{i+1} - T_{f,n}{}^{i}}{\Delta t} \tag{4.52}$$

$$\frac{\partial T_f(x,t)}{\partial x} = \frac{T_{f,n+1}{}^{i} - T_{f,n-1}{}^{i}}{2\Delta x} \tag{4.53}$$

By applying the above derivatives and some rearrangment the following algebric equations obtained

For Glass Envelope

$$T_{g,n}{}^{i+1} = ((\tfrac{1}{\Delta t} - AG - BG - CG - DG)T_{g,n}{}^{i} + (AG + BG)T_{A,n}{}^{i} + CGT_{amb}{}^{i} + DGT_{sky}) * \Delta t \tag{4.54}$$

For Absorber

$$T_{A,n}{}^{i+1} = (I_d \gamma \tau_g \alpha_{ab} r_m W k(\theta) / DA + (\tfrac{1}{\Delta t} - B_1) * T_{A,n}{}^{i} + B_2 * T_{g,n}{}^{i} + CA * T_{F,n}{}^{i}) * \Delta t \tag{4.55}$$

For heat transfer fluid

$$T_{F,n}{}^{i+1} = ((\tfrac{1}{\Delta t} - AF) * T_{F,n}{}^{i} + AF * T_{A,n}{}^{i} - BF(T_{F,n+1}{}^{i} - T_{F,n-1}{}^{i})) * \Delta t \tag{4.56}$$

Where in Equation 4.54,4.55 and 4.56 the coeffficeints are given as follows:

$$AG = \frac{h_{cv,\text{int}}}{\rho_g C_g A_g} \tag{4.57}$$

$$BG = \frac{\pi D_{A,e} h_{r,\text{int}}}{\rho_g C_g A_g} \tag{4.58}$$

$$CG = \frac{\pi D_{g,e} h_{cv,ext}}{\rho_g C_g A_g} \tag{4.59}$$

$$DG = \frac{\pi D_{g,e} h_{r,ext}}{\rho_g C_g A_g} \tag{4.60}$$

$$A_1 = AG + BG + CG + DG \tag{4.61}$$

$$A_2 = AG + BG \tag{4.62}$$

$$AA = \frac{\pi D_{A,e} h_{cv,\text{int}}}{\rho_A C_A A_A} \tag{4.63}$$

$$BA = \frac{\pi D_{A,e} h_{r,\text{int}}}{\rho_A C_A A_A} \tag{4.64}$$

$$CA = \frac{\pi D_{A,i} h_{cv,F}}{\rho_A C_A A_A} \tag{4.65}$$

$$CD = \frac{1}{\rho_A C_A A_A} \tag{4.66}$$

$$B_1 = AA + BA + CA \tag{4.67}$$

$$B_2 = AA + BA \tag{4.68}$$

$$AF = \frac{\pi D_{A,i} h_{cv,F}}{\rho_F C_F A_F} \tag{4.69}$$

$$BF = \frac{\dot{m} C_F}{2\rho_F C_F A_F \Delta x} \tag{4.70}$$

Initial conditions

At $t = t_o$, for $0 \le x \le L$

The glass envelope is at ambient air temperature, $T_g(x,t_o) = T_{amb}(x,t_o)$

The absorber is assumed to be 15°C above the ambient air. $T_g(x,t_o) = T_{amb}(x,t_o) + 15^0 C$

The fluid is assumed to be at an initial temperature of 180 °C.

Boundary condtions

At $t > t_o$,For $x = 0$,Temperature of fluid at the inlet of reciver is equal to the exit fluid temperature of storage tank, $T_F(0,t) = T_{inlet}$

At $t > t_o$,For $x = L$ $\frac{\partial T_F}{\partial x} = 0$.

4.3 Sizing and Layout of Solar Fields with PTSC

The first step in the design of a parabolic trough solar field is to define a set of parameters that determine solar field performance. These parameters are collector orientation, day of the design point, direct solar irradiance and ambient air temperature for the selected date and time, geographical location of the plant site (latitude and longitude), total thermal output power to be delivered by the solar field, solar field inlet/outlet temperatures, working fluid for the solar collectors and working fluid flow rate.

In a typical PTSC field, several collectors connected in series make a row, and a number of rows are connected in parallel to achieve the required nominal thermal power output at design point. The number of collectors connected in series in every row depends on the temperature increase to be achieved between the row inlet and outlet.

The number collectors of in single row that connected in parallel determined based on thermal power demanded Injera baking process.

$$\text{Number of collector} = \frac{\text{Thermal Power demanded}}{\text{The power delivered by single collector}} \tag{4.71}$$

4.4 Design and performance analysis of thermal energy storage

4.4.1 Introduction

Solar energy is a renewable energy available only intermittently or even irregularly. However, the utilization of energy often has a different phase compared to the time of availability of renewable energy. Phase change materials (PCM) have the advantage of high energy storage density and are able to maintain temperature (nearly) constant during the phase change process.

A complete storage process involves at least three steps: charging, storing, and discharging. During the charging process, the HTF is heated inside a solar collector and pumped through the packed bed in the axial direction from top of the bed to the bottom. It is assumed that the initial temperatures of the HTF and the PCM packed bed are equal; after that, the temperature of the HTF increases gradually until it attains the required storage temperature and it remains constant until the occurrence of the equilibrium state between HTF and the packed bed temperatures, then the charging process terminates. During the discharging process, the cold HTF is pumped through the bed in the axial direction from the bottom of the bed to the top.

4.4.2 Selection of PCM material for the latent heat storage

The first parameter considered in selection of PCM material is its melting point. The melting point temperature of the PCM should much the operating temperature of designed thermal system. The PCM melting point selected with interval of about 5 to 10 ^{o}C above the desired operating temperature of the application. Based pervious experimental and numerical study operation temperatures selected for the Injera baking is 250 to 300 ^{o}C, this is temperature of oil should reach under baking pan.

Table 4-3 Thermo-physical properties of selected PCMs (Nergy et al., 2018 and Solomon et al., 2014)

Melting point(^{o}C)	Latent heat of fusion (KJ/kg)	Density (kg/m^3)		Specific heat(J/kg K)		Conductivity W/m K	
		solid	liquid	Solid	Liquid	solid	Liquid
308	176	2260	1900	1588	1650	0.59	0.5

4.4.3 Volume sizing for thermal storage system

PCM storage tank is sized based on the required storage capacity for intended operating application. By considering the energy provided from heat transferring fluid

The size of the PCM storage tank can be expressed as the following equation (Yantong Li, 2018):

$$v_{pst} = \frac{E_{rs}}{c_{pl}\rho_m(1-\varepsilon)(T_i - T_m) + H_m\rho_m(1-\varepsilon) + c_{ps}\rho_m(1-\varepsilon)(T_m - T_s) + c_{pf}\rho_f\varepsilon(T_l - T_s)} \quad (4.72)$$

Where E_{rs} is the required storage capacity of the system; ε is mean void fraction (porosity); c_{pl} and c_{ps} are the liquid and solid specific heat of the PCM, respectively; T_l and T_s are the maximum and minimum operation temperature, respectively; T_m and H_m are the phase change temperature and specific enthalpy of the PCM, respectively

Selection of Geometric parameters

PCM is filled in a cylindrical capsule which is made of 6061 Aluminum. The outer diameter of the capsule is 40 mm , have a wall thickness of 3 mm and the overall capsule length is 250 mm. This capsule is sealed from both ends to prevent leaking of the melted PCM. Aluminum is selected because they show good accessibility for the chosen corrosion protection and applicability of the sealing concept. (Stephan Höhlein, 2018).

- Number of cylindrical capsule

$$n_c = \frac{v_{pst} * 4(1-\varepsilon)}{\pi * D_{out}^{\ 2} * l} \quad (4.73)$$

Where v_{pst} volume of the PCM storage tank; D_{out} and l are the outer diameter and the overall capsule length, respectively.

- Mass of Phase change material.

$$m_{pcm} = \rho_m * \tfrac{\pi}{4} * ID^2 * l * n_c \quad (4.74)$$

Where ρ_m is density of phase change material; ID is inner diameter of cylindrical capsule

4.4.4 Mathematical modelling and performance analysis of PCM tank

To investigate the thermal behavior of storage system two phase model that considers the system as a continuous medium and not as a medium comprised of individual particles is used.

Governing Equations

The following energy equations are written separately for the HTF and PCM(Gracia & Cabeza, 2014):

$$\varepsilon\rho_{eff}C_{peff}\left(\frac{\partial T_f}{\partial t}+v_f\frac{\partial T_f}{\partial x}\right)=k_{fx}\frac{\partial^2 T_f}{\partial x^2}+k_{fr}\left(\frac{\partial^2 T_f}{\partial r^2}+\frac{1}{r}\frac{\partial T_f}{\partial r}\right)+h_{ef}a_p(T_p-T_f)-U_w a_w(T_f-T_{sur}) \quad (4.75)$$

$$(1-\varepsilon)\rho_{efp}C_{efp}\frac{\partial T_p}{\partial t}=k_{sx}\frac{\partial^2 T_p}{\partial x^2}+k_{pr}\left(\frac{\partial^2 T_p}{\partial r^2}+\frac{1}{r}\frac{\partial T_p}{\partial r}\right)+h_{ef}a_p(T_f-T_p) \quad (4.76)$$

The first term of the left hand side of Eq.(4.75) represents the Sum of the rate of change of enthalpy and the net enthalpy associated with the fluid flow in the control volume. The four terms on the right hand represent heat exchanged by conduction in the axial and radial directions of the control volume, heat exchange by convection between the solid particles and the fluid and heat loss from the storage wall to the external ambient ,respectively.

The first term of the left hand side of Eq. (4.76) represents rate of change of enthalpy of the PCM within the control volume and the three terms on the right hand side represent heat transferred by conduction in the axial, heat transferred radial directions in the control volume and heat transferred by convection between the particles and the fluid, respectively.

One dimensional mathematical model formulated from Eq 4.75 and 4.76 by considering the heat conduction occurs only along the axial direction for both HTF and PCM. Further to simplify the mathematical model the following assumptions considered (Yantong Li, 2018):

- ✓ The temperature of the PCM is invariable during the phase change process.
- ✓ The storage tank wall is adiabatic so that there is no heat loss from the tank to the environment.
- ✓ There is no internal heat generation in the PCM tubes.
- ✓ The variation of the PCM and HTF temperature is only along the oil flow direction.
- ✓ The temperature has no effect on the thermo-physical properties of PCM and HTF.

The governing energy balance equation about the heat transfer process between the PCM and the HTF given below

a) HTF

$$\varepsilon \rho_f C_f \left(\frac{\partial T_f}{\partial t} + v_f \frac{\partial T_f}{\partial x}\right) = k_{fx} \frac{\partial^2 T_f}{\partial x^2} + h_{fp} a_p (T_p - T_f) \tag{4.77}$$

Where ρ_f is the density of the HTF, C_f is the specific heat of the HTF, v_f is the mean velocity of the HTF, T_f is the temperature of the HTF, h_{fp} is the effective convective heat transfer coefficient between the HTF and the PCM, k_{fx} is axial effective thermal conductivity of HTF, a_p is the heat transfer area of the capsule per unit bed volume, T_p is the temperature of the PCM and x is the distance.

The mean velocity of the HTF in the tank is determined by (Yantong Li, 2018):

$$v_f = \frac{m_f}{\varepsilon A_c \rho_f} \tag{4.78}$$

Where m_f and A_c are the mass flow rate of the HTF and the cross area of the PCM storage tank, respectively.

b) PCM

$$(1-\varepsilon)\rho_p C_p \frac{\partial T_p}{\partial t} = k_{sx} \frac{\partial^2 T_p}{\partial x^2} + h_{fp} a_p (T_f - T_p) \tag{4.79}$$

Where ρ_p is the density of the PCM, C_p is the specific heat of the PCM and k_{sx} is axial effective thermal conductivity of PCM

For one-dimensional transient advection–diffusion governing equation substituted by finite difference approximation with explicit method, using centered space finite difference scheme for discretizing the convection term. Whereas the spatial second derivative and the time derivative discretized using the second-order accurate central difference formula and the first-order accurate forward differencing formula, respectively.

The domain $0 \leq x \leq L$ is discretized into segments of length Δx, where Δx = L/M thus generating a mesh of (M + 1) nodes in the spatial domain, and time step of Δt =1s used.

$$\frac{\partial T_f}{\partial t} = \frac{T_{f,i}{}^{j+1} - T_{f,i}{}^{j}}{\Delta t} \tag{4.80}$$

$$\frac{\partial T_f}{\partial x} = \frac{T_{f,i+1}{}^{j} - T_{f,i-1}{}^{j}}{2\Delta x} \tag{4.81}$$

$$\frac{\partial^2 T_f}{\partial x^2} = \frac{T_{f,i+1}{}^{j} - 2T_{f,i}{}^{j} + T_{f,i-1}{}^{j}}{\Delta x^2} \tag{4.82}$$

$$\varepsilon\rho_f C_f \frac{T_{f,i}{}^{j+1} - T_{f,i}{}^{j}}{\Delta t} + \varepsilon\rho_f C_f v_f \frac{T_{f,i+1}{}^{j} - T_{f,i-1}{}^{j}}{2\Delta x} = k_{fx} \frac{T_{f,i+1}{}^{j} - 2T_{f,i}{}^{j} + T_{f,i-1}{}^{j}}{\Delta x^2} + h_{fp} a_p (T_{p,i}{}^{j} - T_{f,i}{}^{j}) \tag{4.83}$$

$$T_{f,i}{}^{j+1} - T_{f,i}{}^{j} + \frac{c}{2}\left(T_{f,i+1}{}^{j} - T_{f,i-1}{}^{j}\right) = r\left(T_{f,i+1}{}^{j} - 2T_{f,i}{}^{j} + T_{f,i-1}{}^{j}\right) + F(T_p{}^{j} - T_f{}^{j}) \tag{4.84}$$

Equation 4.84 is rearranged as

$$T_{f,i}{}^{j+1} = \left(1 - F - 2r\right)T_{f,i}{}^{j} + \left(r - \frac{c}{2}\right)T_{f,i+1}{}^{j} + \left(r + \frac{c}{2}\right)T_{f,i-1}{}^{j} + FT_{p,i}{}^{j} \tag{4.85}$$

Where:

$$c = \frac{v_f \Delta t}{\Delta x} \tag{4.86}$$

$$r = \frac{k_{fx}\Delta t}{\varepsilon\rho_f C_f \Delta x^2} \tag{4.87}$$

$$F = \frac{h_{fp} a_p \Delta t}{\varepsilon\rho_f C_f} \tag{4.88}$$

Similarly for the PCM heat transfer:

$$\frac{\partial T_p}{\partial t} = \frac{T_{p,i}{}^{j+1} - T_{p,i}{}^{j}}{\Delta t} \tag{4.89}$$

$$\frac{\partial^2 T_p}{\partial x^2} = \frac{T_{p,i+1}{}^{j} - 2T_{p,i}{}^{j} + T_{p,i-1}{}^{j}}{\Delta x^2} \tag{4.90}$$

$$(1-\varepsilon)\rho_p C_p \frac{T_{p,i}{}^{j+1} - T_{p,i}{}^{j}}{\Delta t} = k_{sx} \frac{T_{p,i+1}{}^{j} - 2T_{p,i}{}^{j} + T_{p,i-1}{}^{j}}{\Delta x^2} + h_{fp} a_p (T_{f,i}{}^{j} - T_{p,i}{}^{j}) \tag{4.91}$$

Equation 4.91 is rearranged as

$$T_{p,i}{}^{j+1} = \left(1 - FP - 2RP\right) T_{p,i}{}^{j} + RP\left(T_{p,i+1}{}^{j} + T_{p,i-1}{}^{j}\right) + FPT_{f,i}{}^{j} \tag{4.92}$$

Where :

$$RP = \frac{k_{sx}\Delta t}{(1-\varepsilon)\rho_p C_p \Delta x^2} \tag{4.93}$$

$$FP = \frac{h_{fp} a_p \Delta t}{(1-\varepsilon)\rho_p C_p} \tag{4.94}$$

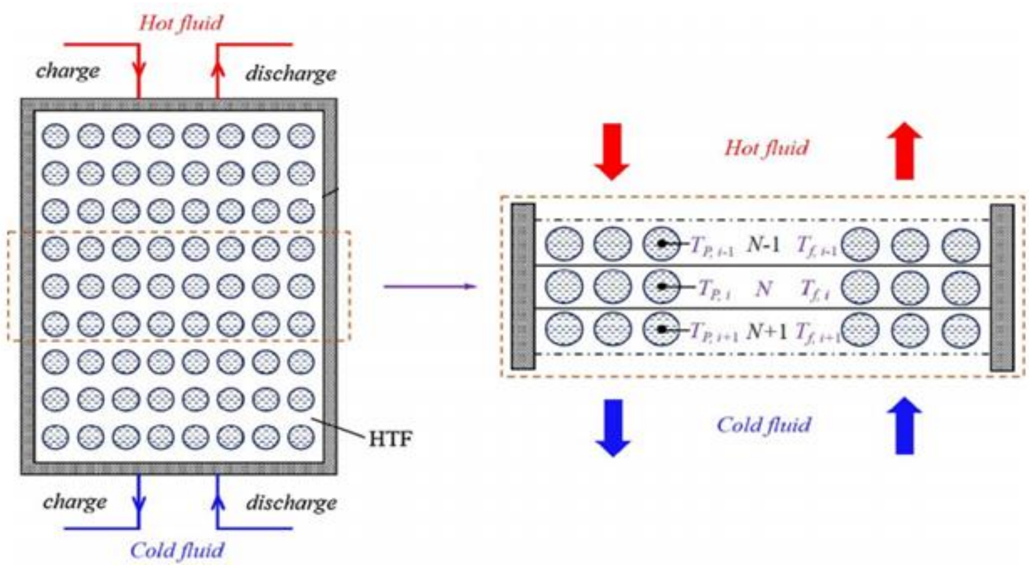

Figure 4-9 The schematic representation of the heat transfer process between the PCM *(Yantong Li, 2018)*

Initial and boundary conditions

At time $t = 0 \quad T_p(x,0) = T_f(x,0) = T_o$

At time $t > 0 \quad T_f(0,t) = T_{inlet}$, $\dfrac{\partial T_f(x,t)}{\partial x} = 0,$ at $x = L$ and $\dfrac{\partial T_p(x,t)}{\partial x} = 0,$ for $x = 0$ and $x = L$

Empirical correlations

The effective convective heat transfer coefficient between the HTF and the PCM is determined as the following equation(Yantong Li, 2018):

$$h_{ef} = \frac{1}{R_f + R_w + R_p} \tag{4.95}$$

Where: R_f , R_w and R_p are the thermal resistance of the HTF, tube walls and PCM, respectively

The convection heat transfer coefficient can be determined from Nusselt number correlation

$$Nu = 0.8\,\mathrm{Re}^{0.4}\,Pr^{0.36} \tag{4.96}$$

Where: Re and Pr are Reynolds and Prandtl numbers, respectively

The convective heat transfer coefficient of the HTF is calculated as the following equation

$$h_f = \frac{k_f Nu}{D_{out}} \tag{4.97}$$

Where k_f and D_{out} are thermal conductivity and outer diameter of cylindrical capsule.

The heat transfer process inside a fixed packed bed storage tank includes conduction, convection, and possibly radiation. These mechanisms of heat transfer are generally included in one parameter called effective thermal conductivity The axial effective thermal conductivity of fluid and PCM stated below as suggested by(Gracia & Cabeza, 2014) :

$$k_{fx} = 0.7\varepsilon k_f \qquad \text{if } \mathrm{Re} \le 0.8 \tag{4.98}$$

$$k_{fx} = 0.5\,\mathrm{Pr}\,\mathrm{Re}\,k_f \quad \text{if } \mathrm{Re} > 0.8 \tag{4.99}$$

The PCM effective thermal conductivity in axial direction is

$$k_{px} = k_{efx} - k_{fx} \tag{4.100}$$

Where

$$k_{efx} = k_e + 0.5\,\mathrm{Re}\,\mathrm{Pr}\,k_f \tag{4.101}$$

And the stagnation effective thermal conductivity k_e is given as

$$k_e = k_f \left(\frac{k_p}{k_f} \right)^m \tag{4.102}$$

$$m = 0.28 - 0.75 \log \varepsilon - 0.057 \log(\frac{k_s}{k_f}) \tag{4.103}$$

The phase change process

The phase change within the encapsulated PCM is accounted for by the apparent heat capacity method(Mawire & Shobo, 2015)

i. During the solid stage, $T_p < T_{m1}$ $\quad c_p = c_{p1};\ \rho_p = \rho_{p1};\ k_p = k_{p1}$

ii. During solid-liquid phase change, $T_{m1} < T_p < T_{m2}$

$$c_p = \frac{c_{p1} + c_{p2}}{2} + \frac{H_m}{T_{m2} - T_{m1}};\ \rho_p = \frac{\rho_{p1} + \rho_{p2}}{2};\ k_p = \frac{k_{p1} + k_{p2}}{2}$$

iii. During the liquid stage, $T_p > T_{m2}$ $\ c_p = c_{p2};\ \rho_p = \rho_{p2};\ k_p = k_{p2}$

4.5 Transient anlysis of baking Pan

Baking pan is a round circular disk with a smooth top surface suitable for Injera baking application. During discharging process heat transferred from thermal energy storage tank to Injera baking assembly. Heat transferred from heated oil to the baking pan by convection and conduction heat transfer mechanisms.

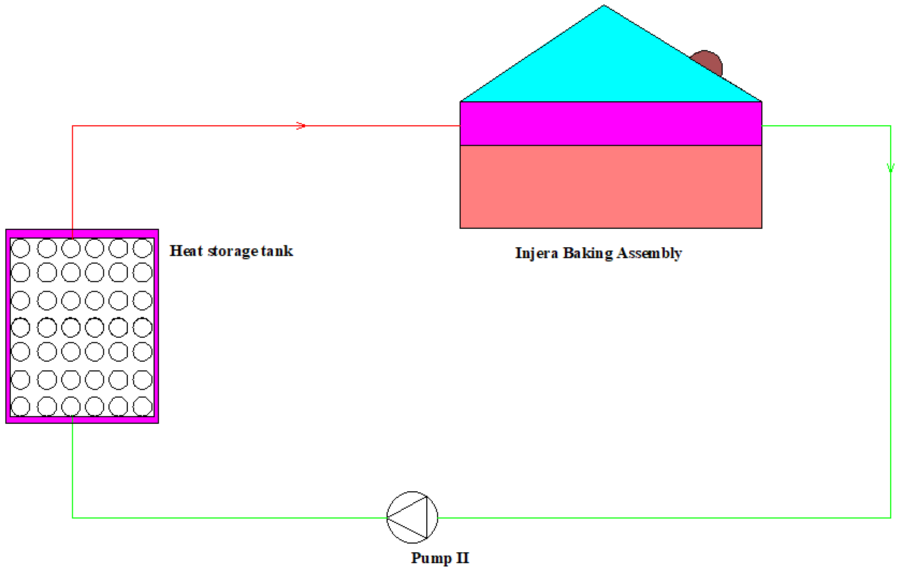

Figure 4-10 Schematic diagram of thermal heat storage tank with Injera baking assembly.

The Injera baking assembly consist of the baking pan, glazing material between oil and the pan and insulation materials.

1. Heat Transfer Coefficient at the Surface of the Baking Pan

a. Convection from Baking Pan to the Atmosphere

There is convection heat loss from the baking pan to the air flow over the baking pan. It is free convection over circular disk. The property of air is determined at the average film temperature. For horizontal plates of various shapes (for example, squares, rectangles, or circles), there is a need to define the characteristic length for use in the Nusselt and Rayleigh numbers. Experiments have shown that a single set of correlations can be used for a variety of different plate shapes when the characteristic length is defined as

$$L_c = \frac{A_s}{p} \tag{4.104}$$

Where: A_s is the surface area and p is the perimeter

To calculate the heat transfer coefficient dimensionless numbers Grashof, Rayleigh and Nusselt determined using the following correlation (Incropera et al., 2011)

Grashof number, $Gr_L = \dfrac{g\beta(T_s - T_\infty)L_c^{\,3}}{v^2}$ (4.105)

Where g is gravitational acceleration, m/s^2, β is coefficient of volume expansion,1/k T_s is temperature of the baking pan surface, ˚C, T_∞ is temperature of the ambient air ˚C v is kinematic viscosity of the fluid, m^2/s and L_c is the characteristic length,m.

Rayleigh number, $Ra_L = Gr_L \Pr$ (4.106)

Nusselt number, $Nu = 0.5Ra_L^{1/4}$ for $10^4 < Ra_L < 10^7$ (4.107)

$Nu = 0.15Ra_L^{1/3}$ for $10^7 < Ra_L < 10^{11}$ (4.108)

Convective Heat Transfer Coefficient

$$h_c = \frac{Nuk}{L_c} \tag{4.109}$$

b. Radiative heat transfer coefficient

The Radiative heat transfer coefficient at the surface of the bake Pan is given by(Incropera et al., 2011):

$$h_r = \sigma\varepsilon\left(\frac{T_s^{\,4} - T_\infty^{\,4}}{T_s - T_\infty}\right) \tag{4.110}$$

2. Convective Heat Transfer Coefficient of Heated Oil

The convection heat transfer coefficient on the surface of the baking pan in contact with the hot oil determined by (Incropera et al., 2011):

$$h_o = \frac{Nuk}{L_c} \tag{4.111}$$

The Nusselt number correlation for free convection between a cold surfaces facing downward is given as (Incropera et al., 2011):

$Nu = 0.27Ra_L^{1/4}$ for, $10^7 < Ra_L < 10^{11}$ (4.112)

Where Rayleigh number, $$Ra_L == \frac{g\beta(T_s - T_\infty)L_c^{\ 3}}{v\alpha} \tag{4.113}$$

Similarly the property of the oil determined at average of temperature of the baking pan bottom surface and heated oil.

4.5.1 Mathematical Modeling for Baking Pan

To analysis the heat up time of the baking the mathematical model for the baking pan developed based on the following assumptions:

- The pan is left uncovered in its initial heating up condition.
- Heat loss due to the glazing material between the pan and the hot oil and losses through the left and right sides are negligible.
- The temperature varies only in axial direction or along the thickness.
- There is no heat generation and thermal conductivity of baking pan is constant.

The transient heat conduction through the baking pan given as:

$$\rho C_p \frac{\partial T}{\partial t} = k \frac{\partial^2 T}{\partial x^2} \tag{4.114}$$

Where ρ is density (kg / m^3),specific heat capacity (J /kg.K) and T is temperature of baking pan vary with space and time.

Initial and boundary conditions

Initial condition at $t = 0$

The baking pan is initially at a constant room temperature.

$T_{\text{intial}} = 20^o C$

Boundary Conditions for $t > o$

At $x = 0$ (at the bottom of the baking pan)

$$-\left(k \frac{\partial T}{\partial x}\right)_{x=o} = h_o (T_s - T_{oil}) \tag{4.115}$$

At $x = L$ (at the top surface of baking pan)

$$-\left(k\frac{\partial T}{\partial x}\right)_{x=L} = h_{ct}(T_s - T_\infty) \tag{4.116}$$

Solution Procedure

The one dimensional parabolic partial differential governing equation solved using MATLAB's built in pdepe solver. The following steps used to solve the given equation with defined initial and boundary condition

1. Rewrite the equation. The PDE rewritten in the below format

$$c\left(x,t,u,\frac{\partial u}{\partial x}\right)\frac{\partial u}{\partial t} = x^{-m}\frac{\partial}{\partial x}\left(x^m f\left(x,t,u,\frac{\partial u}{\partial x}\right)\right) + s\left(x,t,u,\frac{\partial u}{\partial x}\right) \tag{4.117}$$

2. Where m=0 for Cartesian, 1 for cylindrical, 2 for spherical.
3. Code the PDE, initial and boundary condition.
4. Select the mesh points for the solution.
5. Apply the PDE solver.
6. Post processing, view the result and interpreting it.

CHAPTER 5

RESULT AND DISCUSSION

5.1 Hourly Beam Incident Solar Radiation on Horizontal Surface

From the solar radiation model developed in Matlab different input parameter used for thermal and optical analysis of PTC have been simulated. The solar irradiation which is the solar power received over 24 hour for the representative day of each month given in Figure 5.1. The month of February and March presents the highest solar energy potential from winter and spring season respectively. The maximum and minimum horizontal beam solar irradiation is observed during March (5.07 KWh/m^2)and July (3.34KWh/m^2) respectively. Hourly beam incident solar radiation on horizontal surface varies significantly with the months of the year. The hourly beam incident solar radiation on horizontal surface for summer season shown in Figure 5.2. For other seasons it presented at APPENDIX.

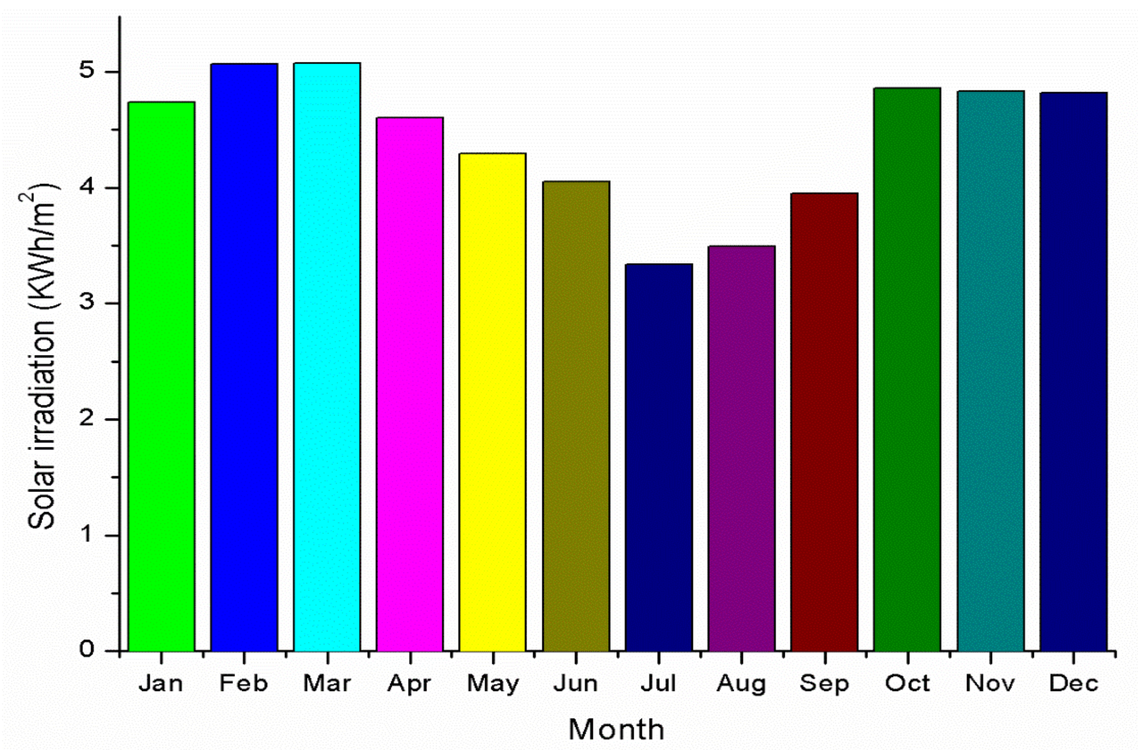

Figure 5-1 Hourly beam incident solar irradiation on Horizontal surface

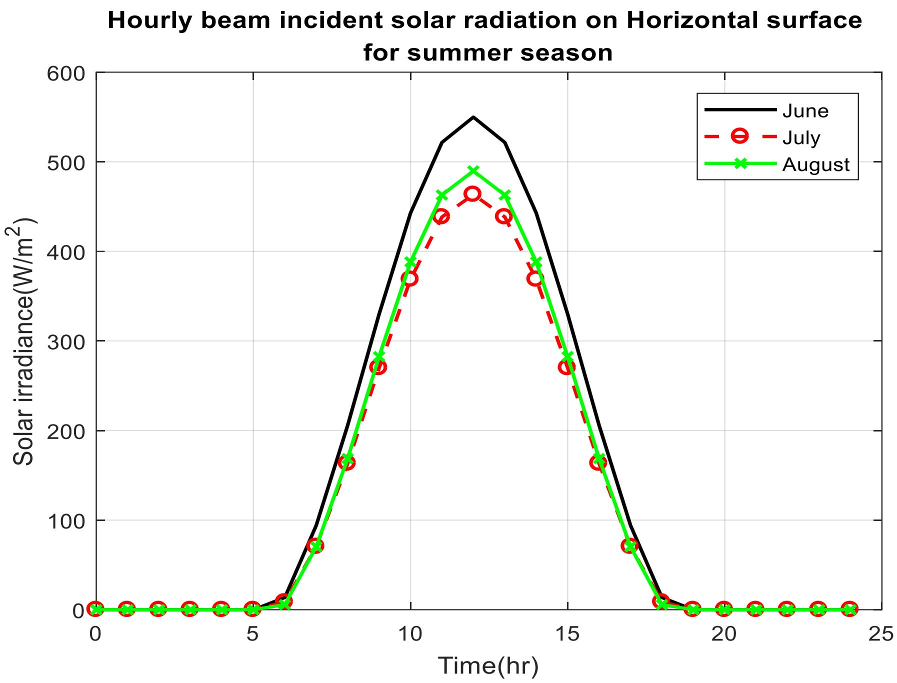

Figure 5-2 Hourly beam incident solar radiation on Horizontal surface for summer season

5.2 Hourly Beam Incident Solar Radiation on Inclined Surface

The hourly variation of the incident beam radiations falling into the collector have been simulated for different tracking mode. Four representative days with lowest beam solar radiation selected from their respective seasons of a year. A month of July, September, January and May considered from summer, autumn, winter and spring season respectively. The Hourly beam incident solar radiation on the inclined surface presented below. From Figs. 5.3,5.4,5.5 and 5.6 the result show that the beam solar radiation incident on the plane of collector largely vary with used tracking mode. In all cases lowest radiation collected during sunrise and sunset, the highest beam radiation collected during peak sun hours. The full-tracking tracking system allows collecting the highest solar energy for the whole year. At peak sun hour incident solar radiation reaches 760.34 W/m^2, 594.06W/m^2, 471.03W/m^2 and 565.40W/m^2 during winter, spring, summer and autumn season of year, respectively. Following the full tracking system maximum solar radiation could be reached with N-S tracking during a mid-day. Following N-S tracking during summer and spring higher solar radiation reaches on the collector surface using East–West horizontal tracking. The collector equipped with two-axis tracking system is most efficient than collector equipped with one tracking system for the whole year. The full-tracking mode permits collecting the highest solar energy

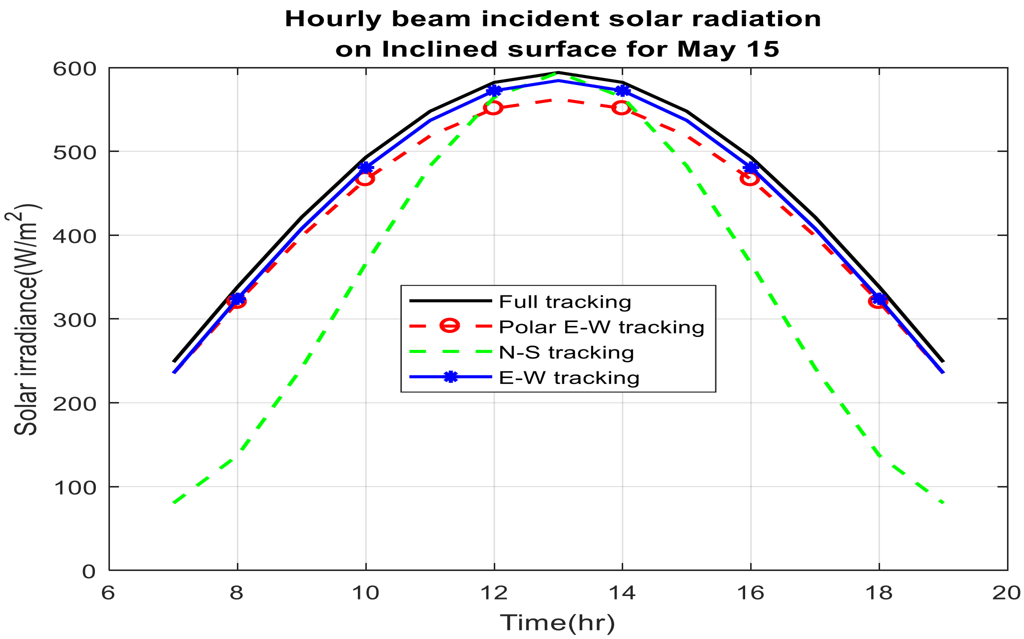

Figure 5-3 Hourly beam incident solar radiation on inclined surface on May 15

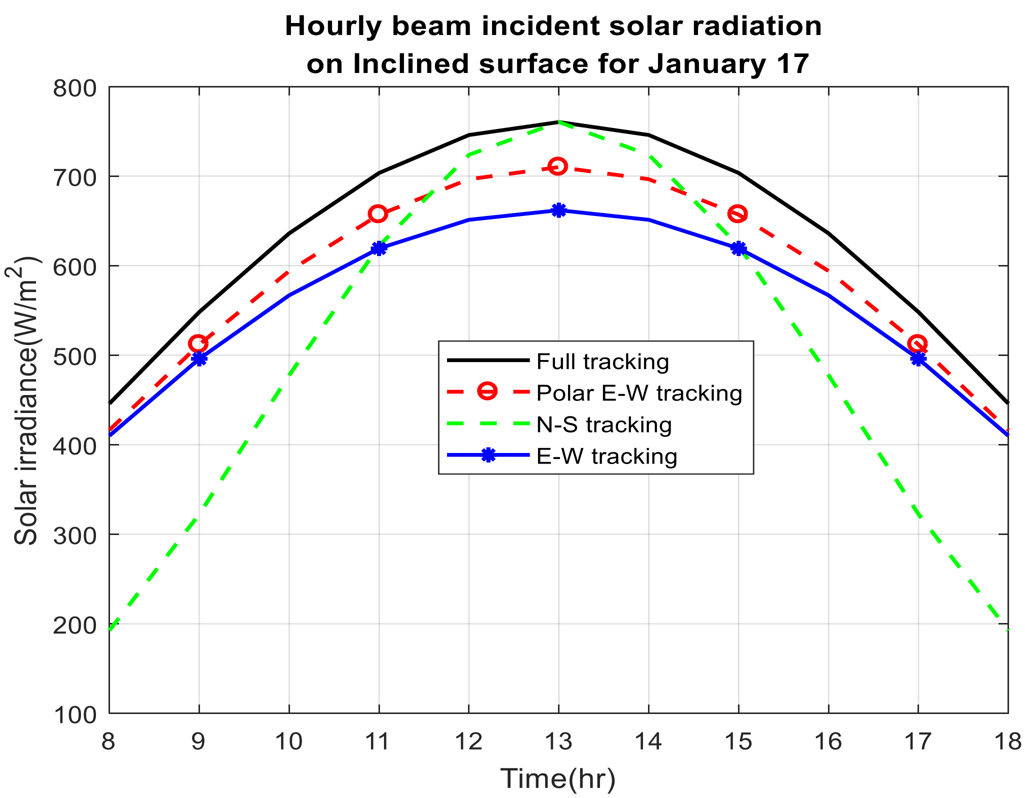

Figure 5-4 Hourly beam incident solar radiation on inclined surface on January 17

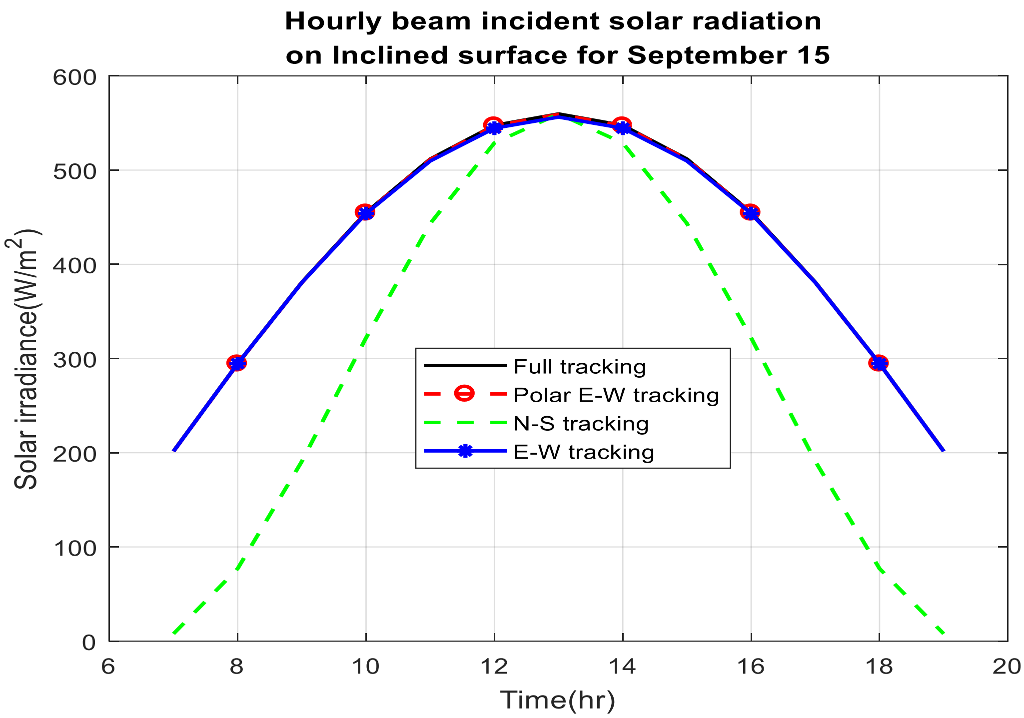

Figure 5-5 Hourly beam incident solar radiation on inclined surface on September 15

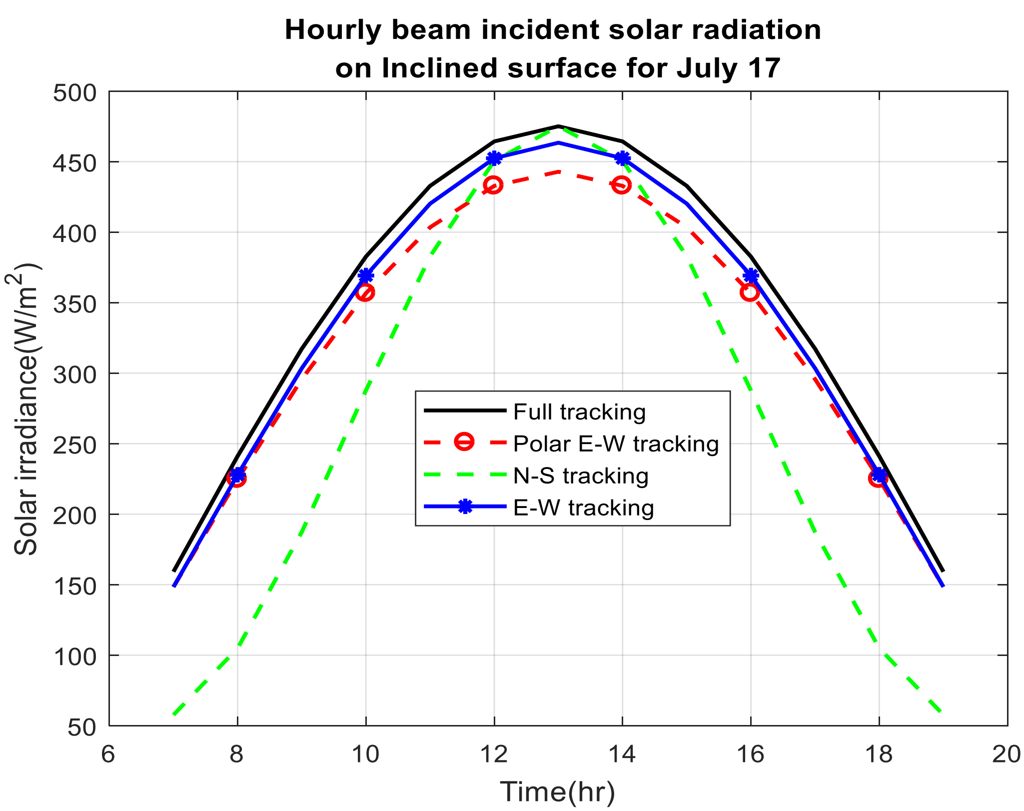

Figure 5-6 Hourly beam incident solar radiation on inclined surface on July 17

As seen from table below the polar East–West and horizontal East–West tracking systems with one axis tracking are enough tracking mode for a parabolic trough collector in the summer, spring and autumn. The horizontal North–South tracking system is more proper tracking mode than East–West horizontal tracking.

Table 5-1 Solar Energy received for different four season of a year

Tracking Mode	Solar Energy Received (KWh/m^2)			
	Winter	Summer	Autumn	Spring
Full tracking	6.92	4.47	5.34	5.85
E-W polar	6.15	4.17	5.34	5.54
E-W horizontal	4.05	4.31	5.32	5.69
N-S horizontal	5.44	3.42	3.69	4.34

5.3 Variation of Outlet temperature

The hourly variation of heat transfer fluid outlet temperature simulated using the transient mathematical model developed using Matlab. As indicated in Figure 5.7 the exit temperature from collector can reaches above temperature of 300^{o}C,the result show that the temperature variation is depend on the available solar radiation. The outlet temperature varies with the season since sunshine hour duration vary from a season to season. The hourly collector HTF oil exit temperature for other seasons are presented at APPENDIX.

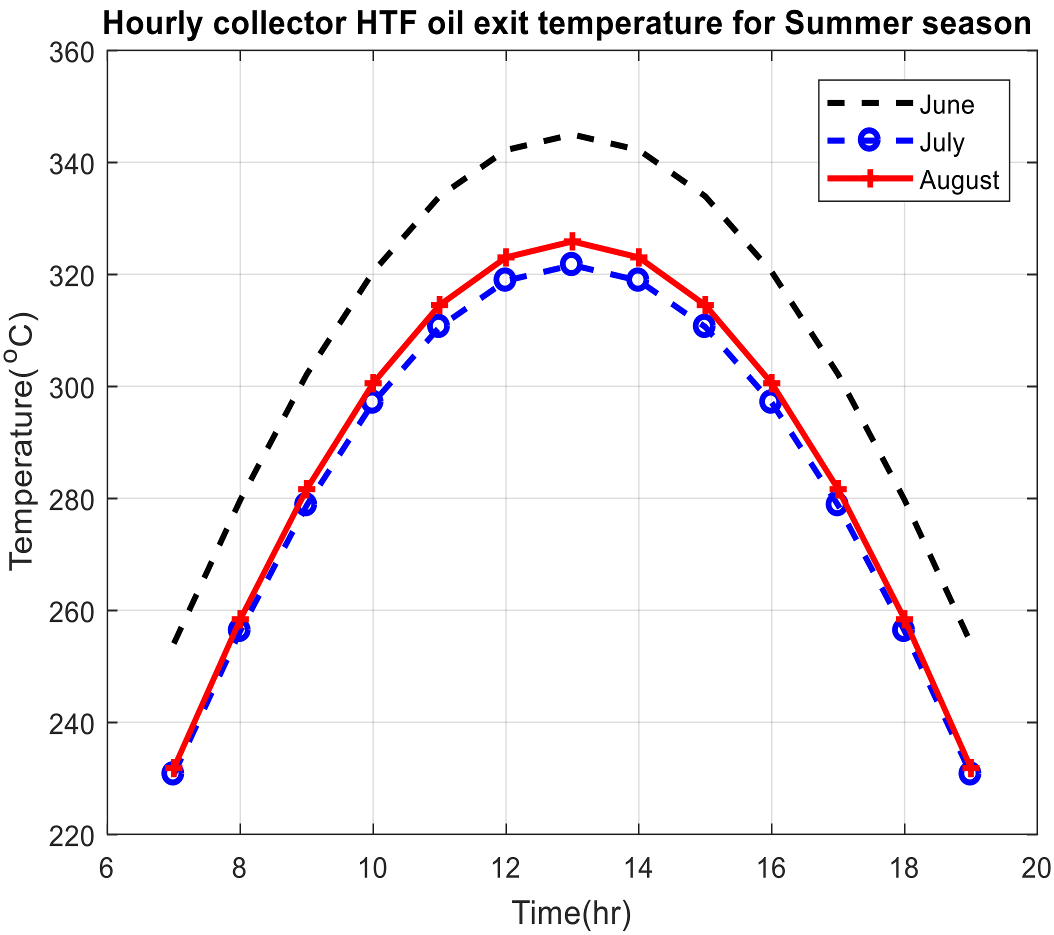

Figure 5-7 Hourly collector HTF oil exit temperature for summer season

5.4 Instantaneous useful heat gained by the collector

Instantaneous useful heat gained by a collector calculated based on the thermal model developed. The result shows that it varies significantly with from a season to season. As it can be seen from Figure 5.8 instantaneous useful heat gained for given day is maximum at solar noon. The instantaneous useful heat gained for other seasons are presented at APPENDIX.

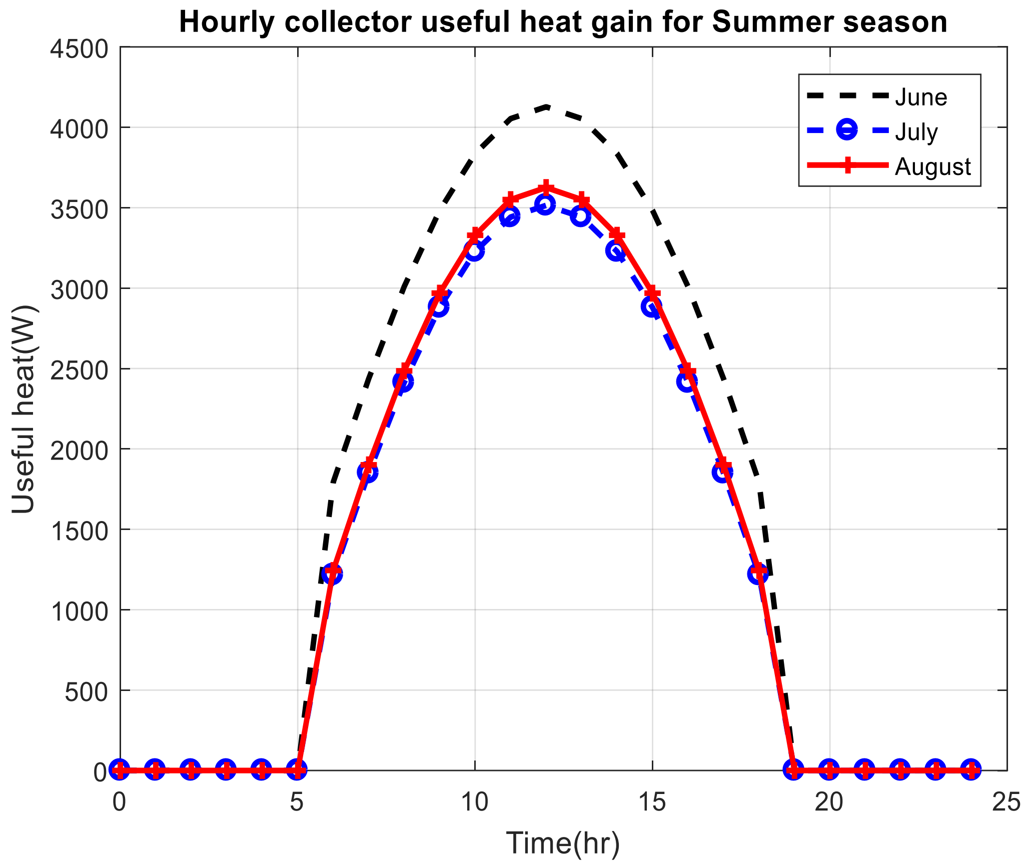

Figure 5-8 Instantaneous useful heat gained for summer season

5.5 Total daily useful heat production of collector

The daily average useful heat gain estimated for each month used for sizing of a collector and the number of collector depend on the amount of heat gain by a single collector. As indicated in figure below 33.5KW is lowest useful heat collected during a month of July using a single collector and maximum of 51.4KW useful heat collected during a month of December.

To satisfy the heat demand of Injera baking for one session cooking activity of average family size 4 parabolic collector modules and 2 parabolic collector modules connected in parallel for July and December months respectively.

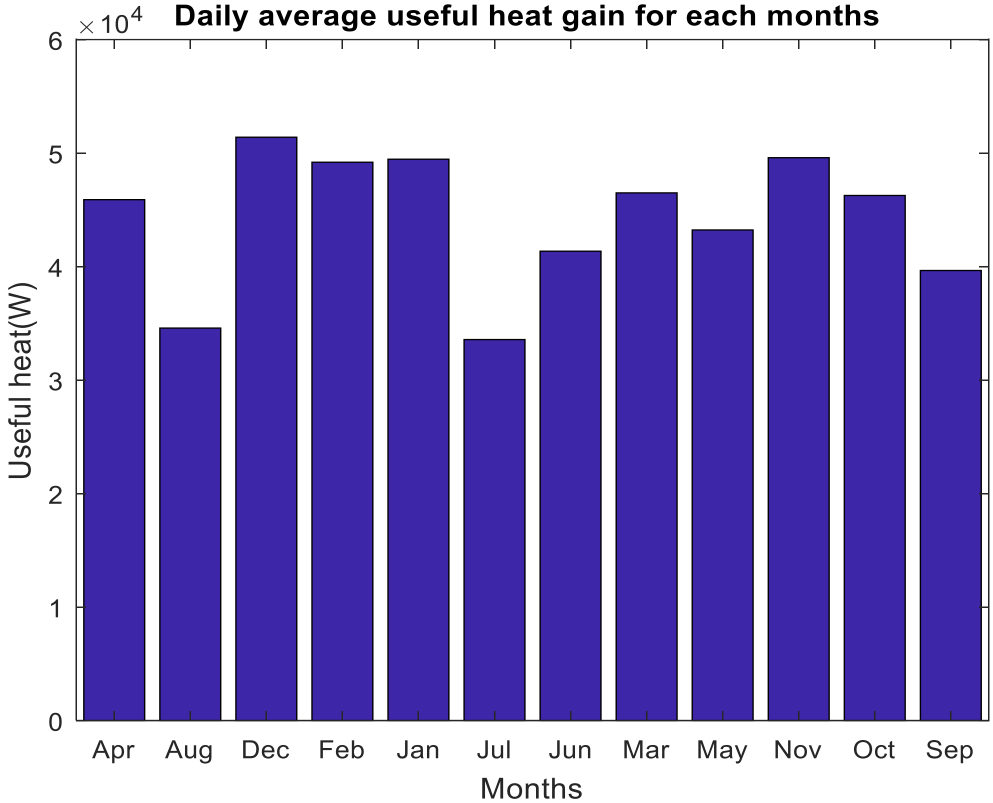

Figure 5-9 Daily average useful heat each months of a year

5.6 Efficency of the PTSC System

Using the optical model developed in the previous chapter the maximum and minimum optical efficiency of the collector calculated is equal to 68.9%% and 63.50% respectively. The Figure 5.10 indicates that lowest and highest efficiency observed during June and September respectively.

The instantaneous thermal efficiency of the solar collector depends on mass flow rate, the heat transfer fluid inlet and outlet temperature of the collector and beam solar radiation. Instantaneous total solar radiation incidence on collector surface and variation is from sunrise to sunset. The Figure 5.11 shows how the Instantaneous thermal efficiency vary throughout a day.

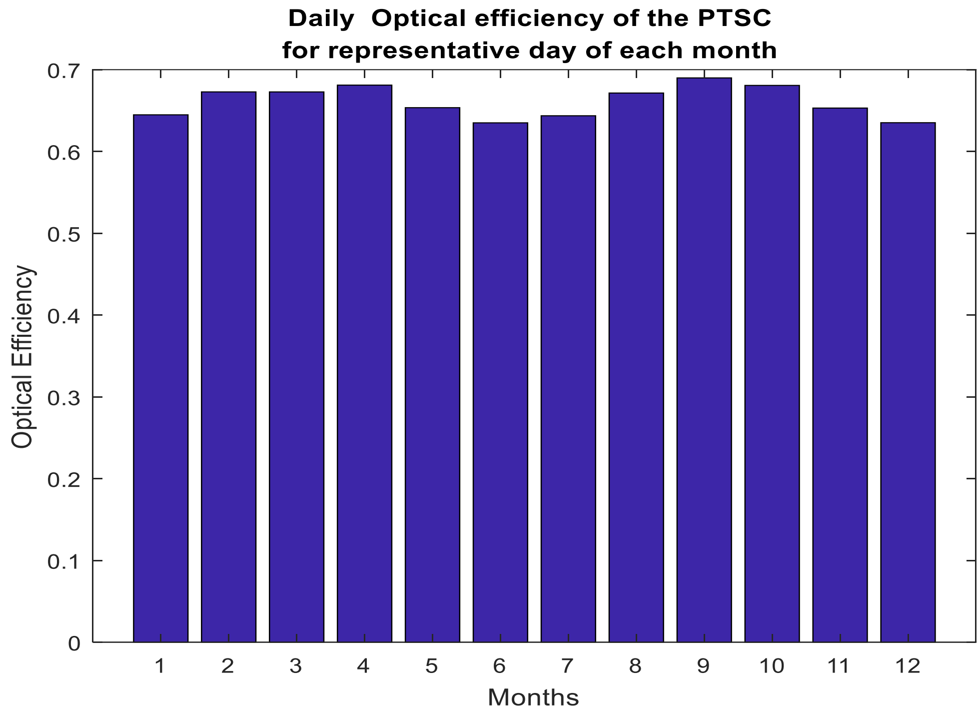

Figure 5-10 Daily optical efficiency of the PTSC for representative days of each month

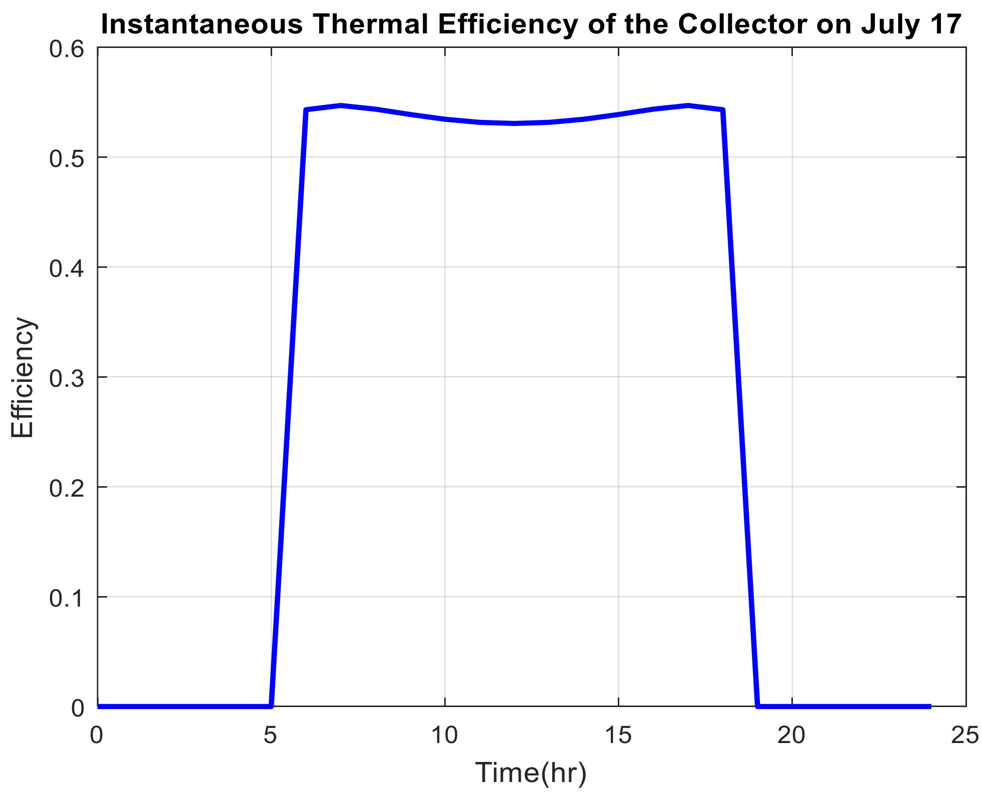

Figure 5-11 Instantaneous thermal efficiency of the collector on July 17

5.7 Temperature Variation of Phase Changing Material During Charging Process

The temperature variation phase change material studied during charging process. Initially the temperature of the PCM and HTF are same. Figure 5.12 indicate that for the first two hours only sensible heating occurs the left six hour is when the phase change process occurs.

To satisfy the heat demand of Injera baking for one session cooking activity of average family size the PCM storage tank with height of 0.3529m and diameter of 0.2352m is required. Cylindrically encapsulated capsule with diameter of 0.04m and length of 0.25m packed with a porosity of 0.25.The result shows that 168.1 Kg PCM, NaNo3 needed to store the required energy and the total number capsule required were 277.

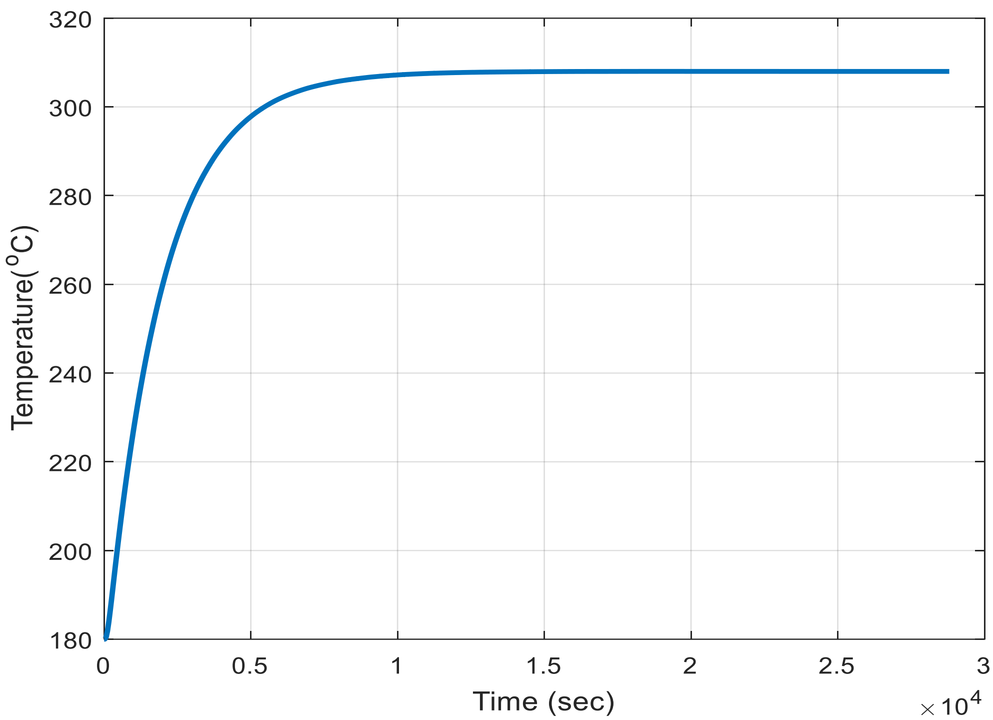

Figure 5-12 Temperature variation of phase change material during charging process on July 7

5.7.1 Validation

The mathematical model used to study the charging behavior of the PCM validated against the experimental work done by (Zheng, 2015). The PCM $NaNo_3$ encapsulated in 50.8mm diameter and 127mm height with mass of 269.6 kg. The Figure 5.13 indicates that the result plots have similar shape.

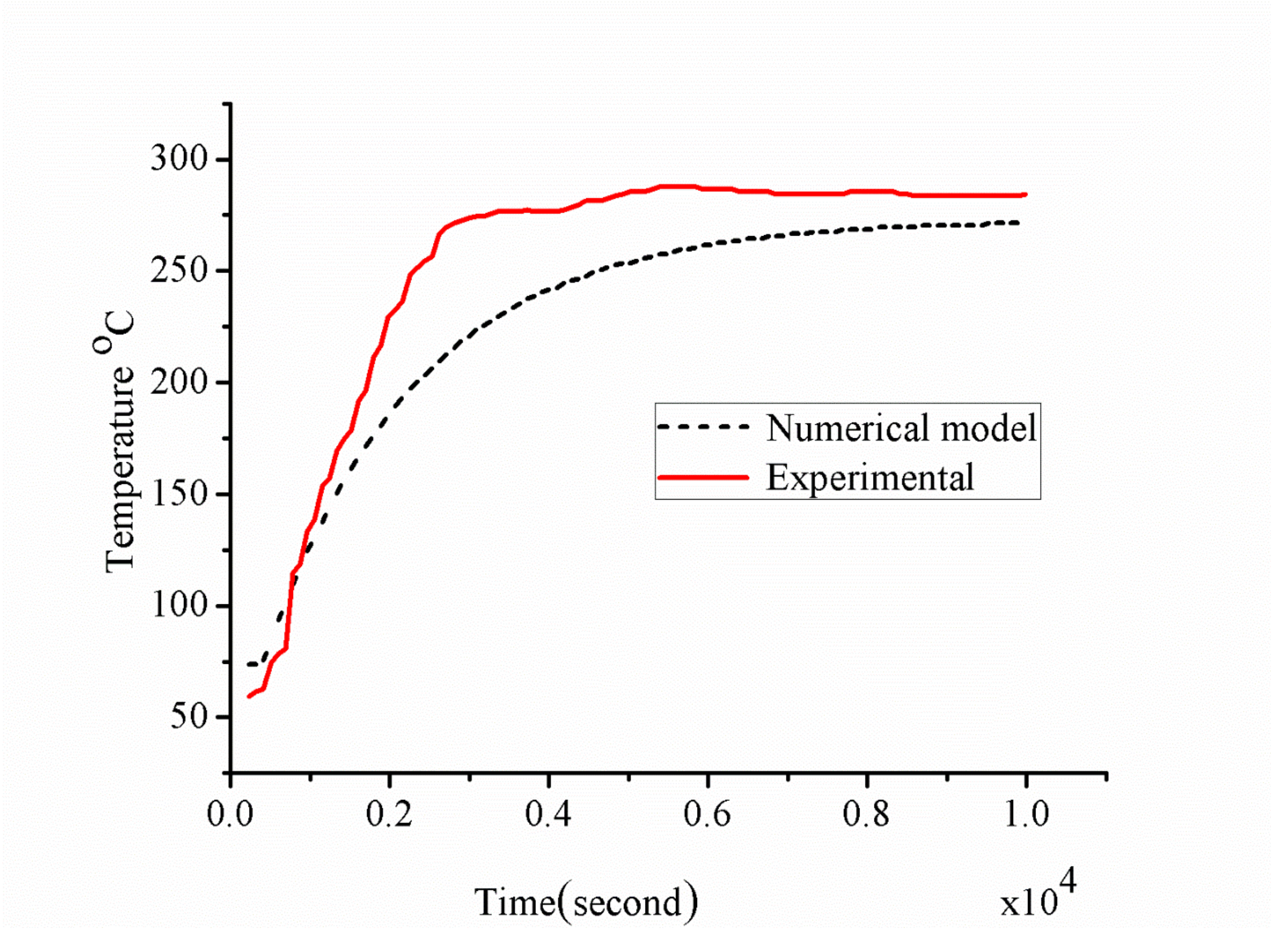

Figure 5-13 Temperature history of the PCM on charging from experiment (Zheng, 2015)

5.8 Transient analysis of baking pan

Form the mathematical modeling developed for the baking pan in the previous chapter the heating up time investigated using two different therma oils. As shown below in the Figure 5.14. The heating up time required to reach pan surface temperature of 200°c is around 385 sec and 432 sec respectively for Shell Thermia oil and Syltherm 800.

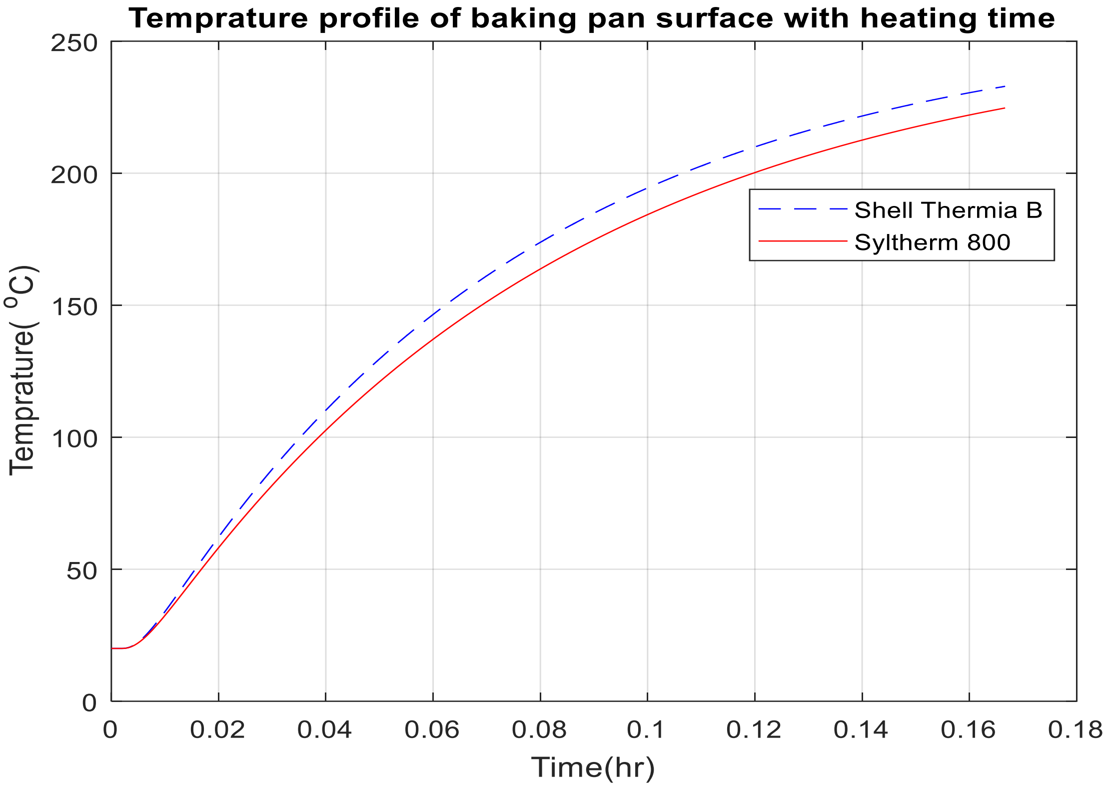

Figure 5-14 Temperature profile of baking pan surface with heating time

CHAPTER 6

CONCLUSIONS AND RECOMMENDATIONS

6.1 Conclusions

The present work composed of numerically modelling the performance of parabolic trough solar collector integrated with latent thermal energy storage for Injera baking application. The cooking demand of Injera baking for average family size consumed for three days were estimated. Based on this demand the size of parabolic trough solar collector and thermal energy storage system designed.

Solar radiation model was developed using a matlab to analysis the solar energy potential based on climate condition of Adama city based on data found from National Metrological Agency. The four sun-tracking techniques have been studied to evidence the best configuration that collect maximum energy. The result shows that Polar East–West and horizontal East–West tracking systems were best appropriate for a parabolic trough collector throughout the entire year.

One dimensional model was developed to analysis parabolic trough solar collector and the heat transfer in latent thermal energy storage. Transient mathematical model was developed and solved using a finite difference method implemented by using the Matlab'spdepe solver

The result of numerical simulations shows that the outlet temperature from the studied collector can reaches above 300^{o}C with mass flow rate of 0.0125kg/s. Four and two parabolic collector modules should be used in order to cover the cooking demand during July and December month. This result shows that the parabolic trough solar collector was the best choice for the problem.

Charging performance of the thermal energy storage was analyzed with NaNo3 as phase change material. The result shows that 168.1 Kg PCM, NaNo3 needed to store the required energy and the total number capsule required were 277

6.2 Recommendations

From the study reviles that besides the Injera baking application it is recommended to consider the concentrating solar thermal power plant using parabolic trough solar collector around Adama city .

Based on the results from this study the following points can be recommended for future work

- ✓ Experimental investigation should be done in order to model the system accurately
- ✓ Cost analysis of the overall system can be used for future commercialization and financial feasibility.
- ✓ Optimizing the system and designing the institutional cooking for large scale cooking demand

REFERENCES

A.Allouhi, Amine, M. B., T.Kousksou, A.Jamil, & k.Lahrech. (2018). Yearly performance of low-enthalpy parabolic trough collectors in MENA region according to different sun-tracking strategies. *Applied Thermal Engineering*, *128*, 1404–1419. https://doi.org/10.1016/j.applthermaleng.2017.09.099

Alva, G., Lin, Y., & Fang, G. (2018). An overview of thermal energy storage systems. *Energy*, *144*, 341–378. https://doi.org/10.1016/j.energy.2017.12.037

Alva, G., Liu, L., Huang, X., & Fang, G. (2017). Thermal energy storage materials and systems for solar energy applications. *Renewable and Sustainable Energy Reviews*, *68*, 693–706. https://doi.org/10.1016/j.rser.2016.10.021

Ambaw, G. (2015). *Performance analysis and reliablity testing of a ceramic bake ware for an electric injera baking stove*. Master Thesis Addis abeba university.

Bellos, E., Tzivanidis, C., & Belessiotis, V. (2017). Daily performance of parabolic trough solar collectors. *Solar Energy*, *158*(September), 663–678. https://doi.org/10.1016/j.solener.2017.10.038

Chahine, K., Murr, R., Ramadan, M., Hage, H. El, & Khaled, M. (2018). Use of parabolic troughs in HVAC applications - Design calculations and analysis. *Case Studies in Thermal Engineering*, *12*(May), 285–291. https://doi.org/10.1016/j.csite.2018.04.016

Crespo, A., Barreneche, C., Ibarra, M., & Platzer, W. (2018). Latent thermal energy storage for solar process heat applications at medium- high temperatures – A review. *Solar Energy*, *April*, 1–32. https://doi.org/10.1016/j.solener.2018.06.101

Duffie, J. A., & Beckman, W. A. (2013). *of Thermal Processes Solar Engineering*.

Getenet, G. (2011). *Heat transfer analysis during the process of injera*. Master Thesis Addis abeba university.

Ghodbane, M., & Boumeddane, B. (2018). A numerical analysis of the energy behavior of a parabolic trough concentrator. *Journal of Fundamental and Applied Sciences*, *8*(3), 671.

https://doi.org/10.4314/jfas.v8i3.2

Goytom, D. (2016). *Finite Difference Modelling of Solar Thermal Powered Injera Baking Oven*. *3*(12). https://doi.org/10.17148/IARJSET.2016.31223

Gracia, A. De, & Cabeza, L. F. (2014). *Numerical simulation of a PCM packed bed system : A review*. 1–29.

Hafez, A. Z., Attia, A. M., Eltwab, H. S., ElKousy, A. O., Afifi, A. A., AbdElhamid, A. G., AbdElqader, A. N., Fateen, S. E. K., El-Metwally, K. A., Soliman, A., & Ismail, I. M. (2018). Design analysis of solar parabolic trough thermal collectors. *Renewable and Sustainable Energy Reviews*, *82*(June 2017), 1215–1260. https://doi.org/10.1016/j.rser.2017.09.010

Hailu, M. H., Tesfay, A. H., & Bayray, M. (2017). *A Direct Solar Fryer for Injera Baking Application*. *July 2018*. https://doi.org/10.18086/swc.2017.24.02

Hassen, A. A., Amibe, D. A., & Nydal, O. J. (2011). *PERFORMANCE INVESTIGATION OF SOLAR POWERED INJERA BAKING OVEN FOR INDOOR COOKING*.

Incropera, F. P., Bergman, T. L., Lavine, A., & Dewitt, D. P. (2011). *Fundamentals of Heat and Mass Transfer*.

Kalogirou, S. A. (2012). A detailed thermal model of a parabolic trough collector receiver. *Energy*, *48*(1), 298–306. https://doi.org/10.1016/j.energy.2012.06.023

Kalogirou, S. A. (2014). Copyright. In *Solar Energy Engineering*. https://doi.org/10.1016/b978-0-12-374501-9.00014-5

Kasaiean, A., Sameti, M., Daneshazarian, R., & Noori, Z. (2018). Heat transfer network for a parabolic trough collector as a heat collecting element using nano fl uid. *Renewable Energy*, *123*, 439–449. https://doi.org/10.1016/j.renene.2018.02.062

Khairul, I. (2016). *PERFORMANCE ANALYSIS OF PARABOLIC TROUGH CONCENTRATED SOLAR SYSTEM MD . KHAIRUL ISLAM DISSERTATION SUBMITTED IN FULFILLMENT OF THE REQUREMENTS FOR THE DEGREE OF MASTER OF PHILOSOPHY INSTITUTE OF GRADUATE STUDIES UNIVERSITY OF MALAYA*.

Kumar, A., & Shukla, S. K. (2018). *Solar thermal energy storage*. *January*.

Kumar, D., & Kumar, S. (2015). Year-round performance assessment of a solar parabolic trough collector under climatic condition of Bhiwani , India : A case study. *Energy Conversion and Management*, *106*, 224–234. https://doi.org/10.1016/j.enconman.2015.09.044

Lamrani, B., Khouya, A., Zeghmati, B., & Draoui, A. (2018). Mathematical modeling and numerical simulation of a parabolic trough collector: A case study in thermal engineering. *Thermal Science and Engineering Progress*, *8*(March), 47–54. https://doi.org/10.1016/j.tsep.2018.07.015

Magendran, S. S., Saleem, F., Khan, A., Mubarak, N. M., Vaka, M., & Karri, R. (2019). *Nano-Structures & Nano-Objects Synthesis of organic phase change materials (PCM) for energy storage applications : A review*. *20*(2019).

Marefati, M., Mehrpooya, M., & Shafii, M. B. (2018). Optical and thermal analysis of a parabolic trough solar collector for production of thermal energy in different climates in Iran with comparison between the conventional nanofluids. *Journal of Cleaner Production*, *175*, 294–313. https://doi.org/10.1016/j.jclepro.2017.12.080

Marif, Y., Benmoussa, H., Bouguettaia, H., Belhadj, M. M., & Zerrouki, M. (2014). Numerical simulation of solar parabolic trough collector performance in the Algeria Saharan region Numerical simulation of solar parabolic trough collector performance in the Algeria Saharan region. *Energy Conversion and Management*, *85*(September), 521–529. https://doi.org/10.1016/j.enconman.2014.06.002

Mawire, & Shobo. (2015). *Numerical investigation of a packed bed thermal energy storage system for solar cooking using encapsulated phase change material*. *May*, 254–259.

Mofijur, M., Meurah, T., Mahlia, I., Silitonga, A. S., Ong, H. C., Silakhori, M., Hasan, M. H., Putra, N., & Rahman, S. M. A. (2019). *Phase Change Materials (PCM) for Solar Energy Usages and Storage : An Overview*. 1–20.

Mokheimer, E. M. A., Dabwan, Y. N., Habib, M. A., Said, S. A. M., & Al-sulaiman, F. A. (2014). Techno-economic performance analysis of parabolic trough collector in Dhahran , Saudi Arabia. *Energy Conversion and Management*, *86*, 622–633.

https://doi.org/10.1016/j.enconman.2014.06.023

Muthusivagami, R. M., Velraj, R., & Sethumadhavan, R. (2010). *Solar cookers with and without thermal storage — A review*. *14*, 691–701. https://doi.org/10.1016/j.rser.2008.08.018

Mwesigye, A., Halil, Y., & Meyer, J. P. (2018). *Numerical analysis of the thermal and thermodynamic performance of a parabolic trough solar collector using SWCNTs-Therminol ® VP-1 nano fl uid*. *119*, 844–862. https://doi.org/10.1016/j.renene.2017.10.047

Nergy, E., Ivision, P. O. E. N. D., Niversity, C. R. U., Edfordshire, B., & Kingdom, U. (2018). *Review of PCMs and heat transfer enhancement methods applied in parabolic trough solar plants thermal storage systems*. *37*(1), 96–107.

Ouagued, M., Khellaf, A., & Loukarfi, L. (2013). Estimation of the temperature , heat gain and heat loss by solar parabolic trough collector under Algerian climate using different thermal oils. *Energy Conversion and Management*, *75*, 191–201. https://doi.org/10.1016/j.enconman.2013.06.011

Padilla, R. V., Demirkaya, G., Goswami, D. Y., Stefanakos, E., & Rahman, M. M. (2011). Heat transfer analysis of parabolic trough solar receiver. *Applied Energy*, *88*(12), 5097–5110. https://doi.org/10.1016/j.apenergy.2011.07.012

Solomon, L., Elmozughi, A. F., Neti, S., & Oztekin, A. (2014). *High Temperature Thermal Energy Storage Using EPCM : The Effect of Void*. *April 2017*. https://doi.org/10.1115/IMECE2014-37306

Tesfay, Asfafaw H, Kahsay, M. B., & Nydal, O. J. (2015). *Solar cookers with latent heat storage for intensive cooking application*. *November*, 8–12.

Tesfay, Asfafaw Haileselas, Bayray, M., & Jørgen, O. (2014). Solar powered heat storage for Injera baking in Ethiopia. *Energy Procedia*, *57*, 1603–1612. https://doi.org/10.1016/j.egypro.2014.10.152

Tiwari, G. ., Tiwari, A., & Tiwari, S. (2016). *Handbook of Solar Energy*.

Tsegay, M. M. (2011). *Design and manufacture of laboratory model for solar powered injera baking oven*. Addis Abeba University.

Tzivanidis, C, Bellos, E., Korres, D., Antonopoulos, K. A., & Mitsopoulos, G. (2015). Case Studies in Thermal Engineering Thermal and optical efficiency investigation of a parabolic trough collector. *Case Studies in Thermal Engineering*, *6*, 226–237. https://doi.org/10.1016/j.csite.2015.10.005

Tzivanidis, Christos, & Bellos, E. (2016). The use of parabolic trough collectors for solar cooling - A case study for Athens climate. *Case Studies in Thermal Engineering*, *8*(October), 403–413. https://doi.org/10.1016/j.csite.2016.10.003

Wei, G., Wang, G., Xu, C., Ju, X., Xing, L., Du, X., & Yang, Y. (2018). Selection principles and thermophysical properties of high temperature phase change materials for thermal energy storage : A review. *Renewable and Sustainable Energy Reviews*, *81*(June 2017), 1771–1786. https://doi.org/10.1016/j.rser.2017.05.271

Yılmaz, İ. H., & Mwesigye, A. (2018). Modeling, simulation and performance analysis of parabolic trough solar collectors: A comprehensive review. *Applied Energy*, *225*(February), 135–174. https://doi.org/10.1016/j.apenergy.2018.05.014

Zheng, Y. (2015). *Thermal Energy Storage with Encapsulated Phase Change Materials for High Temperature Applications*.

APPENDIX

ANNEX A: Variation of Outlet temperature

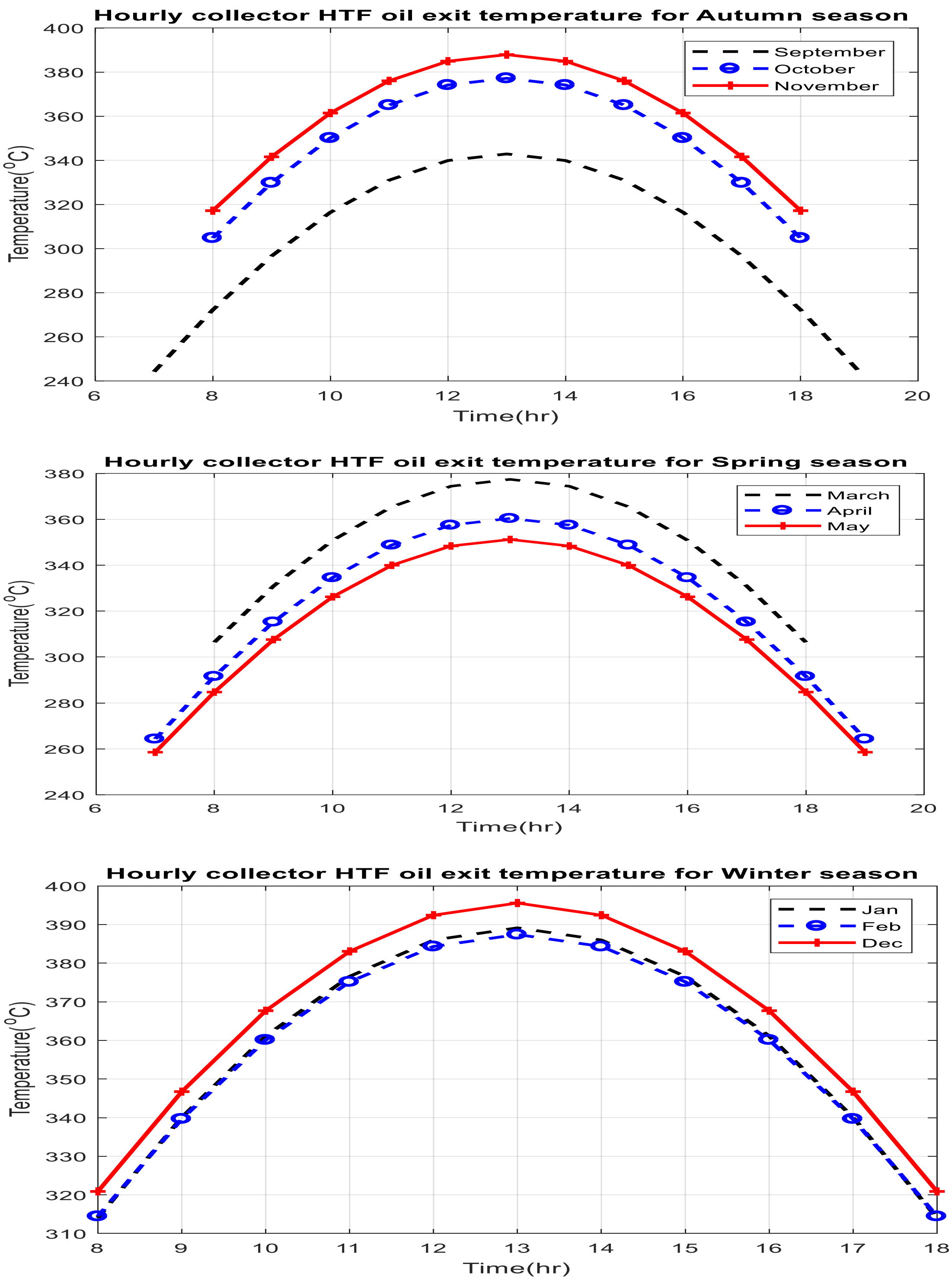

Figure A.1: Hourly variation of outlet Temperature for different season

ANNEX B: Hourly beam incident solar radiation on inclined surface

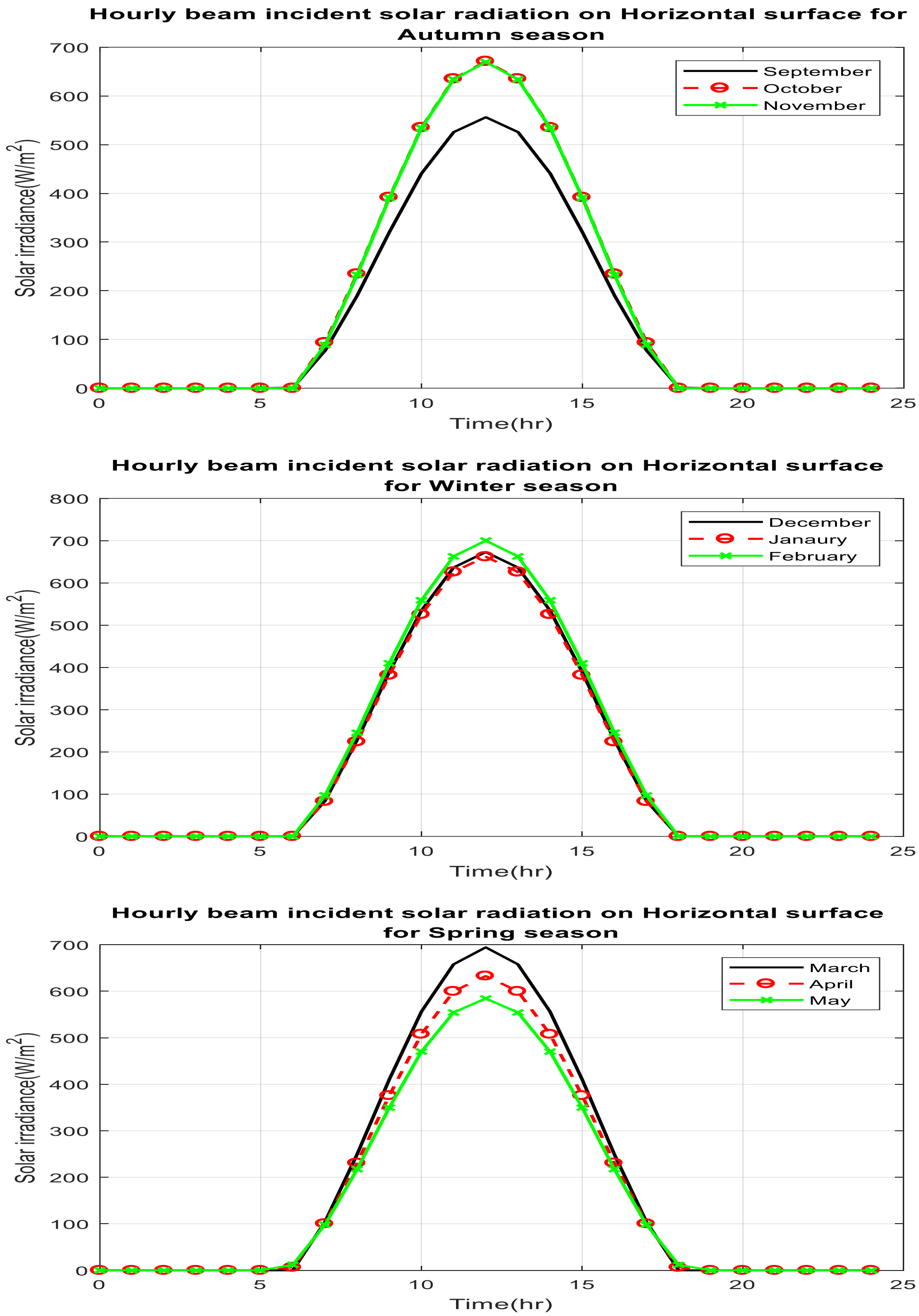

Figure B:1 Hourly beam incident solar radiation on inclined surface for different season

ANNEX C :Instantaneous useful heat gain

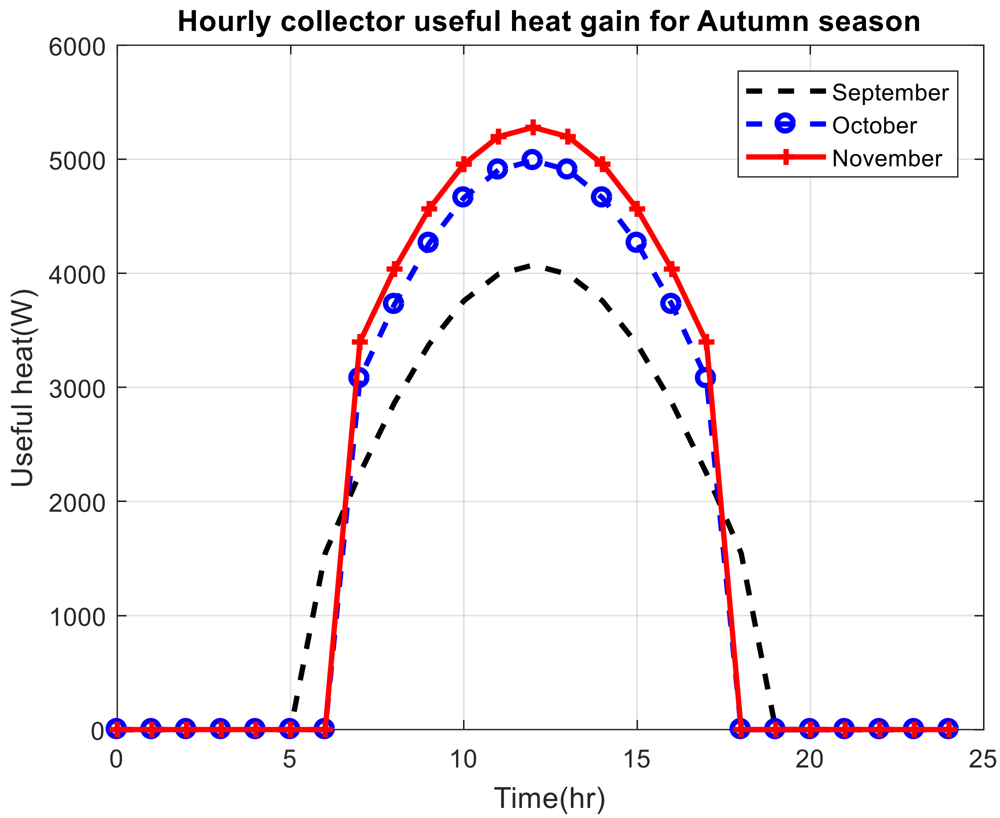

ANNEX D:Heat transfer oil properties

a) Syltherm 800

CARACTERISTIQUES PHYSIQUES DES FLUIDES THERMIQUES
PHYSICAL DATA OF THERMAL FLUIDS

SYLTHERM 800 d'après les données de la société **DOW CHEMICAL**
from ***DOW CHEMICAL*** *data*

température θ *temperature*	masse volum. ρ *density*	chaleur spécifique Cp *specific heat*		viscosité dynamique μ *dynamic viscosity*		conductivité thermique λ *thermal conductivity*		pression de vapeur Ps *vapor pressure*	
°C	kg/m3	J/kg.K	kcal/kg.°C	Pa.s	kg/m.h	W/m.K	kcal/h.m.°C	Pa (abs)	bar(rel.) *barg*
-40	991	1506	0,360	0,051050	183,780	0,1463	0,1258		
0	953	1574	0,376	0,015330	55,188	0,1388	0,1194		
40	917	1643	0,393	0,007000	25,200	0,1312	0,1128	100	
80	882	1711	0,409	0,003860	13,896	0,1237	0,1064	1460	
120	846	1779	0,425	0,002360	8,496	0,1162	0,0999	9300	-0,92
160	810	1847	0,441	0,001540	5,544	0,1087	0,0935	35000	-0,66
200	773	1916	0,458	0,001050	3,780	0,1012	0,0870	94600	-0,07
240	734	1984	0,474	0,000740	2,664	0,0936	0,0805	204800	1,03
280	693	2052	0,490	0,000540	1,944	0,0861	0,0741	380200	2,79
320	648	2121	0,507	0,000410	1,476	0,0786	0,0676	630500	5,29
360	600	2189	0,523	0,000310	1,116	0,0711	0,0612	961200	8,60
400	547	2257	0,539	0,000250	0,900	0,0635	0,0546	1373000	12,72

b) Shell thermia B

Temperature °C	0	20	40	100	150	200	250	300	340
Density Kg/m^3	876	863	850	811	778	746	713	681	655
Specific Heat Capacity KJ/kg K	1.809	1.882	1.954	2.173	2.355	2.538	2.72	2.902	3.048
Thermal Conductivity W/m K	0.136	0.134	0.133	0.128	0.125	0.121	0.118	0.114	0.111
Prandtl No	3375	919	375	69	32	20	14	11	9

ANNEX E: Matlab code

The following matlab code used to calculate the hourly beam solar irradiation on horizontal surfice (solar power received over 24 hr for representative day of each month) and hourly beam incident sola radiation on horizontal surface.

```
% January
phi=8.51447;%latitude of Adama
H1=22.0136;%Monthly mean daily Global radiation (MJ/m^2)
Hd1=6.193538816;%%Monthly mean daily diffuse radiation (MJ/m^2)
ws1=86.71978842; %the sunset-hour angle
n1=17;%n for the mean day of the month
dec1=23.5*sind((360*(284+n1)/365));%Declination
i=0:24;% Time of the day
w=(i-12)*(15);
a1=0.409+0.5016*sind((ws1-60));
b1=0.6609-0.4767*sin((ws1-60)*pi/180);
rt1=(pi()/24)*(a1+b1*cos(w*pi/180)).*(cos(w*pi/180)-cos(ws1*pi/180))/(sin(ws1*pi/180)-
(pi/180)*ws1*(cos(ws1*pi/180)));
I1=(rt1.*H1)*10^6/3600;%Monthly average hourly Global radiation in (W/m^2)
I1(I1<0)=0;
rd1=(pi()/24)*(cos(w*pi/180)-cos(ws1*pi/180))/(sin(ws1*pi/180)(pi/180)*ws1*(cos(ws1*pi/180)));
ID1=(rd1.*Hd1)*10^6/3600;
ID1(ID1<0)=0;
IB1=I1-ID1;%hourly beam solar radiation on horizontal surface for January
%February
H2=23.6287;%Monthly mean daily Global radiation (MJ/m^2)
Hd2=6.68517;%Monthly mean daily diffuse radiation
```

```
ws2=88.02644528; %the sunset-hour angle
n2=47;%n for the mean day of the month
dec2=23.5*sin((360*(284+n2)/365)*pi/180);
a2=0.409+0.5016*sin((ws2-60)*pi/180);
b2=0.6609-0.4767*sin((ws2-60)*pi/180);
rt2=(pi()/24)*(a2+b2*cos(w*pi/180)).*(cos(w*pi/180)-cos(ws2*pi/180))/(sin(ws2*pi/180)-
(pi/180)*ws2*(cos(ws2*pi/180)));
I2=(rt2.*H2)*10^6/3600;%Monthly mean hourly Global radiation
I2(I2<0)=0;
rd2=(pi()/24)*(cos(w*pi/180)-cos(ws2*pi/180))/(sin(ws2*pi/180)-(pi/180)*ws2*(cos(ws2*pi/180)));
ID2=(rd2.*Hd2)*10^6/3600;
ID2(ID2<0)=0;
IB2=I2-ID2;%hourly beam solar radiation on horizontal surface for February
% march
H3=24.76619285;%Monthly mean daily Global radiation (MJ/m^2)
Hd3=7.775268886;
ws3=89.63782515; %the sunset-hour angle
n3=75;
dec3=23.5*sin((360*(284+n3)/365)*pi/180);
a3=0.409+0.5016*sin((ws3-60)*pi/180);
b3=0.6609-0.4767*sin((ws3-60)*pi/180);
i=0:24;
w=(i-12)*(15);
rt3=(pi()/24)*(a3+b3*cos(w*pi/180)).*(cos(w*pi/180)-cos(ws3*pi/180))/(sin(ws3*pi/180)-
(pi/180)*ws3*(cos(ws3*pi/180)));
I3=(rt3.*H3)*10^6/3600;%Monthly mean hourly Global radiation
I3(I3<0)=0;
rd3=(pi()/24)*(cos(w*pi/180)-cos(ws3*pi/180))/(sin(ws3*pi/180)-(pi/180)*ws3*(cos(ws3*pi/180)));
ID3=(rd3.*Hd3)*10^6/3600;
ID3(ID3<0)=0;
IB3=I3-ID3;%hourly beam solar radiation on horizontal surface for March
% April
H4=24.65469271;%Monthly mean daily Global radiation (MJ/m^2)
Hd4=9.048121748;
ws4=91.4224681; %the sunset-hour angle
n4=105;
dec4=23.5*sin((360*(284+n4)/365)*pi/180);
```

```
a4=0.409+0.5016*sin((ws4-60)*pi/180);
b4=0.6609-0.4767*sin((ws4-60)*pi/180);
i=0:24;
w=(i-12)*(15);
cozeta4=(sin(phi*pi/180))*(sin(dec4*pi/180))+(cos(phi*pi/180))*(cos(dec4*pi/180))*(cos(w*pi/180));
rt4=(pi()/24)*(a4+b4*cos(w*pi/180)).*(cos(w*pi/180)-cos(ws4*pi/180))/(sin(ws4*pi/180)-
(pi/180)*ws4*(cos(ws4*pi/180)));
I4=(rt4.*H4)*10^6/3600;%Monthly mean hourly Global radiation
I4(I4<0)=0;
%may
phi=8.51447;
H5=23.90551221;%Monthly mean daily Global radiation (MJ/m^2)
Hd5=9.361648174;
ws5=92.92000521; %the sunset-hour angle
n5=135;
dec5=23.5*sin((360*(284+n5)/365)*pi/180);
a5=0.409+0.5016*sin((ws5-60)*pi/180);
b5=0.6609-0.4767*sin((ws5-60)*pi/180);
i=0:24;
w=(i-12)*(15);
cozeta5=(sin(phi*pi/180))*(sin(dec5*pi/180))+(cos(phi*pi/180))*(cos(dec5*pi/180))*(cos(w*pi/180));
rt5=(pi()/24)*(a5+b5*cos(w*pi/180)).*(cos(w*pi/180)-cos(ws5*pi/180))/(sin(ws5*pi/180)-
(pi/180)*ws5*(cos(ws5*pi/180)));
I5=(rt5.*H5)*10^6/3600;%Monthly mean hourly Global radiation
I5(I5<0)=0;
costetap5=cos(dec5*pi/180);%Polar N–S axis with E–W tracking
%June
H6=23.21478797;%Monthly mean daily Global radiation (MJ/m^2)
Hd6=9.489043309;
ws6=93.65869767; %the sunset-hour angle
n6=162;
dec6=23.5*sin((360*(284+n6)/365)*pi/180);
a6=0.409+0.5016*sin((ws6-60)*pi/180);
b6=0.6609-0.4767*sin((ws6-60)*pi/180);
i=0:24;
w=(i-12)*(15);
cozeta6=(sin(phi*pi/180))*(sin(dec6*pi/180))+(cos(phi*pi/180))*(cos(dec6*pi/180))*(cos(w*pi/180));
```

```
rt6=(pi()/24)*(a6+b6*cos(w*pi/180)).*(cos(w*pi/180)-cos(ws6*pi/180))/(sin(ws6*pi/180)-
(pi/180)*ws6*(cos(ws6*pi/180)));
I6=(rt6.*H6)*10^6/3600;%Monthly mean hourly Global radiation
I6(I6<0)=0;
rd6=(pi()/24)*(cos(w*pi/180)-cos(ws6*pi/180))/(sin(ws6*pi/180)-(pi/180)*ws6*(cos(ws6*pi/180)));
%July
H7=21.91360564;%Monthly mean daily Global radiation (MJ/m^2)
Hd7=10.58101182;
ws7=93.32613512; %the sunset-hour angle
n7=198;
dec7=23.5*sin((360*(284+n7)/365)*pi/180);
a7=0.409+0.5016*sin((ws7-60)*pi/180);
b7=0.6609-0.4767*sin((ws7-60)*pi/180);
i=0:24;
w=(i-12)*(15);
rt7=(pi()/24)*(a7+b7*cos(w*pi/180)).*(cos(w*pi/180)-cos(ws7*pi/180))/(sin(ws7*pi/180)-
(pi/180)*ws7*(cos(ws7*pi/180)));
I7=(rt7.*H7)*10^6/3600;%Monthly mean hourly Global radiation
I7(I7<0)=0;
%August
H8=22.51708448;%Monthly mean daily Global radiation (MJ/m^2)
Hd8=10.64483905;
ws8=92.05263537; %the sunset-hour angle
n8=228;
dec8=23.5*sin((360*(284+n8)/365)*pi/180);
a8=0.409+0.5016*sin((ws8-60)*pi/180);
b8=0.6609-0.4767*sin((ws8-60)*pi/180);
i=0:24;
w=(i-12)*(15);
rt8=(pi()/24)*(a8+b8*cos(w*pi/180)).*(cos(w*pi/180)-cos(ws8*pi/180))/(sin(ws8*pi/180)-
(pi/180)*ws8*(cos(ws8*pi/180)));
I8=(rt8.*H8)*10^6/3600;%Monthly mean hourly Global radiation
I8(I8<0)=0;
% September
H9=23.34159419;%Monthly mean daily Global radiation (MJ/m^2)
Hd9=9.917736322;
ws9=90.3320562; %the sunset-hour angle
```

```
n9=258;
dec9=23.5*sin((360*(284+n9)/365)*pi/180);
a9=0.409+0.5016*sin((ws9-60)*pi/180);
b9=0.6609-0.4767*sin((ws9-60)*pi/180);
i=0:24;
w=(i-12)*(15);
rt9=(pi()/24)*(a9+b9*cos(w*pi/180)).*(cos(w*pi/180)-cos(ws9*pi/180))/(sin(ws9*pi/180)-
(pi/180)*ws9*(cos(ws9*pi/180)));
I9=(rt9.*H9)*10^6/3600;%Monthly mean hourly Global radiation
I9(I9<0)=0;
%October
H10=23.68631637;%Monthly mean daily Global radiation (MJ/m^2)
Hd10=7.435655378;
ws10=88.54912629; %the sunset-hour angle
n10=288;
dec10=23.5*sin((360*(284+n10)/365)*pi/180);
a10=0.409+0.5016*sin((ws10-60)*pi/180);
b10=0.6609-0.4767*sin((ws10-60)*pi/180);
i=0:24;
w=(i-12)*(15);
rt10=(pi()/24)*(a10+b10*cos(w*pi/180)).*(cos(w*pi/180)-cos(ws10*pi/180))/(sin(ws10*pi/180)-
(pi/180)*ws10*(cos(ws10*pi/180)));
I10=(rt10.*H10)*10^6/3600;%Monthly mean hourly Global radiation
I10(I10<0)=0;
%November
H11=22.32049595;%Monthly mean daily Global radiation (MJ/m^2)
Hd11=6.284973344;
ws11=87.05990279; %the sunset-hour angle
n11=318;
dec11=23.5*sin((360*(284+n11)/365)*pi/180);
a11=0.409+0.5016*sin((ws11-60)*pi/180);
b11=0.6609-0.4767*sin((ws11-60)*pi/180);
i=0:24;
w=(i-12)*(15);
rt11=(pi()/24)*(a3+b3*cos(w*pi/180)).*(cos(w*pi/180)-cos(ws11*pi/180))/(sin(ws11*pi/180)-
(pi/180)*ws11*(cos(ws11*pi/180)));
I11=(rt11.*H11)*10^6/3600;%Monthly mean hourly Global radiation
```

```
I11(I11<0)=0;
%December
H12=21.55855517;%Monthly mean daily Global radiation (MJ/m^2)
Hd12=5.477873791;
ws12=86.34773254; %the sunset-hour angle
n12=344;
dec12=23.5*sin((360*(284+n12)/365)*pi/180);
a12=0.409+0.5016*sin((ws12-60)*pi/180);
b12=0.6609-0.4767*sin((ws12-60)*pi/180);
i=0:24;
w=(i-12)*(15);
rt12=(pi()/24)*(a12+b12*cos(w*pi/180)).*(cos(w*pi/180)-cos(ws12*pi/180))/(sin(ws12*pi/180)-
(pi/180)*ws12*(cos(ws12*pi/180)));
I12=(rt12.*H12)*10^6/3600;%Monthly mean hourly Global radiation
I12(I12<0)=0;
rd12=(pi()/24)*(cos(w*pi/180)-cos(ws12*pi/180))/(sin(ws12*pi/180)-(pi/180)*ws12*(cos(ws12*pi/180)));
ID12=(rd12.*Hd12)*10^6/3600;
ID12(ID12<0)=0;
IB12=I12-ID12;%hourly beam solar radiation on horizontal surface for December
%Hourly Ambient temperature
%The code for calculation of hourly ambient variation for January. For other %months we can calculate in similar
manner
Tmax=[27.69032258 29.54091133 31.28258065 31.00426667 30.49677419 30.70666667 28.95612903
26.97483871 28.02 28.56064516 27.66583908 26.40774194];
Tmin=[13.7 15.7 17.4 17.3 17.4 18.1 16.6 16.7 16.0 15.5 14.8 12.9];
DR=Tmax-Tmin;
Tamean=(Tmax+Tmin)/2;
thmax=14;
t=0:1:24;
n=length(Tmax);
Tam=zeros(n,length(t));
for i=1:n
   for k=1:length(t)
   Tam(n,k)=Tamean(n)+((DR(n))/2*(cos(2*pi*(t-thmax)/24)));
   end
end
```

Code for simulation of collector performance

```
% optical performance
 L=6.1;%length of the collector
w=2.3;%width of the collector
di=0.047;%inner diameter of the receiver pipe
do=0.051;%outer diameter of the receiver pipe
Dco=0.074;%outer diameter of the Glass cover
Dci=0.070;%inner diameter of the Glass cover
Ar=pi*di*L;%
er=0.10;%receiver tube emittance
eci=0.88;%Glass Cover emittance
eco=0.88;%
TRc=0.85;%Glass Cover transmittance
ABr=0.95;% Receiver tube absorbance
RLt=0.90;%Trough reflectance
In=0.95;%intercept factor
n1=17;%n for the mean day of the month
dec1=23.5*sin((360*(284+n1)/365)*pi/180);%Declination
costeta1=cos(dec1*pi/180);%Polar N–S axis with E–W tracking;
teta1=acos(costeta1);
kteta1=costeta1+0.0003178*(teta1)-0.00003985*(teta1).^2;% modifier
opeff1=In*TRc*ABr*RLt*kteta1;%Optical effeciency
costeta2=cos(dec2*pi/180);%Polar N–S axis with E–W tracking;
teta2=acos(costeta2);
kteta2=costeta2+0.0003178*(teta2)-0.00003985*(teta2).^2;%Incident angle modifier
opeff2=In*TRc*ABr*RLt*kteta2;%Optical effeciency
costeta3=cos(dec3*pi/180);%Polar N–S axis with E–W tracking;
teta3=acos(costeta3);
kteta3=costeta2+0.0003178*(teta3)-0.00003985*(teta3).^2;%Incident angle modifier
opeff3=In*TRc*ABr*RLt*kteta3;%Optical effeciency
costeta4=cos(dec4*pi/180);%Polar N–S axis with E–W tracking;
teta4=acos(costeta4);
kteta4=costeta4+0.0003178*(teta4)-0.00003985*(teta4).^2;%Incident angle modifier
opeff4=In*TRc*ABr*RLt*kteta4;%Optical effeciency
costeta5=cos(dec5*pi/180);%Polar N–S axis with E–W tracking;
teta5=acos(costeta5);
kteta5=costeta5+0.0003178*(teta5)-0.00003985*(teta5).^2;%Incident angle modifier
```

```
opeff5=In*TRc*ABr*RLt*kteta5;%Optical effeciency
costeta6=cos(dec6*pi/180);%Polar N–S axis with E–W tracking;
teta6=acos(costeta6);
kteta6=costeta6+0.0003178*(teta6)-0.00003985*(teta6).^2;%Incident angle modifier
opeff6=In*TRc*ABr*RLt*kteta6;%Optical effeciency
costeta7=cos(dec7*pi/180);%Polar N–S axis with E–W tracking;
teta7=acos(costeta7);
kteta7=costeta7+0.0003178*(teta7)-0.00003985*(teta7).^2;%Incident angle modifier
opeff7=In*TRc*ABr*RLt*kteta7;%Optical effeciency
costeta8=cos(dec8*pi/180);%Polar N–S axis with E–W tracking;
teta8=acos(costeta8);
kteta8=costeta8+0.0003178*(teta8)-0.00003985*(teta8).^2;%Incident angle modifier
opeff8=In*TRc*ABr*RLt*kteta8;%Optical effeciency
costeta9=cos(dec9*pi/180);%Polar N–S axis with E–W tracking;
teta9=acos(costeta9);
kteta9=costeta9+0.0003178*(teta9)-0.00003985*(teta9).^2;%Incident angle
opeff9=In*TRc*ABr*RLt*kteta9;%Optical effeciency
costeta10=cos(dec10*pi/180);%Polar N–S axis with E–W tracking;
teta10=acos(costeta10);
kteta10=costeta10+0.0003178*(teta10)-0.00003985*(teta10).^2;%Incident angle modifier
opeff10=In*TRc*ABr*RLt*kteta10;%Optical effeciency
costeta11=cos(dec11*pi/180);%Polar N–S axis with E–W tracking;
teta11=acos(costeta11);
kteta11=costeta11+0.0003178*(teta11)-0.00003985*(teta11).^2;%Incident angle modifier
opeff11=In*TRc*ABr*RLt*kteta11;%Optical effeciency
costeta12=cos(dec12*pi/180);%Polar N–S axis with E–W tracking;
teta12=acos(costeta12);
kteta12=costeta12+0.0003178*(teta12)-0.00003985*(teta12).^2;%Incident angle modifier
opeff12=In*TRc*ABr*RLt*kteta12;%Optical effeciency
y=[opeff1 opeff2 opeff3 opeff4 opeff5 opeff6 opeff7 opeff8 opeff9 opeff10 opeff11 opeff12];
bar(y)
%thermal performance of the PTSC

clear all
clc
L=6;  %length of the collector
W=2.3;  % width of the collector
Dai=0.047;%Absorber pipe internal diameter
```

```
Dao=0.051;%Absorber pipe outer diameter
Dgi=0.070;%Glass envelop internal diameter
Dgo=0.074;%Glass envelop external diameter
In=0.95;  % intercept factor
ema=0.10;%Absorber pipe transmittance
emg=0.88;%Glass envelop transmittance
aba=0.95;%Absorber pipe thermal absorptance
rs=0.9;%Reflected surface reflectivity
trg=0.85;%Glass envelop transmittance
%working HTF,air properties
Ta=25+273.5;
Tsky=Ta-8;
kc=1.04;%pyrex glass thermal conductivity
ema=0.10;%Absorber pipe transmittance
emg=0.88;%Glass envelop transmittance
rhoair = 1.1614;%air density
kair = 0.0263;%thermal conductivity of air
cpair = 1007.0;%specific heat of air
dvair= 1.846*10^-5;%dynamic viscosity of air
prair=0.7;%average temprature of glass and ab pipe
g=9.81; %gravity
L=6;  %length of the collector
w=2.3;  % width of the collector
Dgo=0.074;
Dai=0.047;%Absorber pipe internal diameter
Dao=0.051;%Absorber pipe outer diameter
Dgi=0.070;%Glass envelop internal diameter
Vair=3.5;
Reair=(rhoair*Vair*Dgo)/dvair;
if Reair<100 && Reair>0.1
   Nuout=0.4+0.54*(Reair)^0.52;
else
   Nuout=0.3*(Reair)^0.6;
end
hcvext=(kair/Dgo)*Nuout;
%calculating Tgo
Aa=pi*L*(Dao-Dai);
```

```
Ag=pi*L*(Dgo-Dgi);
Af=pi*Dai*L;
boltZ=5.67*10^-8;
a=Ta+27;
b=Ta+80;
Tgo=(Ta+0.1)*ones(1,b-a+1);
Tr=325.15:378.15;
A=(1/ema+(1-emg)*(Dao)/(Dgi*emg));
Qloss1=100*ones(1,b-a+1);
Qloss2=200*ones(1,b-a+1);
Tgi=zeros(1,b-a+1);
kvair=20.92*10^-3;
leff=(Dgi-Dao)/2;
Grair=(g*0.00294*(78*(leff)^3))/(kvair)^2;
Rac=((log(Dgi/Dao))^4/((leff^3)*(Dao^-0.6+Dgi^-0.6)^5))*(Grair*prair);
keff=(0.38*43.9*10^-3)*(prair/(0.861+prair))^0.25*((Rac)^0.25);
for i=1:b-a+1
    while(abs((Qloss1(i)-Qloss2(i))/Qloss2(i))>0.0025 && Tgo(i)<Tr(i))
        Qloss1(i)=pi*Dgo*L*w*(Tgo(i)-Ta)+pi*Dgo*L*emg*boltZ*((Tgo(i))^4-(Tsky)^4);
        Tgi(i)=(Qloss1(i)*log(Dgo/Dgi))/(2*pi*kc*L)+Tgo(i);
       Qloss2(i)=pi*Dao*L*boltZ*((Tr(i))^4-(Tgi(i))^4)/A;
       Tgo(i)=Tgo(i)+0.001;
    end
    hrext=boltZ*emg*(Tgo(1,end)^2+Tsky^2)*(Tsky+Tgo(1,end));
    hrint=(boltZ*((Tr(1,end)^2)+(Tgo(1,end)^2))*((Tr(1,end)-1)+Tgo(1,end)))/((1/ema)+((1-emg)/emg)*(Dao/Dgi));
    UL=Qloss1(i)/(Aa*(Tr(i)-Ta));
    hcvint=2*pi*keff/(log(Dgi/Dao));
end
mfl=0.025;% mass flow rate
cpf= 1916;%specific heat of working HTF(J/kg.k)
dvf=0.00105; % dynamic viscosity of HTF Pa.s
kf=0.102;%thermal conductivity of fluid w/m.k
rhof=773;%density of HTF
Vf1=(mfl)/(rhof*Af);%velocity
Ref=rhof*Vf1*Dai/dvf;
prf=(dvf*cpf)/kf;
f=(1.82*logm(Ref)-1.64)^-2;
```

```
if Ref<=2300
   Nuf=4.36;
else
   Nuf=((f/8)*(Ref-1000)*prf)/((1+12.7)*(f/8)^0.5)*(prf^(2/3)-1);
end
hcf=(kf/Dai)*Nuf;
cpab= 435.0;%Specific heat of absorberpipe
rhoab= 8073;%Densityof absorberpipe
cpgl=500;%Sclcpecific heat of glass envelope
rhogl=200;%Density of glass envelope
mg=rhogl*cpgl*Ag;
AG=hcvint/mg;
BG=pi*Dao*hrint/mg;
CG=pi*Dgo*hcvext/mg;
DG=pi*Dgo*hrext/mg;
ma=rhoab*cpab*Aa;
AA=pi*Dao*hcvint/ma;
BA=pi*Dao*hcvint/ma;
CA=pi*Dai*hcf/ma;
DA=1/ma;
mf=rhof*cpf*Af;
dx=0.25;
AF=5;%AF=pi*Dai*hcf/mf;
BF=(mfl*cpf)/(mf*dx);
nn=(L/dx)+1;%%number of node
dt=1;
nt=86400;
load IBi
Tg=zeros(24,3600);
TA=zeros(24,3600);
Tf=zeros(24,3600);
nr=3600;
for i=1:24
Tg(i,1)=25+273;%column vector
TA(i,1)=25+273;
Tf(i,1)=25+273.5;
Tf(1,:)=180+273.5;
```

```
end
for i=1:24
   for j=2:3600
        Tg(i,j)=(((1/dt)-(AG+BG+DG))*Tg(i,j-1)+(AG+BG)*TA(i,j-1)+(CG*(25+273))+DG*Tsky)*dt;
        TA(i,j)=(IBi(2*j)*6*DA+(1/dt-AA-BA-CA)*TA(i,j-1)+(AA+BA)*Tg(i,j-1)+CA*Tf(i,j-1));


          Tf(24,:)=(1/dt-AF)*Tf(i,j-1)+AF*TA(i,j-1);
             Tf(i,j)=(1/dt-AF)*Tf(i,j-1)+AF*TA(i,j-1)-BF*(Tf(i,j-1)-Tf(i,j-1))*dt;
   end
end
%sizing of PCM storage system and analysis of Charging
clear
clc
rhs=2260;%density of solid pcm kg/m3
rhl=1900;%density of liquid pcm kg/m3
cps=1.588;%specific heat capacity solid pcm kJ/kg
cpl=1.650;%specific heat capacity liquid pcm KJ/kg
cp=(cps+cpl)/2;
rhf=773;%density of HTF kg/m3
Hm=176;%Latent heat of fusion (KJ/kg)
deltT=2;
deltT2=2;
cpf=1.916;%specific heat KJ/kg.K
e=0.25;
Er=30224.025;%Energy required in KJ
%vst=Er/(cpl*rhl*deltT+Hm*rhl+cps*rhs*deltT2);
vst=Er/(cpl*rhl*deltT*(1-e)+Hm*rhl*(1-e)+cps*rhl*deltT*(1-e)+cpf*rhf*e*deltT);
% H=1.5*D;
% vst=pi*D*H;
D=sqrt(vst/pi*1.5);
H=1.5*D;
Do=0.04;
Di=0.037;
l=0.25;
nc=vst*4*(1-e)/(pi*Do^2*l);
mpcm=rhs*(pi/4)*Di^2*l*nc;
vpcm=(pi/4)*Di^2*l*nc;
```

```
mwf=0.001050;%dyanamic viscosity N/m2.s
mf=0.0125;
kf=0.1012;
prf=(mwf*cpf)/kf;
Ac=(pi/4)*D^2*H;
vf=mf/(e*Ac*rhf);
A=e*cpf*rhf;
B=A*vf;
Rep=(rhf*vf*Do)/mwf;
Nu=2+1.1*(6*(1-e))^0.6*(Rep^0.6)*prf^(0.3);
%Nu=0.8*(Rep^0.4)*prf^(0.3);
hp=kf*Nu/Do;
Lc=(pi*(Do/2)^2*l)/(2*pi*(Do/2)^2+2*pi*(Do/2)*l);
ks=177;
Bi=hp*Lc/ks;
hep=hp/(1+0.2*Bi);
kfx=0.5*prf*Rep*kf;
kp1=0.59;
kp2=0.5;
a=(kp1+kp2)/2;
b=(cps+cpl)/2;
c=(rhs+rhl)/2;
%during solid stage
m1=0.28-0.757*log10(e)-0.057*log10(kp1/kf);
ke1=kf*(kp1/kf)^m1;
kefx1=kf*(ke1/kf+0.58*prf*Rep);
ksx1=kefx1-kfx;
A1=(1-e)*rhs*cps;
%During solid-liquid phase change
m2=0.28-0.757*log10(e)-0.057*log10(a/kf);
ke2=kf*(a/kf)^m2;
kefx2=kf*(ke2/kf+0.58*prf*Rep);
ksx2=kefx2-kfx;
A2=(1-e)*b*c;
%During the liquid stage
m3=0.28-0.757*log10(e)-0.057*log10(kp2/kf);
ke3=kf*(kp2/kf)^m3;
```

```
kefx3=kf*(ke3/kf+0.58*prf*Rep);
ksx3=kefx3-kfx;
A3=(1-e)*rhl*cpl;
pef=e*rhf;
pes=(1-e)*rhs;
cef=e*cpf;
ces=(1-e)*cps;
ap=(2*pi*(Do/2)^2+2*pi*(Do/2)*l)/vst;
C=hep*ap;
S1=B/A;
f1=kfx/A;
C1=C/A;
SS1=ksx1/A1;
SS2=ksx2/A2;
SS3=ksx3/A3;
ff1=C/A1;
ff2=C/A2;
ff3=C/A3;
dx=0.04;
r=kfx/(e*rhf*cpf);
F=(hep*ap)/(e*rhf*cpf);
cp2=(cps+cpl)/2;
rhf2=rhf
F2=(hep*ap)/(e*rhf*cpf);
c=vf/dx;
A=1-F-2*r;
B=r-c/2;
C=r+c/2;
kps=0.495;
kpl=0.565;
kp2=(kps+kpl)/2;
RP1=kpl/(1-e)*(rhl)
rh2=(rhs+rhl)/2;
RP2=kp2/(1-e)*(rh2)
RP3=kps/(1-e)*(rhs)
cp2=(cps+cpl)/2+(Hm/2);
FP1=(hep*ap)/(1-e)*(rhl*cps);
```

```
FP2=(hep*ap)/(1-e)*(rh2*cp2);
FP3=(hep*ap)/(1-e)*(rhs*cps);
D=1-FP-2*RP;
nn=(0.36/Do)+1;
dt=0.1;
nts=43200;
Tp=zeros(nn,43200);
Tf=zeros(nn,43200);
Tp(:,1)=180;
Tf(:,1)=180;
Tf(1,:)=320;
for j=2:nts
    for i=2:nn-1
       Tf(i,j)=A*Tf(i-1,j-1)+B*Tf(i+1,j-1)+C*Tf(i-1,j-1)+F*Tp(i-1,j-1);
       Tp(i,j)=D*Tp(i-1,j-1)+RP1*(Tp(i+1,j-1)+Tp(i-1,j-1))+FP1*Tf(i-1,j1);
    end
  Tf(nn,j)=A*Tf(nn-1,j-1)+(B+C)*Tf(nn-1,j-1)+F*Tp(nn-1,j-1);
    Tp(nn,j)=D*Tp(i,j)+2*RP1*Tp(i-1,j)+FP1*Tf(i,j);
    Tp(1,nts)=D*Tp(i,j)+2*RP1*Tp(i-1,j)+FP1*Tf(i,j);
 end
```